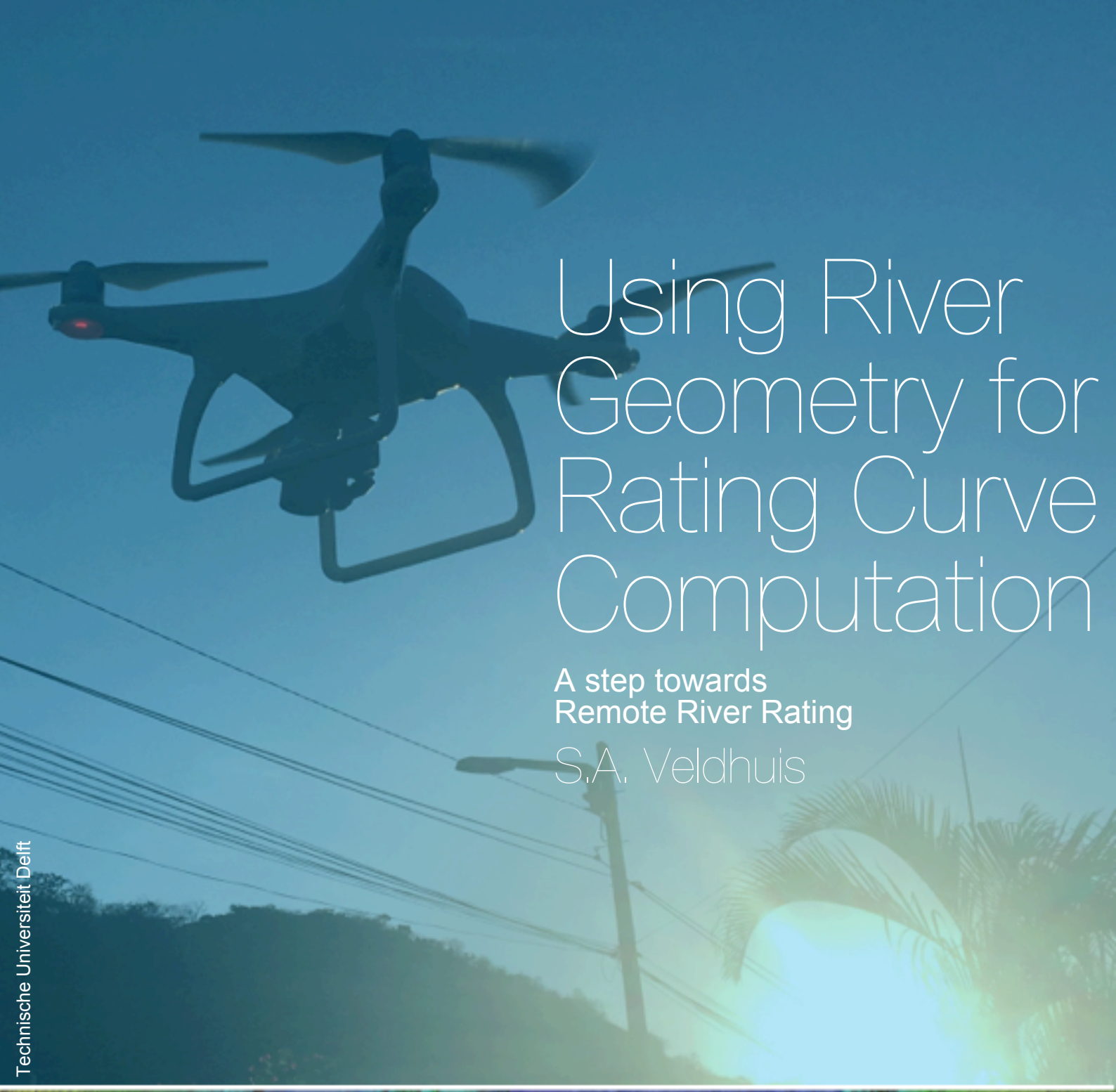

Using River Geometry for Rating Curve Computation

A step towards Remote River Rating

S.A. Veldhuis

Technische Universiteit Delft

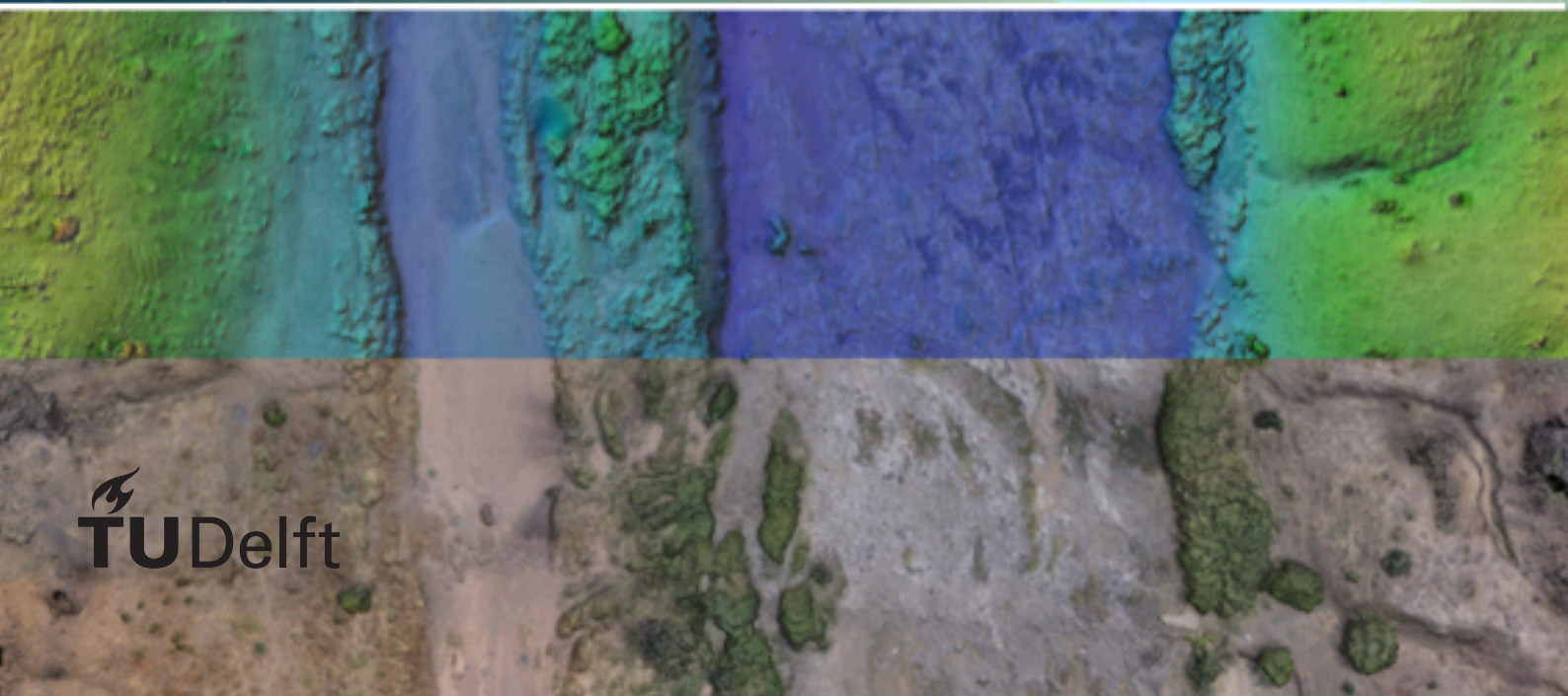

TU Delft

Using River Geometry for Rating Curve Computation

A step towards Remote River Rating

by

S.A. Veldhuis

to obtain the degree of Master of Science
at the Delft University of Technology,
to be defended publicly on Thursday June 28, 2018 at 10:00 AM.

Student number:	4205634	
Project duration:	July 15, 2017 – June 28, 2018	
Thesis committee:	Prof. dr. ir. H.H.G. Savenije,	TU Delft, chair
	Prof. dr. ir. M. Kok,	TU Delft
	Ir. W.M.G. Luxemburg,	TU Delft

This thesis is confidential and cannot be made public until July 1, 2018.

TU Delft

Preface and Acknowledgement

This thesis study is performed as part of the requirements for obtaining the degree of Master of Science at Delft Technical University (TUD), faculty of Civil Engineering and Geosciences, department of Water Resource Management, subgroup Hydrology. This thesis is the product of approximately ten months of research which was done for aforementioned educational institution.

Even though the majority of work was done behind university walls, an important part of this research involved a two-month period of fieldwork in the Tete province of north-western Mozambique. I was able to travel there in accordance with a newly established Memorandum of Understanding (MoU) between TUD and Hidroeléctrica de Cahora Bassa (HCB), one of Mozambique's main hydro-power companies. In addition, the regional water authority Administração Regional de Águas do Zambeze (ARA Zambeze) was also involved. The logistical and technical support that I received from both parties was essential to the successful outcome of this research.

I would like to express my sincere gratitude to a number of people who have provided me with opportunities, motivation, ideas, information, and any other type of support.

First and foremost a word of appreciation should be directed at the people who have guided me through the whole process, prof.dr.ir. Huub Savenije and ir. Willem Luxemburg. In the first place I want to thank them for the opportunity to partake in this very interesting and exciting research. Secondly I thank them for all the advice, ideas and above all enthusiasm they have provided me with over the course of this study.

I am of course very grateful to all the people from HCB: Engº Nelson Beete (CEO HCB), MSc, Engº Gustavo Jessen, BSc, Engº Rosaque J. Guale, MSc, Engº José Matola, MSc Humberto Levesseni and Juma Matsinhe, as well as the people from ARA-Zambeze: Engº Francisco Macaringue, MSc, Engº Manuel J. Mahunguana, MSc and Nellio Julio who have helped and supported me during my stay in Mozambique. As I already mentioned, their support was essential to me and this research, both on a personal and a professional level and I hope to see them again some day.

Last but not least a word of thanks to prof.dr.ir. Matthijs Kok for being part of my thesis committee by being involved in the assessment of this study and to my girlfriend MSc Marcia Merenciana for proofreading this report.

S.A. Veldhuis
Delft, June 20, 2018

Contents

Abstract

This thesis study aims to provide a solution for the shortcomings concerning conventional rating curve computation. Conventional rating curve computation struggles with the issues of being data-intensive, inaccurate in high-flow regimes and susceptibility to changes in cross-sectional geometry. In the view of the researchers, an answer can be found in a more physically-based rating curve that allows for substantiation through a detailed representation of the river's geometry. For a detailed reconstruction of the geometry, we see a big potential in the use of state of the art remote sensing technologies. Apart from (1) increasing accuracy by removing the need for extrapolation to high-flow regimes, the physically-based rating curve would (2) be less susceptible to changes in geometrical changes due to scouring and sediment-deposition, (3) be more easily to update if geometrical changes do occur, and (4) would require less data and is therefore likely to be cheaper to establish. The physically-based rating curve is based on Manning's formula for steady uniform flow.

The research included two months of fieldwork in the north-western province of Mozambique, Tete. Here, as a guest of HCB in Songo, the researcher collaborated with local parties HCB and ARA-Zambeze to perform measurements on a set of tributaries to the Zambezi river. A small commercial drone was used and aerial photographs were converted into Digital Elevation Models (DEMs). Eight rivers were visited in total, of which two the data was of insufficient quality and quantity to be used in further analysis.

Three factors seem to be of main influence to accuracy of the DEM: size of the measurement area, coverage of the area by Ground Control Points (GCP)s and presence of vegetation. Absolute errors in the DEMs, i.e. the average error of GCPs per river, ranged from $0.16\ m$ to $2.57\ m$ in the horizontal plane and from $0.01\ m$ to $0.30\ m$ in the vertical direction. It can be concluded that a high resolution elevation model can be computed showing very little relative error in both the horizontal plane (max 1.90%) and the vertical plane (max 3.65%).

A lack of flowing water in the observed rivers gave rise to the need for an alternative way of quantifying slope (i). A solution was found by using the increase of the conveyance (C or $AR^{2/3}$) in downstream direction (Y) for a constant water level ($i = 0$). By enforcing a slope on the water surface, $^{dC}/_{dY}$ can be brought down to zero, which in theory corresponds to the situation for uniform-flow. Through this process, the theoretical 'local' slope corresponding to uniform flow in the measured reach can be established. A comparative measure was formed by deriving the 'regional' slope from Advanced Spaceborne Thermal Emission and Reflection Radiometer Global Digital Elevation Model (ASTGDEM) by looking at the elevation profile of a reach of $20\ km$ around the measuring location. A factor two difference showed that the slope is likely to be influenced by the water level (i.e. local slope will dominate low flows and regional slope will dominate high flows) and stipulates the importance of (1) calibration or real time measurements of i and (2) the need to validate proposed method for slope calculation.

Taking into account parameter uncertainty, it can be concluded that the physically-based rating curve shows sufficient similarity with that of ARA-Zambeze's to assume the validity of the method for physically-based rating curve computation. Theory of error propagation is used to quantify the relative contribution of the uncertainties in the parameter values. The error in Q can be seen to lie between 67% and 30% where the roughness coefficient (n) is estimated based on literature, but this decreases to values between 50% and 13% when n is calibrated. An important observation is that the uncertainty of h_0 has a very big influence for low water levels (42% at $h = 1.6\ m$) and becomes significantly lower at higher water levels (4.2% at $h = 4.6\ m$). This analysis shows that, in exception for very low-flows, accuracy of the physically based rating-curve will benefit most from decreasing uncertainty in n. For low flows, the major contribution to the error comes from uncertainty in h_0. Another important conclusion is that in contrast to conventional rating curves, the physically based rating curve shows an increasing accuracy for increasing water levels due to the decreasing influence of the error in h_0. This resolves the biggest flaw in conventional rating curve computation, the decreasing predictive capability for high flows due to extrapolation of low flow data.

The biggest overall limiting factor to accuracy is the need to calibrate n which requires at least one relevant flow measurement under the assumption of uniform roughness as is done in this study. When

the roughness coefficient is calibrated, the error in the physically based rating curve is roughly 10% for high flows, but can still be reduced. Further improvement can be achieved by accounting for the non-uniformity in n. This would however require multiple discharge measurements.

List of Acronyms

ARA-Zambeze Administração Regional de Águas do Zambeze.

ASTGDEM Advanced Spaceborne Thermal Emission and Reflection Radiometer (ASTER) Global Digital Elevation Model (GDEM).

DEM Digital Elevation Model.

DGPS Differential Global Positioning System.

DPC Dense Point Cloud.

GCP Ground Control Point.

GSD Ground Sampling Distance.

HCB Hidroeléctrica de Cahora Bassa.

HGL Hydraulic Grade Line.

ISO International Organisation of Standardization.

MoU Memorandum of Understanding.

NaN Not a Number.

ODM OpenDroneMap.

RMSE Root Mean Square Error.

SPC Sparse Point Cloud.

TIFF Tagged Image File Format.

TUD Delft Technical University.

UAV Unmanned Aerial Vehicle.

Glossary

aperture A hole within a lens, through which light travels into the camera body. The larger the hole, the more light passes to the camera sensor. Aperture also controls the depth of field, which is the portion of a scene that appears to be sharp. Typically expressed in ”f” numbers (also known as ”focal ratio”) [19].

ARA-Zambeze Administração Regional de Águas do Zambeze. The governmental water authority of all water management related issues concerning the Zambezi basin in Mozambique. ARA-Zambeze is managed by the Ministry of Public Works, Housing, and Water Resources.

channel control A cross section where change in the physical characteristics of the channel downstream to it is of effect on the flow at the gauging section is called to be under channel control).

Dense Point Cloud The dense point cloud represents the actual constructed 3D model. A point cloud can be seen as a set of data points in space.

Ground Sampling Distance A measure for the real life distance between two pixel-centres of an image [cm/pixel].

Ground Control Point A reference point on the ground with known location and elevation. Used to scale and possibly georeference the 3D model of the river section.

HCB Hidroeléctrica de Cahora Bassa. One of Mozambique’s main hydro-electricity companies. Their power is generated by a dam in the Zambezi river, situated near Songo in the Tete province. They export power to countries such as South-Africa, Zimbabwe, Zambia, and Malawi.

hydrograph A graph showing the variation of flow (y-axis) over time (x-axis).

ISO A way to brighten your photos if you can’t use a longer shutter speed or a wider aperture. A higher numbers means a brighter image. However, raising your ISO increases noise in your images [19].

orthomosiac A set of overlapping aerial photo’s matched to form one geometrically corrected image. The orthomosaic (or orthophoto) can be used to measure true distances because it has been adjusted for topographic relief, lens distortion, and camera tilt.

rating-curve A mathematical representation of the relation between discharge and water-level, plotted as a curve. The most widely accepted form of the mathematical relation is that of a power-law function: $a(h - h_0)^b$.

Root Mean Square Error The RMSE represents the sample standard deviation of the differences between predicted values and observed values. RMSE is the square root of the average of squared errors. The effect of each error on RMSE is proportional to the size of the squared error; thus larger errors have a disproportionately large effect on RMSE. Consequently, RMSE is sensitive to outliers. [28].

Shutter Speed The length of time a camera shutter is open to expose light into the camera sensor. Shutter speeds are typically measured in fractions of a second. Slow shutter speeds allow more light into the camera sensor [19].

Sparse Point Cloud The sparse point cloud represents the result of photo alignment. To obtain the sparse point cloud Photoscan searches for common points on photographs and matches them, as well as finds the position of the camera for each picture and refines camera calibration parameters. The sparse point cloud is required for further 3D model reconstruction.

stage The water level in a river or stream with respect to a chosen reference height.

List of Symbols

Q Discharge [m^3/s].

h Water level / Stage [m].

h_0 Stage at zero flow [m].

i Slope of the water surface [m/m].

n Manning's roughness coefficient [$s/m^{\frac{1}{3}}$].

a_1 Parameter of the physically based rating curve: $a_1 = n^{-1} i^{\frac{1}{2}}$ [$m^{\frac{1}{3}}/s$].

a_2 Geometry-parameter of the physically based rating-curve [$m^{\frac{8}{3}-b}$].

b Power function exponent / Geometry-parameter [-].

z Elevation [m].

B River width [m].

L River Length [m].

A (Conveyance) Area [m^2].

P Wetted Perimeter [m].

R Hydraulic Radius: $R = A/P$ [m].

C Conveyance: $C = AR^{\frac{2}{3}}$ [$m^{\frac{8}{3}}$].

List of Figures

List of Tables

1 Introduction

1.1. Research Motivation

Hydrological models are of high importance for making meaningful predictions about water availability, accurate flood-forecasting and of course for our understanding of the natural world. The most popular method for parameter calibration of the hydrological model is by means of comparing the modelled hydrograph to the observed hydrograph. Naturally, this requires the availability of discharge data for the modelled catchment. As directly measuring flow is a tedious and labour-intensive venture, the observed hydrograph is usually computed by using a rating-curve, depicting the relation between discharge (Q) and stage (h) to transform measured water-levels into a time series of indirect flow-measurements.

The researchers see a big opportunity to improve discharge monitoring with state of the art remote sensing products. In this off-site 'remote river rating', both big- (e.g. satellites) and small- (e.g. UAVs) scale remote sensing technologies can play a part. The ultimate goal would be to use satellite images for the acquirement of discharge-data in ungauged river basins. This in itself is not something new, however, both resolution of images and satellite trajectories are known to impose a limiting factor on both the precision, accuracy, and the location of the data that can be obtained [4] [29].

This thesis will present a step towards this concept of remote river rating by using a simple commercial UAV for an improved computation procedure for rating-curves. As mentioned, it is general practice to use rating curves for indirect measurements of discharge. However, even ground stations for measuring stage are often difficult to keep operational and come with significant unreliability [11] [20] [26].

It is here that the researchers see room for improvement as the common method of rating-curve computation falls short in certain aspects. Computation of the rating-curve is commonly done by performing a series of corresponding Q and h measurements over time, and fitting a (power-)function through these data-points. The problem here is that due to their often difficult measurability, these measurements usually do not include data in the high-flow regimes of a river. Therefore the curve needs to be extrapolated in order to include high flows, resulting in increasing uncertainty of its accuracy. Secondly, as the measurements are generally done in only one certain cross-section, possible errors induced by non-uniformities are not averaged out. In addition, river-geometry and therefore the Q-h relation is usually non-stationary due to scouring of the riverbed and deposition of sediments [13]. This results in the necessity for the rating curve to be updated regularly. All of this is hampered by the fact that performing Q-h measurements are costly and time-consuming.

In response to these shortcomings, the researchers argue that it would be beneficial to produce a more physically-based rating-curve that reduces the need for extrapolation to high-flow regimes and also averages out non-uniformities in the cross-section, making it less sensitive to geometrical changes. This physically-based rating curve allows for substantiation of the exponent in the power function [12], which depends on the geometry of the river section.

In doing so we see a big opportunity in making use of some of the technological advances in the field of remote sensing, resulting in a more accurate and more easily applicable method for rating curve computation. The benefits we see in the proposed method include:

1. Fewer field measurements needed to update rating curves. Per rating section, only one set of

drone measurements and one discharge measurement are required instead of multiple stage- and discharge measurements over time.

2. In-situ measurements with a drone are easy thus regular updating of the rating curve is cheaper.
3. The entire section geometry, i.e. including floodplains, can be included leading to a more physically-based rating procedure eliminating the need for extrapolation.
4. More accurate presentation of river section as many cross-sections within a river stretch are averaged as opposed to using a single section. Local non-uniformities are therefore averaged out and the rating is less sensitive to changes in the section.

1.2. Aim of This Research

As explained in the previous section, this study aims to provide a solution for the many problems concerning conventional river rating. It is considered to be of high importance that the developed method provides an accessible way of performing river rating in those areas where local water authorities are limited to do so by either financial-, logistical- or political factors. This because those areas are more likely to be poorly gauged and could therefore benefit most from such advancements. This will ultimately also increase our overall understanding of the various river-systems in the world which are influenced by different climatological and geological environments.

A second aspect of key importance is making use of the technological advances that science has made in the field of remote sensing. Both state of the art remote sensing equipment and products are becoming more and more accessible to science and society in general. One very good example of this are the advancements of drone-technology. The researchers feel that with the technologies currently available, it should be possible to perform accurate river rating remotely. This would (1) greatly increase the amount of high-flow flow measurement in ungauged river catchments and (2) thereby greatly benefit water resources management and flood-forecasting in those areas. In summation, the aim of this study is thereby described by providing an answer to the following research question:

> **How can state-of-the-art remote sensing techniques be used to improve conventional river rating practices in terms of accuracy, applicability, and accessibility, thereby aiding in the development of remote river rating?**

Accuracy relates to the indirect flow measurements being a better representation of real-life values than is achieved through conventional rating practises. Applicability relates to the decreasing effort of performing multiple measurements in both space and time, and accessibility relates to the method being more accessible for companies/water authorities with limited financial means for such research/data collection.

It is important for the reader to keep in mind that the focus of this study lies on the development of the proposed method. Although explained and reasoned for, actual quantification of the three mentioned factors of improvement is not the aim of this study. Another note of relevance is that this research can be seen as a successive study to a similar thesis that was performed for the TUD [24]. However, mentioned study had not been completed yet when this research commenced.

Hypothesis and Objectives

The hypothesis of this study is formulated as follows:

> The conventional method for rating curve computation, i.e. by means of fitting a curve to a series of Q-h measurements, can be improved in terms of accuracy, applicability and accessibility by making use of drone technology.
>
> 1. Accuracy will be improved by computation of a more physically-based rating curve that does not rely on extrapolation to the high-flow regime of the rating curve.
> 2. Applicability will be improved by both simplifying measurement performance and increasing feasibility of measurements in areas that are hard to reach.
> 3. Accessibility will be improved by making use of simple and affordable technologies and by reducing the amount of measurements needed.

In order of achieving aforementioned research-goal and testing above-mentioned hypothesis, a set of underlying research objectives have been defined to be:

1. Perform drone- and supplementary measurements in Tete, Mozambique to test feasibility of the proposed method.
2. Use drone- and supplementary measurements to compute rating curves of a set of rivers in the area of interest and compare with currently used rating curves to judge performance.
3. Based on the proceedings of the above two objectives, identify challenges and limitations on the proposed method for rating curve computation.
4. Establish a set of recommendations for involved parties on (improvement of the) applicability of proposed method for rating curve computation.

1.3. Report Structure

This chapter has provided the reader with the motivation of this research and the supporting hypotheses and objectives. Chapter 2 will provide a very basic theoretical framework to better understand the theory behind the concept of photogrammetry and the foundation of the physically-based rating curve: Manning's Formula. In Chapter 3 a detailed explanation of the used materials and applied methods is given, followed by a comprehensive documentation of the two months of fieldwork in Mozambique in Chapter 4. Results are analysed and discussed in Chapter 5, leading to a set of recommendations in Chapter 6. Chapter 7 summarizes this thesis and states drawn conclusions.

2

Theoretical Basis

2.1. (Stereo-)Photogrammetry

The essence of the proposed method for rating curve computation relies on turning plain aerial photographs into a 3D model. This is done through the method of (stereo)photogrammetry. Photogrammetry refers to making measurements from photographs. The principle of stereo-vision, i.e. the capability to perceive depth, lies at the core of this method. In order to see in stereo-vision by means of 2D images, a stereo-pair is needed. A stereo-pair refers to a set of two images showing the same object but from different locations. The difference between the two photos in representation of that object on the 2D image is called the parallax, i.e. the apparent displacement in the position of an object with respect to a reference point caused by a shift in the point of observation. In photogrammetry, parallax refers to the relative difference in position of an image point that appears in each of the overlapping photo of the stereo-pair. Parallax can differ in the two direction of the 2D plane and is calculated quite simply by determining the difference in coordinates (Figure 2.1). An example of parallax in aerial photography is the effect of high buildings that appear to 'keel over' in the direction away from the centre of the photograph.

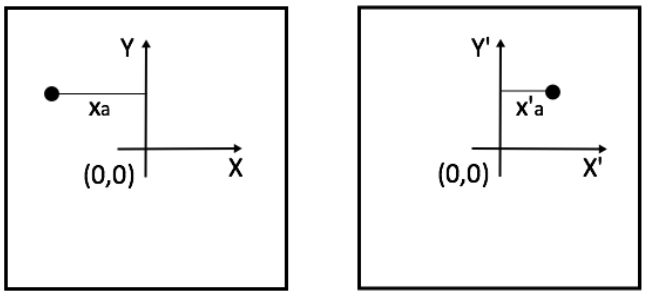

Figure 2.1: Parallax.

In combination with information on camera locations, altitude and focal length, the parallax allows for the calculation of that object's height in the 3D plain (see Figure 2.2 and Equation 2.1). Note that this figure portrays the situation where both pictures are taken from exactly the same height and the photos are taken vertically downwards. A difference in camera-altitudes and photographic tilt will induce an additional parallax in the Y-direction of the photograph.

A variety of software products have been developed for the purpose of photogrammetry and for this study the Photoscan software by Russian developer Agisoft [1] is used (see Section 3.1.4). In order to create a 3D model of the area of interest, every pixel needs to be captured, and recognized from at least two camera-positions. Automation of this process is a big part of where the software comes in

to make sure matching pixels are identified. To ensure this is done with sufficient precision, the aerial images need to be taken with a certain degree of overlap (also see Figure 3.5).

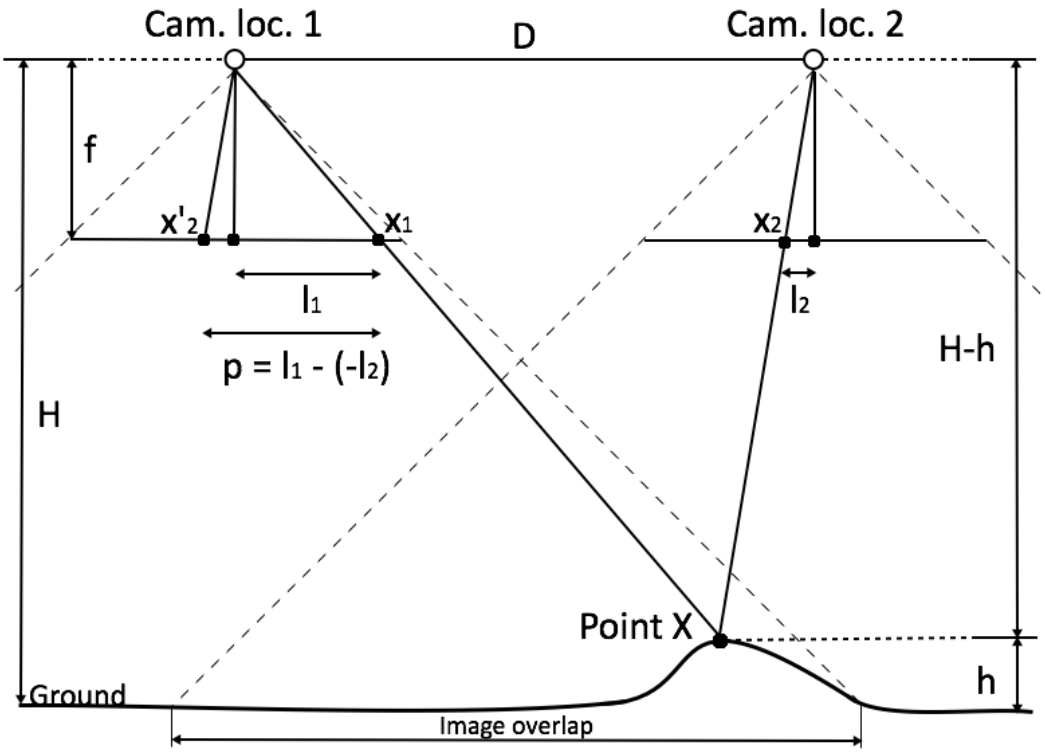

Figure 2.2: Using stereo-vision (and parallax) to determine the height of a point (also see Equation 2.1). H = flight altitude, h = object altitude, f = camera focal length, D = distance between camera positions and p = parallax. (Image partly copied from: http://www.seos-project.eu/)

$$H - h = \frac{Df}{p} \tag{2.1}$$

2.2. River Flow

The 3D geometrical model of the river reach is used to compute a theoretical value for river flow for a given water level. In doing so, the flow conditions are assumed to be both steady and uniform. Steady flow refers to flow velocity at a given location not changing over time. Generally, the flow in rivers is variable in time meaning it is unsteady. However, for practical applications the variation is often considered to be so slow that a steady flow situation can be assumed. Uniform flow refers to the hydraulic condition in which the velocity and cross-sectional area, and therefore also discharge, are constant throughout the length of a channel. The likeliness of this condition to be present increases in upstream direction of disturbances such as waterfalls, confluence points, cross-sectional changes, etc.

Several physical relations have been developed to quantify steady uniform open channel flow, the most famous being the Chézy- and the Manning(-Strickler) formulas. Both are equally applicable and the decision to use one or the other is usually based on tradition [5]. The difference between the two lies in the determination of the roughness coefficient. In this study Manning's formula [18] will be used.

In rating curve computation, the most widely accepted way to consider discharge as a single function of water level is by means of a power-law function as in (2.2) [22].

$$Q = a(h - h_0)^b \tag{2.2}$$

Here Q $[m^3/s]$ is the discharge, h $[m]$ is the water level, h_0 $[m]$ represent the water level at zero flow and a $[m^{3-b}]$ and b $[-]$ are parameters which value is determined through curve-fitting. Whereas

the b parameter is solely linked to cross-sectional geometry, parameter a does not have a clearly defined physical meaning [10] and is used as a dust-bin parameter accounting for a multitude of physical processes. However, in reality the flow capacity of a river channel and adjacent floodplains is affected by the cross-sectional geometry, the slope of the water surface (equal to slope of riverbed in case of uniform flow) and to the bed-roughness which depends on bed material and land cover among things. This is captured by the Manning formula (2.3), where n $[s/m^{\frac{1}{3}}]$ is Manning's roughness coefficient, i $[m/m]$ is the longitudinal slope of the water surface, A $[m^2]$ the cross-sectional area, and R $[m]$ the hydraulic radius. This formula describes the discharge of steady uniform flows and is compatible with the power-law function through (2.4). Through this approach it is reasoned that Equation (2.5) is therefore more physically-based than Equation (2.2).

$$Q = \frac{1}{n}\sqrt{i}AR^{\frac{2}{3}} \tag{2.3}$$

$$Q = \underbrace{\frac{1}{n}\sqrt{i}}_{a_1} \quad \underbrace{AR^{\frac{2}{3}}}_{a_2(h-h_0)^b} \tag{2.4}$$

$$Q = a_1 a_2 (h - h_0)^b \tag{2.5}$$

The second part of Equation 2.4, $AR^{\frac{2}{3}} = a_2(h - h_0)^b$, is seen as a function of water level and can completely be described by the geometry of the river section (also see Figure 2.3). This part will be referred to as the conveyance (C). C $[m^{\frac{8}{3}}]$ is not to be mistaken with the also commonly referred to conveyance term: $\frac{1}{n}AR^{\frac{2}{3}}$ that includes roughness. The geometry can be measured in the field in great detail by means of aerial imagery. This only leaves a_1 $[m^{\frac{1}{3}}/s]$ to be determined which depends on the slope (i) and roughness ($\frac{1}{n}$) of the riverbed. The slope can theoretically be measured but roughness is more difficult due to the fact that it depends on many different factors and is not constant over the entire profile of the river. However, [25] showed that a uniform Manning's coefficient can be used for the entire river profile due to parameter compensation. Floodplains usually have a higher roughness than the main channel due to vegetation, but this is compensated by the decrease in roughness caused by a higher water level. Still, due to its complexity, ideally the roughness coefficient is included in a calibration process. Otherwise it can be estimated based on available literature.

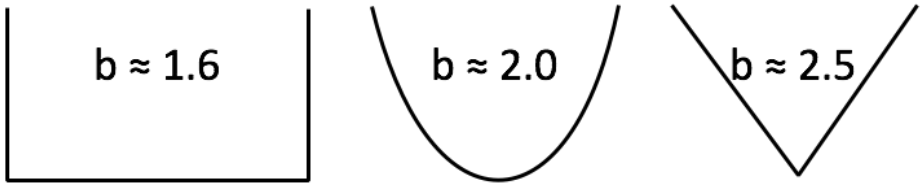

Figure 2.3: The value of the b-exponent depends on geometrical shape of the channel [10].

3

Materials and Methods

3.1. Materials

3.1.1. UAV

Aerial imagery collection for 3D geometry determination of the river reach was done by means of an UAV (popularly known as a drone). For this study we used the DJI Phantom 4. Due to their wide range of possible applications, their popularity with both the general public, scientists, and military does not come as a surprise. This has led drone technology to rapidly advance over the last years and commercial drones to drop significantly in price. Variations in camera quality, battery life and stabilisation mechanisms among things will influence the price of the UAV but a fully equipped DJI Phantom 4 was already available at ±€ 1100 (The Netherlands, May 2018). The Phantom 4 has an effective control range of about 5000 m in unobstructed areas [2].

In the preparation phase of this study the slightly older DJI Phantom 3 Pro has also been used (±€ 560: The Netherlands, May 2018). Although this drone performs slightly less well in terms of battery life and camera specifics this drone has also been used successfully. This information is just to show that a suitable UAV does not require a large investment.

3.1.2. Ground Control Points

The GCP can theoretically be made from any object or material as long as it will be clearly visible on the aerial images. Of course there are some practical considerations to be made in choosing a suitable marker to function as GCP. A selection of different markers with different sizes have been tested on visibility from different heights (Figure 3.1). The marker that came out best was a square plate of $40 \times 40\ cm$ with a two by two chessboard pattern. The markers used in Mozambique were made from wooden square plates of $50 \times 50\ cm$ due to practical reasons for the woodworker.

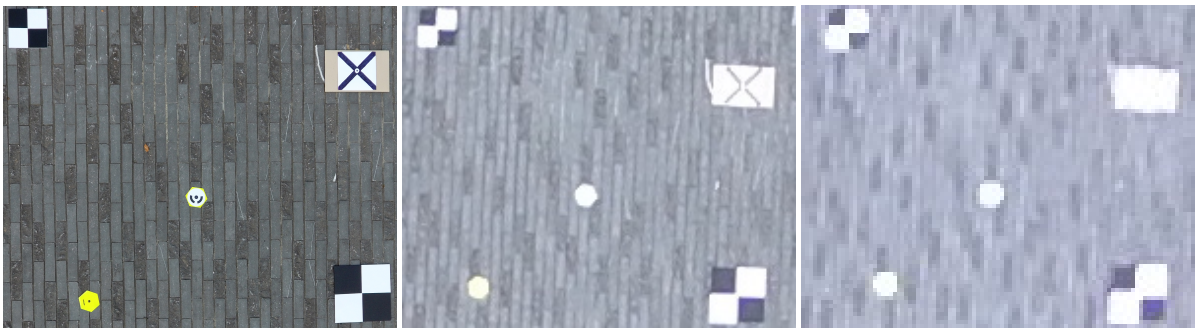

(a) Altitude: 3m (b) Altitude: 40m (c) Altitude: 80m

Figure 3.1: Set of different try-out markers to use as GCPs.

Figure 3.2: A way-point based flight-route in the Litchi application

3.1.3. Spatial Referencing Equipment

Spatial referencing equipment is used to determine the location and elevation of the GCPs. This can be based on a known coordinate system (i.e. WGS84, UTM) or on a locally set up grid system. It goes without saying that a higher accuracy of the coordinates will be beneficial for the resulting DEM. During the preparation phase in The Netherlands, and the fieldwork phase in Mozambique, different types of equipment have been used. The easiest method and most accurate results have been achieved by using a Differential Global Positioning System (DGPS). This does require high investment costs however as DGPS equipment is relatively expensive. Regular GPS can also be used but is (even more so than DGPS) reliable on satellite reception and is notoriously inaccurate for measuring altitudes. Another option is the use of more conventional surveying equipment such as an dumpy/auto level, theodolite or total station.

The decision depends on several aspects such as costs, local availability, and available expertise and manpower. As mentioned, it is important for the researchers that the proposed method is applicable for local companies and water authorities in those areas where investments in water governance are possible to pose limitations. Availability of equipment during the fieldwork phase in Mozambique meant that a dumpy level was used for data collection in this study. During the two phases of the fieldwork, levelling equipment with and without degree circle were used in phases one and two respectively. In combination with the level without degree circle (fieldwork phase two), a measuring tape was used to determine distances between the GCPs. These distances were used to set up a local grid system through the principle of triangulation.

3.1.4. Software

Drone Control

The UAV is controlled by connecting the drone's controller to the user's smartphone or tablet. In this case only a smartphone was available.

Flight planning and control was done by means of two applications. The DJI Go 4 application, default to the control of the DJI Phantom 4, and an external application named Litchi [27]. DJI Go 4 is only used for some initial pre-flight checks. For all other drone control Litchi has been used (Figure 3.2). The advantage of Litchi over DJI's default application is the possibility to (pre)plan flight routes. Using a Google Maps interface, way-points can be added to form a flight route. Many other specifics such as altitude, camera tilt and speed can be included in the flight plan and Litchi also offers an online version allowing the user to plan the flight with the additional comforts of using a computer. Creating a proper flight plan requires some knowledge of the measuring site and expected weather conditions. Preparing a set of flight plans for different scenarios prior to going to the measuring site will really reduce time and effort spent on site.

Photogrammetry
The photogrammetry-software used in this study is called Agisoft Photoscan [1]. The programme has a clear interface and offers a wide variety of options to manually edit parts of the 3D model.

GCPs can be used for georeferencing and to scale the model. If the GCPs are accurately measured, this will highly increase the accuracy of the 3D model. In addition, adding GCPs allows the programme to calculate the Root Mean Square Error (RMSE) of these GCPs in both X, Y, and Z direction, thereby given a good indication of the accuracy of the DEM

A big plus is the user-friendliness of the software and the clear output. A big disadvantage is the lack of insight in what happens behind the screen, making Agisoft Photoscan a so-called 'Black-Box' programme. This hinders the user in understanding the reason behind possible unexpected GCP-errors in the DEM. Another disadvantage is the price of the licence that is needed after the 30-day trial period. Licences come at different prices but DEM exportation requires the professional version. As an educational institution this is available at $ 550 but a regular licence costs $ 3500. The licence is however unlimited and Agisoft offers an official platform for resellers.

Post Processing
For post processing of the DEM that is retracted from Agisoft Photoscan, Python [23] scripting language was used in combination with the Anaconda Spyder environment [14].

3.2. Methods

3.2.1. Ground Surveying

After reconnaissance of the measurement site and settling on the best suitable part of the river reach, the first step involves ground surveying of the GCPs. Section 3.1.4 elaborates on the need for GCPs and Section 3.1.2 on the type of markers used in this study. Section 3.1.3 provides more information on the type of equipment used for ground surveying.

To maximize added value for the photogrammetry software two principles have to be adhered to when placing the markers :

1. Spread the markers out over the measurement area as much as possible.
2. Make sure the markers cover the natural variety in elevation (put the markers at different heights in the terrain).

Activities for ground surveying obviously depend on the equipment that is used and the manpower that is available. Due to the occurrence of several beginner's errors during the first phase of fieldwork, here an example of the ground surveying work-flow is provided as has been implemented during the second phase of fieldwork (consult Sections 3.1.3 and 4.3 for more information). Several data-sheets have been created to organize data collection (Appendix A).

1. Placement of markers for GCPs. In doing so, use two markers to form a line (more or less) perpendicular to the flow direction (this can function as X-axis of the DEM during later editing). Make sure the markers are anchored to the ground.
2. Start filling in the site-form to capture local conditions and site information (Figure A.1).
3. Make a sketch of the measuring site showing the position of the GCPs in the area (Figure A.2).
4. Collect elevation data of the markers by means of the dumpy level and measure inter-marker distances with a measuring tape. Measure distances in such a way that triangulation can be applied to set up a local grid system that includes all GCPs. Use the sketch and the data-form (Figure A.3) to write down all information.

   Keep in mind that when using a degree circle for location computations, that when the level needs to be relocated during measurements, one needs to measure at least two of the same markers as measured from other level-locations in order to use the measured angles to link marker locations. One overlapping measurement will suffice when the level is only used for elevation measurements (no degree circle).
5. Verify if the average of the upper and lower elevation marks equals the middle elevation reading. An error up till $5\ mm$ was deemed acceptable in this step. Redo the reading in case of a higher error.

It should be noted that using a dumpy level and a measuring tape to capture the necessary data on GCP location and elevation is a very time consuming activity and requires a lot of focus. Personal experience taught that measuring 14 points across a river reach of about $250 \times 250\ m$, can take five to six hours with two to three people, depending on local conditions. Usage of more advanced equipment is expected to significantly reduce efforts and errors.

It should also be mentioned that distances can be measured with a basic levelling device as well, however, as the level-readings will have a precision of about $1\ mm$ at most, the derived distances ((upper reading - lower reading) x 100) will have a precision of $1\ dm$ in best case scenario, but this is likely to decrease with increasing distance.

In some cases a GPS device was used to provide additional data on the GCP locations. As accuracy of the GPS-coordinates relies on satellite signal and accuracy is generally less than manual measurements, the GPS-coordinates were mainly intended as a backup. In addition, they were only used for location determination as the inaccuracy of the altitude measurements was too high (more information in the following sub-section).

Measurement Errors of Ground Surveying

Measurements always go hand in hand with measurement errors. Random errors (i.e. experimental errors) of dumpy level measurements were minimized by:

- Double checking all level readings.
- Verify if the average of upper- and lower level reading differ from the middle level reading by a maximum of $5\ mm$.

  The $5\ mm$ was chosen by the author to be a reasonable error-margin. The levelling-rod has a marker every cm, but measurements were done in mm by means of visual estimation. When measurements are performed with care one should be able to make a reading with $0.5\ cm$ accuracy.
- Using the average of all three[1] readings for elevation calculations.

Another intended way to reduce random errors was to have two people do the same reading. This was however not possible due to a lack in available manpower. Measuring-tape measurements were minimized by:

- Letting one person do the reading and let another person read it back before writing it down.
- Always have the tape as tight (i.e. no slack) as possible without over-stretching it.

Errors in distance measurements by measuring-tape are induced by (1) not having a straight line-of-sight between two marker-points (e.g. rocks or bushes in between) and (2) by faulty allignments when having to measure in twofold for distances over $50\ m$ (i.e. the maximum length of the tape). The latter induces a sideways error when the two lines are not in perfect extension of each other, also see Figure 3.3. Because no detailed information on obstructions and sideways-displacement was collected for individual tape measurements, one overall error-estimate has been made and applied to all distance measurements. In doing so, a separation is made between obstacle-induced errors and skewed alignment-induced errors. They will be referred to as obstacle- and alignment errors respectively. The example showed in Figure 3.3 can be regarded as the maximum possible error as obstacle-heights did not exceed $2.0\ m$. The same is assumed for miss-alignments. In the corresponding Table 3.1 it can be seen that in a situation like this, on average the obstacle error is of order magnitude $0.18\ m$ and the alignment error of order magnitude $0.13\ m$. Combining both errors (obstacles and alignment) for the twofold measurements results in an error estimate of $0.22\ m$ ($\sqrt{0.18^2 + 0.13^2}$). A safety margin to account for the possible slack/stretching of the tape is applied which results in an error-estimation of $\varepsilon_T = 0.25\ m$ for twofold distance measurements above $50\ m$.

With regards to errors of the GPS measurements, a separation between the two phases of fieldwork should be made due to two different GPS devises being used. A hand-held GPS device was used during the first phase, whereas a smartphone was used during the second phase due to unavailability

[1] A level measurement requires three readings from an upper, middle and lower bar. The middle bar indicates the level elevation reading. The upper and lower bars can be used to estimate distance and double-check the middle bar reading

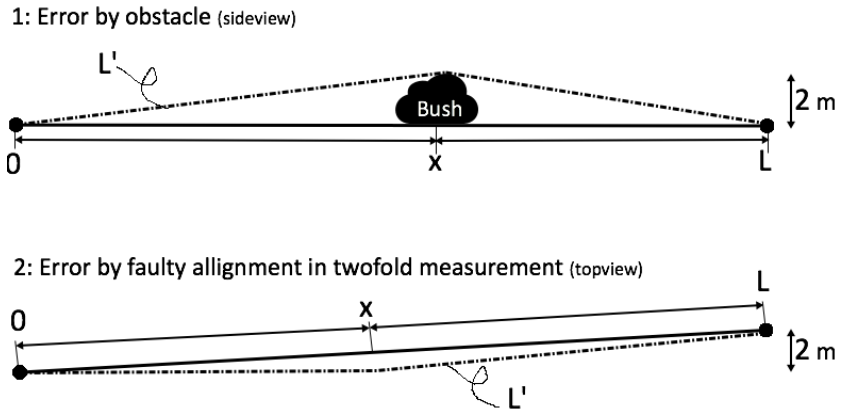

Figure 3.3: Example of a measurement error of measuring distance with a measuring-tape. L = real distance and L' = measured distance

L = 50 m			L = 100 m		
x	L'	ε	x	L'	ε
5	50.241	0.241	10	100.220	0.220
10	50.223	0.223	20	100.125	0.125
20	50.133	0.133	35	100.088	0.088
25	50.120	0.120	50	100.080	0.080
Mean		0.182			0.128

Table 3.1: Errors (ε) in measured length (L') for different distances of the obstacle (x). The left and right side of the table refer to (1) and (2) in Figure 3.3 respectively.

of alternative GPS equipment. The hand-held GPS displayed the error of the given coordinates in both horizontal and vertical direction. In general these varied between 0.5 and $2.0\ m$ for errors in the horizontal plane and between 1.5 and $4.0\ m$ (with outliers up to $11.0\ m$) in the vertical plane. The GPS on the smartphone only showed one measurement of coordinate accuracy which was $5.0\ m$ at minimum. Coordinates were only recorded when the smartphone's GPS had reached this maximum accuracy.

Looking at the accuracy of the GCP coordinates, more accurate results were deemed to be achieved with manual location calculations based on the distances between the GCPs measured by measuring-tape. The estimated magnitude of the errors in distance and elevation measurements are of importance for establishing the accuracy of the computed GCP-coordinates in the local grid-system. This will be further elaborated upon in Section 3.2.4.

3.2.2. Aerial Surveying

Success of aerial photo collection is highly dependent on preparation of the UAV's flight plan. Aspects that have to be taken into account during flight planning include:

1. Flight speed, distance and battery life.
2. Flight altitude.
3. Ground Sampling Distance (Figure 3.4).
4. Camera settings such as Shutter Speed, ISO and aperture.
5. Camera tilt and photo interval.

Collecting a good data set comes down to making sure the images are (1) not blurry, (2) have a proper amount of lighting and (3) have sufficient overlap. Blurriness mostly depends on the flight speed relative to the Ground Sampling Distance (GSD) and on shutter speed. Proper lighting is influenced by shutter speed, ISO and aperture. Flight altitude relates to GSD and together with speed influences the photo interval. Speed and battery life determine the distance that can be flown.

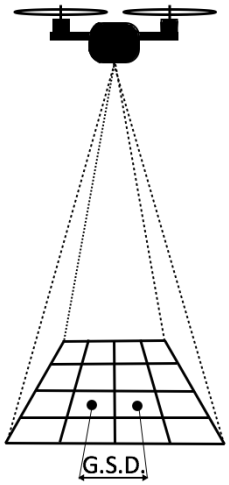

Figure 3.4: Ground Sampling Distance. Depends on altitude, sensor width, focal length, and image resolution.

Sufficient overlap of the photo's is required to optimize the photogrammetry software's ability to match pixels and compute the Dense Point Cloud (DPC) as accurate as possible. In this case Agisoft Photoscan recommends to assure an image overlap of 80% in the forward direction and a sideways overlap of 60%. This means that one needs to first determine the flight altitude in order to determine the maximum distance between parallel flight lanes (see Figure 3.5).

Determining at which altitude to fly mainly depends on the size of the measurement site. Flying higher means being able to capture a bigger ground area per image but will also increase the GSD (i.e. decrease detail of the image). More detailed images (i.e. lower GSD) improve pixel matching. Avoiding blurry images is also important in deciding for a flight altitude and corresponding GSD. A general rule of thumb to avoid blurriness is to keep the GSD at least 3 times bigger than the distance the drone has moved during the taking of a photo [15]. This will therefore depend on flight speed and shutter speed. The difficulty here is that selecting a suitable shutter speed depends on local light conditions which is hard to predict.

An example of making a flight-plan, as done in this study, is included in Appendix C.

3.2.3. Wet-data Collection

For the new river rating method that is proposed, the ideal situation is one where there is a relatively low but still substantial amount of water flowing through the river channel. This because this allows for both measurements of the water slope as well as flow measurements which can be used in order to calibrate the roughness n. When slope measurements are not possible, a flow measurement can be used to calibrate the a_1 parameter in Equation 2.5. In addition to measuring discharge, the geometry of the inundated area is also required to complete the DEM

However, during this study the data collection took place in the end of the Mozambican dry season, resulting in all but one of the measured river to be without flowing water. The only river with a substantial flow was Aruãngua (Luangwa). Unfortunately no discharge measurements could take place here (more on this in Chapter 4).

For above reason no further deliberation of wet-data collection will be provided in this report.

3.2.4. Data Processing

The aim of processing the data is to combine results of both aerial- and ground- surveying practices into the acquired data for DEM computation in the photogrammetry software. This comes down to two things:

1. A set of photographs covering the area of interest.
2. Detailed information on both location and elevation of all GCPs within the area of interest.

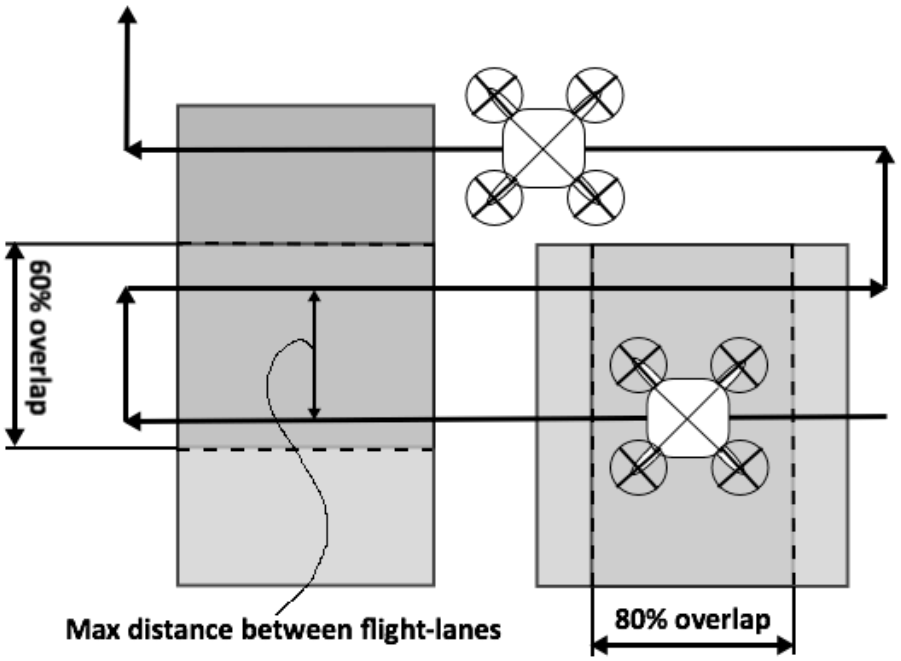

Figure 3.5: Schematization of needed overlap from aerial photo's.

Regarding to point 1, processing activities consist of identifying and deleting photos that are unusable (e.g. by blurriness or other distortions) or cover areas that are outside of the area of interest. The latter is to reduce computational time and to save (working) memory. For the optimization of image collection please refer to Section 3.2.2.

With regards to point 2, the amount of work and the degree of difficulty are highly dependent of the type of equipment used for ground surveying. For example, acquirement of a GCP-location by using a DGPS, only requires one to retract the (geo-referenced) coordinates and altitudes from the device's memory card. Whereas having used a dumpy level (without degree circle) and a measuring tape requires the researcher to set up a local grid system and calculate all GCP location- and elevation data manually. The latter is obviously much more time-consuming but can still provide very good results (even better than an ordinary GPS).

According to the experiences obtained in this particular study, the rest of this section describes how data collected with a dumpy level and measuring tape is processed to input for photogrammetry software. This makes use of a spreadsheet of which an example can be seen in Appendix A: Figure A.3.

1. Type over all readings into the spreadsheet (Figure A.3) and verify again if the check for a maximum error of $5\ mm$ says is uphold (see Section 3.2.1). If not, that means there either is a typo in the data or the in-field check has not been performed properly.
2. The average elevation used for further use is calculated by taking the average of all three readings (i.e. upper, middle and lower mark)
3. Measured elevations from the different level-locations are linked relative to one and the same point. The lowest GCP is used as vertical datum ($Z = 0$).
4. The inter-GCP distances are corrected for elevation differences between the points.
5. By means of the sine- and cosine-rule, the corrected inter-GCP distances are used to determine the angles of the assumed triangles (Figure 3.6).
6. Determine the locations of all GCPs relative to one and the same point. When two points have been used to form a line normal to the flow direction, this line is used to form the X-axis with the most left point having the coordinates $(X, Y) = (0, 0)$ (e.g. GCPs 12 and 13 in Figure 3.6b).

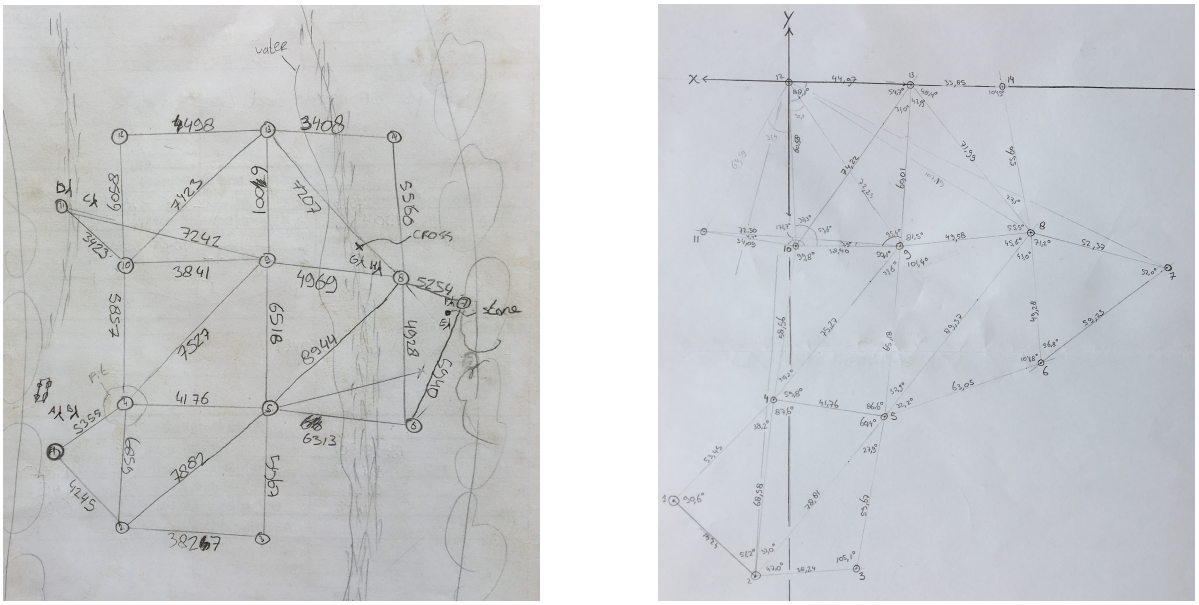

(a) Made on measuring site (b) Same sketch after processing

Figure 3.6: Data processing into local grid system for Rio Luia. (b) shows an improved sketch of the same measuring site as correct angles are implemented and distances have been scaled properly.

7. Calculated GCP elevations and locations are combined to finalize local grid coordinates.

Note that when the above enumerated procedure is followed, points 3 and 6 mean that the reference points for the XY-coordinates and the Z-coordinates do not necessarily have to be the same points. E.g. in this example case of Rio Luia, the reference point in the horizontal plane was set to GCP-12, and that of the vertical plane to GCP-3. This has been a choice of the researcher based on practical reasons for the manual calculations, but can of course be altered to let the reference points for both planes coincide. In that case it is advisable to first determine the reference point in the horizontal plane (as this is more difficult to calculate) and then adapt the reference point for the vertical plane accordingly. This discrepancy does not influence DEM accuracy.

Local Grid

Information on both location and elevation of the ground control points needs to be supplied to the programme, as well as their individual accuracies (Table 3.2). To improve computational speed and post-processing possibilities it is preferable to use georeferenced information. However, when this can not be obtained with sufficient accuracy, a local grid system can be used based on simple XYZ-coordinates. This is the option that is used in this study. The local grid is set up with the information gathered during ground surveying (Section 3.2.1). During ground measurements, all GCPs are connected by a system of triangles, thereby allowing for their relative location to be calculated. When measurement of angles was not possible, only distances were used to create the system of triangles and angles had to be calculated afterwards. For each triangle, the cosine-rule (Equation 3.1) is used to determine one of the angles, followed by the sine-rule (Equation 3.2) to calculate the remaining angles. In the example-triangle of Figure 3.7, the X- and Y- location of GCP B relative to the location of GCP C can then easily be determined by means of $a \cdot \cos\gamma$ and $a \cdot \sin\gamma$ respectively.

Name	X	Y	Z	$X_{Accuracy}$	$Y_{Accuracy}$	$Z_{Accuracy}$
GCP1	X1	Y1	Z1	Accuracy X1	Accuracy Y1	Accuracy Z1
...	...	...	...	...	...	...
GCPn	Xn	Yn	Zn	Accuracy Xn	Accuracy Yn	Accuracy Zn

Table 3.2: Example of output from ground-survey data processing.

The error in the determined local GCP coordinates are influenced by the measurement errors of inter-marker distances. As can be read in Section 3.2.1, distance measurements by measuring-tape have an estimated maximum error of $0.25\ m$. This error obviously propagates into an error for the calculated location through both of the above-mentioned calculation steps (angle and location). Ideally, the magnitude of this error is determined for each GCP-location individually. However, due to a lack of required information, and a lack of time to acquire that information, one general error value for GCP-location is determined.

Going back to taking Figure 3.7 as an example, with C to be the reference point (0,0), the error in the location of point B (ε_B) depends on the error of a (ε_a) and the error of γ which in its turn depends on the error of a, b and c. To come to a representable error estimate, a set of 10000 ε_B-calculations are performed with lengths of a, b and c varying between 30 and $175\ m$. These values more or less form the range of values encountered during local grid computation. The sample mean is used as a overall estimate for GCP location error (ε_{XY}) and is calculated to be $0.60\ m$.

A similar reasoning is used to determine the general error for GCP elevation calculations. Section 3.2.1 explains the estimated measurement error of the elevation measurements to be $5\ mm$. As calculation of the Z-coordinates only require one simple calculation-step to determine one GCP's elevation relative to that of another, the general error of the Z-coordinates (ε_Z) is set to $10\ mm$. These values of 0.6 and $0.01\ m$ are used as overall accuracy estimates for XY and Z respectively and have been applied to all GCPs.

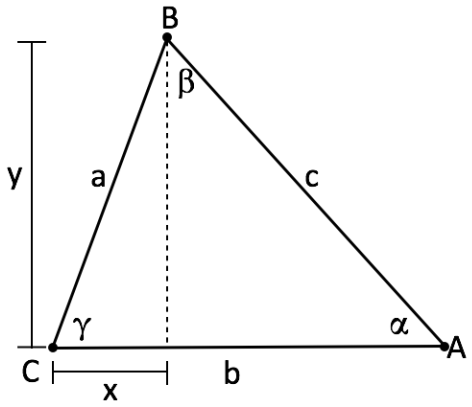

Figure 3.7: Example of triangle between GCPs A, B and C. (Reference for Equations 3.1 and 3.2)

$$c^2 = a^2 + b^2 - 2ab\cos\gamma \ \rightarrow\ \gamma = \cos^{-1}\left(\frac{c^2 - a^2 - b^2}{-2ab}\right) \tag{3.1}$$

$$\frac{a}{\sin\alpha} = \frac{b}{\sin\beta} = \frac{c}{\sin\gamma} \tag{3.2}$$

3.2.5. DEM Computation

Computation of the 3D model is done by means of the photogrammetry software Agisoft Photoscan (also see Sections 2.1 and 3.1.4).

In the process, the software follows three main steps. The first step is camera alignment where it searches for stable features on the photographs and uses these to create scene geometry as well as a map of the camera-positions relative to each other. Camera positions recorded by the drone help to speed up this process. The result is called a Sparse Point Cloud (SPC), which is a 3D reconstruction of the matches features. This reconstruction is still in an arbitrary coordinate system however.

Now the SPC can be scaled by matching the internal coordinate system of the SPC to real-life (geographic) coordinates. The real-life XYZ-coordinates can either be based on a georeferenced grid system (such as WGS84 or UTM) or a locally established grid. This is done by supplying the model with a set of GCPs with known location and elevation.

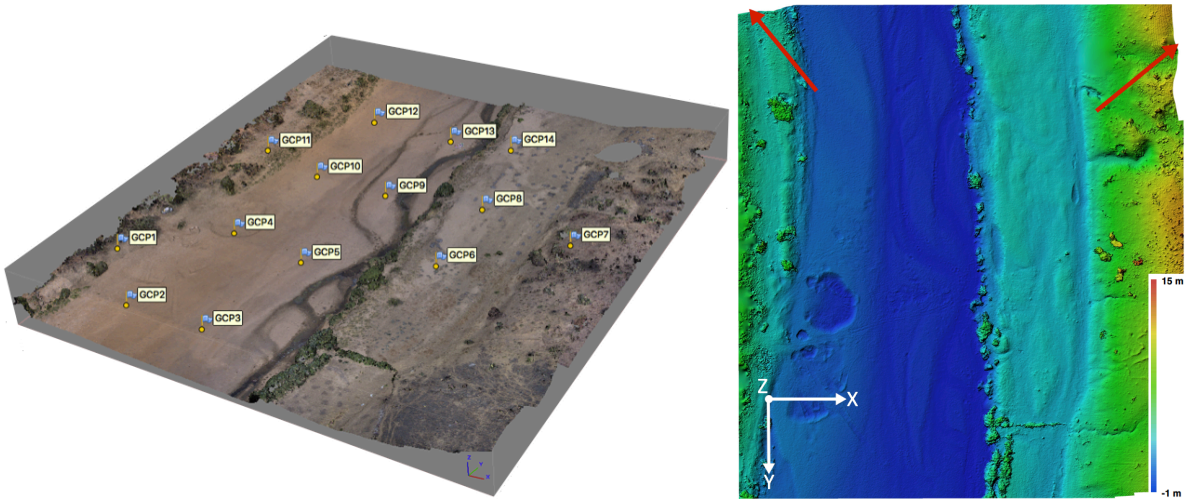

(a) Dense Point Cloud with Ground Control Points (b) Coloured representation of DEM

Figure 3.8: Photogrammetry results from Agisoft Photoscan of Rio Luia. The red arrows show flaws in the exported DEM.

The next step the program undergoes results in the creation of a so-called DPC (Figure 3.8a). The DPC is created by systematically searching over pixel-grids to find best matches between images which leads to significantly more data points than the SPC. The DPC already contains all depth information required for the DEM and is scaled by means of GCPs. See Section 3.2.4 for more information on computation of sofware input with regards to the GCPs. The DPC can be edited manually to e.g. remove noise-inducing objects such as people or vegetation.

The last step in the process is converting the DPC into a DEM or an orthomosiac. The DEM is a rasterized representation of the DPC data and the wanted pixel-size can be specified by the modeller. During DEM creation, data-gaps from the DPC are filled by means of interpolation. Now the DEM can be exported and used for further analysis and calculations. For the DEM a pixel resolution of $10 \times 10\ cm$ is used. In addition to DEM computation, an orthomosiac can be produced to create a geometrically correct image of the entire measuring site (Figure 5.1a).

The DEM is exported as a raster file (TIFF format). Because the model of the river reach often does not neatly correspond to the rectangular size of the raster file, or because the edges had too little image overlap, some unwanted information can be stored at the edges in the form of zero or (-)inf values (see Figure 3.8b). The latter can be stored as NaN-values during exportation. To simplify further usage of the DEM, rows and columns that contain these unwanted information are removed first.

3.2.6. Rating Curve Computation

When the 3D geometry model (i.e. the DEM) has been successfully computed, the actual process of determining the Q-h relation can start. Python is used for DEM editing and analysis. Manning's formula rewritten to a power function (Equation 2.4) for the physically-based rating curve is stated again in Equation 3.3.

$$Q = \underbrace{\frac{1}{n}\sqrt{i}}_{a_1} \quad \underbrace{AR^{\frac{2}{3}}}_{a_2(h-h_0)^b} \tag{3.3}$$

In conventional rating curve computation, parameters are generally determined by taking the logarithmic values of the discharge (Q) and the effective stage $(h - h_0)$ variables and use linear regression to determine a straight line relationship between the two. Equation 3.4 shows the log-transformed version of Equation 2.2. It is clear that the relation resulting from the linear regression will present the parameter values of a and b as being the line's intercept and the slope respectively. In this process, the value for h_0 (stage at zero flow) can be determined in an iterative manner by aiming for the best fit from the linear regression procedure.

$$log(Q) = log(a) + b \cdot log(h - h_0) \tag{3.4}$$

The method proposed here takes a small detour from this straight forward route as the rating curve is not (solely) based on Q-h measurements, but on geometry measurements. After preparation of the DEM two main steps can be distinguished which include:

- Calculation of geometry parameters a_2, b, and h_0
- Calculation of parameter a_1

These steps will be elaborated upon in the following subsections.

When geometry of the cross-section undergoes a significant change, usually a widening of the section induced by floodplains, the relation between discharge and water level usually consists of two parts. This is called a compound rating curve. The compound rating curve therefore consists of a combined set of two equations, one corresponding to the main channel of the river and one corresponding to situation where floodplains are included. As slope and roughness are assumed to be constants, computation of the compound equations only translates to additional calculation of the a_2, b and h_0 parameters.

Calculating the a_2, b and h_0 Parameters

Referring to Equations 2.4 and 2.5, the first step in computing the Q-h relation is determining the a_2 $[m^{3-b}]$ and b $[-]$ parameter values. For further reference, $AR^{\frac{2}{3}} = a_2(h - h_0)^b$ will be referred to as the conveyance (C). This is not to be mistaken with the also commonly referred to conveyance term: $\frac{1}{n}AR^{\frac{2}{3}}$ that also includes roughness. As the equation reveals, C depends on water depth and is therefore a function of water level h. a_2, b and h_0 are constant for a certain river section but can change when the geometry of the section changes.

Calculation of the a_2 and b parameters is done by calculating the relation between C and effective stage $(h - h_0)$ and then fitting a power-law function (Equation 2.2) through this curve by means of non-linear regression. In order to do so, firstly the value for h_0 needs to be established. The measured sections are assumed to mainly be under channel control conditions as no natural or artificial narrowing of the sections (e.g. water-fall, rock-bar, weir) to create a zone of acceleration is known to be present at any of the measured sections. An absence of such a zone of acceleration results in infleunces from downstream distrubances being able to propogated upstream, meaning the rating curve depends upon the geometry and the roughness of the river downstream of the control section [10]. This assumption could however be unrealistic for the case when debries get's stuck between bridge pillars and is thereby blocking water to flow through, creating an artificial narrowing of the section. For a channel controlled gauging section, the level of the deepest point is deemed to give a good indication of h_0 [10] which is used as a best estimate in this study. Influence of h_0 on model performance is analysed (Section 3.2.8).

Computation of the relation between C and $(h - h_0)$ can be approached in two different manners. Say the DEM has dimensions $n \times m$ (rows x columns), then a river reach with a longitudinal length L $[m]$ and a width B $[m]$ contains $n = L \times 10$ and $m = W \times 10$ rows and columns respectively as the DEM has a pixel resolution of 10×10 cm. Here L corresponds with the Y-axis of the DEM and W corresponds with the X-axis (see Figure 3.8b). As the measured river reach can have a length of around 250 m, this means that up to 2500 individual cross-sections can be drawn from the file.

With the first approach, these cross-sections are reduced to a single cross-section by averaging all elevation (z) values in the DEM's columns. This reach-average cross-section is then used to determine the hydraulic parameters needed (A, P and R) to compute the conveyance for a certain water level (see Equations 3.5 to 3.8 and Figure 3.9). Parameters a_2 and b can be determined thereafter. Note that the effect of h_0 is not incorporated into the equation. This is because as soon as the water level has exceeded h_0, the entire section will participate.

For the second approach, all n rows are used individually to compute the C-h relation and identify the values of a_2 and b per cross-section. In this case h_0 is set to the minimum elevation value of the individual cross-section as well. All n values for a_2, b and h_0 are stored and are then averaged to compute the reach-average values.

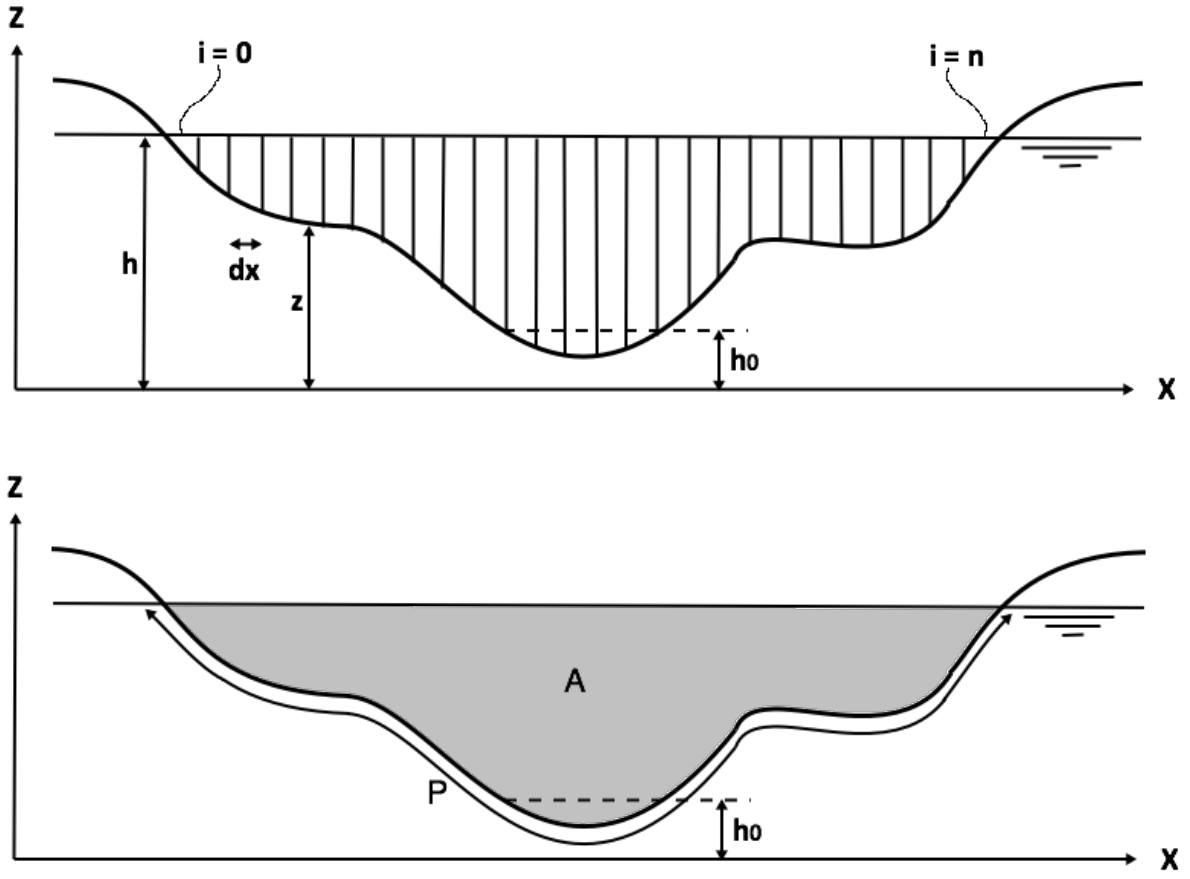

Figure 3.9: Hydraulic parameters of a cross-section. Also see Equations 3.5 to 3.8.

$$A = \sum_{i=0}^{n} dA \quad \text{with} \quad dA = \frac{(h - z_i) + (h - z_{i+1})}{2} dx \tag{3.5}$$

$$P = \sum_{i=0}^{n} dP \quad \text{with} \quad dP = \sqrt{((h - z_i)(h - z_{i+1}))^2 + dx^2} \tag{3.6}$$

$$R = \frac{A}{P} \tag{3.7}$$

$$C = AR^{2/3} \tag{3.8}$$

Due to the fact that irregularities caused by vegetation exist within the DEM, a different approach of parameter calculation needs to be applied when using all cross-section, as opposed to using one average cross-section. When using one average cross-section, these irregularities have been averaged out, leaving the modeller with a clean cross-section for further analysis. This makes it possible to split the section up in a main channel with a threshold elevation value, and a floodplain that only starts participating after that threshold is reached. When using each individual cross-section, the irregularities can cause a cross-section to be split up in multiple segments (referred to as chunks) and do not allow for a clear threshold procedure to be applied. For a certain water level, intersection points with the cross-section (z-values) are found. Using these intersection-points, the cross-section is divided into two or more chunks. For each chunk within the cross-section, A, P, R and C are calculated and

these are summed up to determine the C for the entire individual cross-section. This latter approach is significantly more time consuming and sensitive to errors than the prior one.

For that reason, further analysis performed in this study will be done with the method based on one reach-average cross-section where non-uniformities in computed geometry have been averaged out. This also allows for a compound rating curve to be formed, separating the Q-h equation in two parts. One for the main channel of the river and one for the floodplains. In order to do so, inspection of the reach-average cross-section is done first to determine the threshold water level at which the flood plains will start to participate. Once this level is known, two different power-functions are fitted, resulting in two different a_2- and b values. For the upper segment (i.e. floodplain), h_0 does not have a physically ascertainable value but equals the level at which the floodplains start to participate. The floodplain segment of the compound equation contains a constant that equals the maximum value of the main channel segment, i.e. at the threshold water level. So when subscripts $_M$, $_F$ and $_T$ represent 'main channel', 'floodplain' and 'threshold' respectively, the compound equation looks like:

$$AR^{\frac{2}{3}} = \begin{cases} a_{2,M}(h-h_0)^{b_M} & \text{if } h < h_T \\ \underbrace{a_{2,M}(h_T-h_0)^{b_M}}_{\text{constant}} + a_{2,F}(h-h_T)^{b_F} & \text{if } h \geq h_T \end{cases} \tag{3.9}$$

Calculating the a_1 Parameter

As can be seen in Equation 2.4, the a_1 parameter depends on the slope i and Manning's roughness coefficient n. Roughness is notoriously difficult to quantify as it depends on various factors and is usually not uniform over the cross-section. It goes without saying that this makes the roughness impossible to quantify directly by field measurements. Therefore, it is recommended to calibrate this value. Even though slope is in theory much easier to quantify than roughness, in-field slope measurements can also prove to be difficult mainly due to one or both of the following two reasons:

1. There is no/insufficient flowing water to measure the slope of the water surface.
2. To average out measurement errors it is recommended to measure elevation difference over a longitudinal difference of at least $1000\ m$. This can be difficult/impossible due to:
    - Local conditions at the measuring site such as a lack of infrastructure, dense vegetation, wildlife, climate, etc.
    - State and availability of needed equipment, resources and manpower.

When the data was collected in Mozambique at the end of the dry season, both points proved to be applicable.

Ideally one would be able to perform accurate slope-measurements in the field and then use a discharge measurement to calibrate n. When (accurate) slope measurements are not possible, a discharge measurement can also be used to calibrate the a_1 parameter in its entirety. This is because when the C-h relation is known, this can be transformed with a linear line to compute discharge as transforming with a linear line is equivalent to multiplying with a constant (a_1 in this case) in a formula (see Figure 3.10). When in the absence of flowing water and therefore slope and discharge measurements, a_1 requires to be quantified differently.

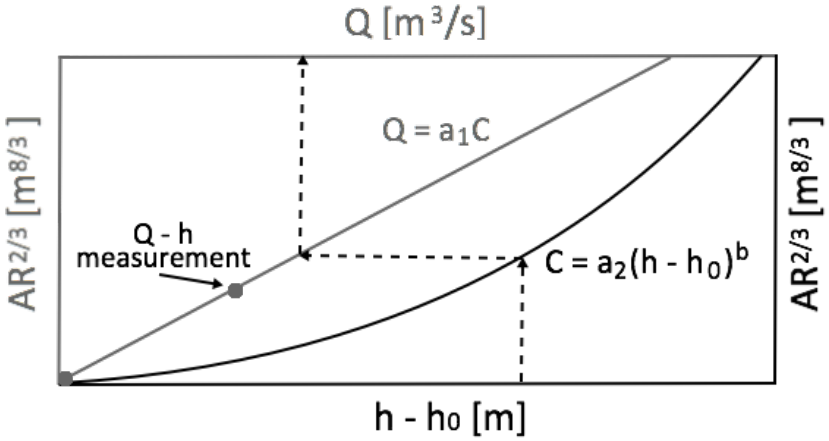

Figure 3.10: When the C-h relation is known, one Q measurements allows for calibration of a_1

As mentioned in Chapter 2, using Manning's formula implies the assumption of uniform flow, which implies the slope of the water surface being equal to that of the riverbed. During this study the only way to determine i was by means of measuring the slope of the riverbed. An accurate slope measurement however requires the elevation difference between two points at least $1\ km$ apart (especially in relatively flat areas). This is because otherwise the possible measurement errors will out way accuracy of the calculated elevation difference. Difficulties induced by a harsh terrain, climate and limited manpower did not allow for accurate slope measurements to take place. Slope calculation based on the DEM seems like a straight forward solution, but this is problematic for the reason that a river's flow-paths usually don't follow a straight line. Meaning one can not simply subtract downstream elevation from upstream elevation as it is unknown which values correspond to the same flow-path. Therefore, an alternative method has been thought of.

The approach taken in this study is to make use of the detailed river geometry data that is obtained from the aerial imagery. This approach uses the relation between the conveyance and the effective stage. See Figure 3.11, when the slope of the water surface is equal to that of the the river bed ($HGL_{i>0}$), C will remain constant in the longitudinal direction of the river reach (for a constant Q, n and i). If there would be no slope of the water surface in downstream direction ($HGL_{i=0}$), C would increase in downstream direction as d would also increase. Note that in that case uniform flow does not apply any more.

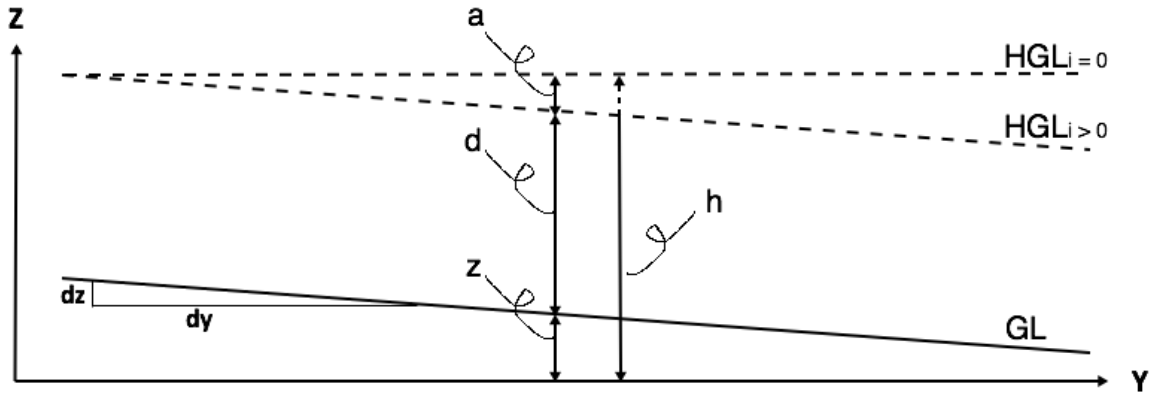

Figure 3.11: Slope calculations. GL = Ground Level, HGL = Hydraulic Grade Line, i = dz/dy = slope.

Two different approaches have been applied in the attempt to use the aforementioned relation to determine slope. The first approach is an analytical one by deriving an equation to use the slope of the conveyance ($\frac{dC}{dy}$) to approximate the theoretical slope of the water surface. The second way is

somewhat simpler and more straight forward. Firstly, the derivation and corresponding assumptions are represented: (also see Figure 3.11):

$a\ [m]$ is the additional depth as a result from the absence of a sloping water surface
$B >> d \ \rightarrow \ A \approx B \cdot d$ and $R \approx d$, where:
$B\ [m]$ is width
$d\ [m]$ is depth
$A\ [m^2]$ is cross-sectional area
$R\ [m]$ is hydraulic radius
$i << 1 \ \rightarrow \ a << d \ \rightarrow \ a + d \approx d$
$i = S_{GL}$ (uniform flow for $i \neq 0$), where:
$i\ [{}^{m}/_{m}]$ is slope of the water surface
$S_{GL}\ [{}^{m}/_{m}]$ is slope of the ground level

$$C = AR^{\frac{2}{3}} = BR^{\frac{5}{3}} \approx \ B(a+d)^{\frac{5}{3}} \tag{3.10}$$

$$\left.\begin{aligned} \frac{\mathrm{d}C}{\mathrm{d}(a+d)} &\approx \frac{5}{3}(a+d)^{\frac{2}{3}}B \\ B &\approx \frac{C}{(a+d)^{\frac{5}{3}}} \end{aligned}\right\} \qquad \frac{\mathrm{d}C}{\mathrm{d}(a+d)} \approx \frac{5C(a+d)^{\frac{2}{3}}}{3(a+d)^{\frac{5}{3}}} \approx \frac{5}{3}\frac{C}{(a+d)} \approx \frac{5}{3}\frac{C}{R} \tag{3.11}$$

$$\left.\begin{aligned} i = \frac{\mathrm{d}z}{\mathrm{d}y} = \frac{\mathrm{d}a}{\mathrm{d}y} &= \frac{\mathrm{d}(a+d)}{\mathrm{d}y} \\ \frac{\mathrm{d}C}{\mathrm{d}y} &= \frac{\mathrm{d}C}{\mathrm{d}(a+d)}\frac{\mathrm{d}(a+d)}{\mathrm{d}y} \end{aligned}\right\} \frac{\mathrm{d}C}{\mathrm{d}y} = \frac{\mathrm{d}C}{\mathrm{d}(a+d)}i \tag{3.12}$$

From Equations 3.11 and 3.12 then follows that:

$$\frac{\mathrm{d}C}{\mathrm{d}y} \ \approx \ \frac{5}{3}\frac{C}{R}i \ \rightarrow \ i \approx \frac{3}{5}\frac{\frac{\mathrm{d}C}{\mathrm{d}y}}{C}R \tag{3.13}$$

As can be seen from Equation 3.13 the slope i can now be approximated by means of $\frac{dC}{dy}$, C and R. The former can be calculated by assuming a constant water level h and plot the variation of C over y.

As mentioned the second approach is a bit more straight forward. Just as for the previous approach, the variation of the conveyance is calculated in downstream direction of the river reach. However, instead of assuming a constant value for the water level, now a slope is enforced on the water surface. Through an iterative manner, a slope can be found that results in a constant value of C over y, i.e. $\frac{dC}{dy} = 0$.

The slope computed with above-mentioned method is compared with a slope that is derived from the ASTGDEM Version 2 [21]. Here, the slope is derived by following the course of the river for a reach starting at $10\ km$ upstream of the measuring site and going down to $10\ km$ downstream of the measuring site, and using QGIS to determine the elevation profile over the course of this section. Linear regression is applied to this data in order to establish the overall slope along the $20\ km$ section.

Computation of the slope only leaves n to be quantified. When calibration is not a possibility, the only option is to use literature to estimate Manning's roughness coefficient. Various methods have been proposed ranging from predefined single values depending on bed-material/compositions to composite values that also include effects of vegetation and stream course [25] [7] [6].

3.2.7. Performance of the Rating Curve

Performance of the (compound) rating curve is evaluated by comparing the computed relation with historical data. Only two of the visited measuring-sites have historical Q-h data, being Rio Aruãngua (Luangwa) and Rio Luia. As the measurements at Rio Aruãngua were not sufficient for rating curve computation (see Chapter 4), only Rio Luia allows for comparison of the rating curve. Flow- and stage data from Rio Luia has been received from ARA-Zambeze, together with the rating curve equation they themselves have calculated and applied.

Comparing the computed rating curve with that of ARA-Zambeze comes with two challenges. The first of which is caused by the fact that the elevation scales do not match. This is because a stand-alone grid system has been applied based on elevation- and location measurements in the field and insufficient data was collected to link this to the elevation-scale used by ARA-Zambeze. The second challenge results from the fact that the used control-sections are likely to deviate. As mentioned, the control-section used in this study is a reach-average cross-section derived from a reach of about $250\ m$ in length. Exact information on the shape of the control-section used by ARA-Zambeze is not available.

Performance of the computed (compound) rating curve is done in a qualitatively manner by means of visual analysis and expert knowledge. In doing so, a separation is made between the low- and high-flow regimes (i.e. main channel and floodplains).

3.2.8. Parameter Sensitivity

Uncertainty of parameter-values is obviously of direct influence on rating curve performance. In order to quantify this influence of the individual parameters a sensitivity analyses is performed. The mathematical relation describing the rule of error propagation [17] is used to determine the total error of the wanted parameter Q and to investigate which of the parameter is most critical to this total error. If a certain value q is a function of two parameters $q(x, y)$, and x and y are measured, then the standard error of q becomes:

$$\sigma_q^2 = \left(\frac{\partial q}{\partial x}\right)^2 \sigma_x^2 + \left(\frac{\partial q}{\partial y}\right)^2 \sigma_y^2 + 2\frac{\partial q}{\partial x}\frac{\partial q}{\partial y}\sigma_{xy}^2 \tag{3.14}$$

If the parameters x and y are independent, then the covariance will approach zero and the equation reduces to:

$$\sigma_q^2 = \left(\frac{\partial q}{\partial x}\right)^2 \sigma_x^2 + \left(\frac{\partial q}{\partial y}\right)^2 \sigma_y^2 \tag{3.15}$$

In addition, an equal percent change in parameter values is applied to establish how this translates a change in the (compound) rating curve.

4

Fieldwork

4.1. Fieldwork Motivation and Objectives

As discussed in Chapter 1, it is of importance to the researchers that the developed method provides an accessible way of performing river rating in those areas where local water authorities are limited to do so by either financial-, logistical- or political factors. This is because those areas are more likely to be poorly gauged and could therefore benefit most from such advancements. With this in mind, combined with the extensive network the Water Management department of TUD has with both private and public companies in the Zambezi river basin, it only seemed logical to field-test the application of proposed method in this area. Therefore it was decided to travel to the Tete province in north-western Mozambique to conduct a cooperative fieldwork session with local involvement. For a total duration of two months, the writer stayed in the town of Songo to work on this research. The objectives during these two months were as followed:

1. Collect data to test proposed method and hypotheses (Section 1.2).
2. Test and advice on applicability of proposed method in the Zambezi river basin.
3. Provide introductory training on proposed method to HCB.

4.2. Collaborations and Educational Framework

With regards to point 3 in the enumeration above, and to receive the necessary support to successfully perform field measurements, an MoU was set up between TU Delft and HCB. Additionally, support and involvement from ARA-Zambeze was informally discussed and received. HCB provided both professional and logistical support to the writer during his stay in Mozambique and in exchange the writer provided some initial training in order to familiarize local H.C.B. staff (two juniors in the company's hydrology department) with the proceedings of proposed method for improved river rating. In order to do so, a set of learning goals have been determined.

- Basic theoretical framework of the proposed new method.
- Drone characteristics and control.
- Data requirements and collection for DEM computation.
- Initial data processing for DEM computation.

The first three goals have been achieved by intensive cooperation during the fieldwork and the preparation phases. The last has proved to be more difficult due to the fact that (1) the researcher was also still in a learning process and (2) quality data had not been collected till the very last moment of the two months in Mozambique.

Tributaries phase 1	Tributariers phase 2
R. Duângua (R. Luangua)	R. Cherisse
R. Mucanha	R. Capoche
R. Muze	R. Luia
R. Aruãngua (R. Luangwa)	
R. Tongoé	

Table 4.1: Measuring sites of the two phases of fieldwork (also see Figure 4.1b). Placed in chronological order of measurements.

4.3. Area Description

Songo is situated in the Tete province of north-western Mozambique (Figure 4.1a) and is home to the hydro-power dam of HCB that lies downstream of the homonymous Cahora Bassa reservoir. The reservoir is part of the Zambezi river (Figure 4.1b). Fieldwork was organized and executed from Songo and focussed on the tributaries on the northern banks of the Cahora Bassa reservoir and Zambezi river. Fieldwork was performed in two phases and consisted of five and three days of in field activities respectively. The first phase focussed on a set of tributaries upstream of the Cahora Bassa dam and the second phase on a set of tributaries just downstream of the dam (Figure 4.1 and Table 4.1). The writer has tried to adhere to local names. For the first measured tributary, the name seemed to vary between R. Duângua and R. Luangua depending on who was asked. In this report the name of Duângua will be used henceforth. The border river of R. Aruãngua is internationally also known as the Luangwa river. The prior name is used in this report.

Figure 4.2 shows images made on the each of the measuring sites. In order to offer some perspective the images are arranged in increasing size of channel width. As can be seen in the images by the lack of water, the fieldwork took place at the end of the dry season (late September till early November). Riverbed composition and vegetation very much varied from place to place. For example Duângua and Luia have very sandy riverbeds whereas Capoche's is very rocky.

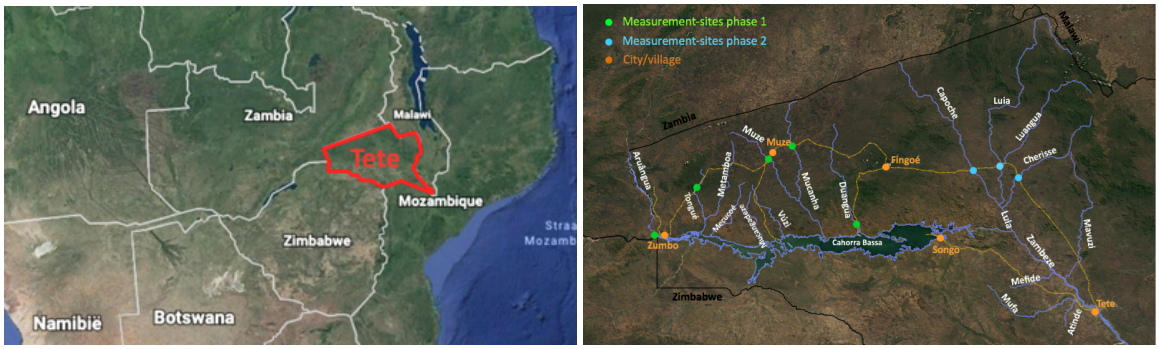

(a) Area of interest zoomed out.(Source: Google Earth)

(b) Schematic of area of interest including relevant tributaries and measurement locations.

Figure 4.1: Area of interest.

4.4. Site Requirements

This section will cover practical information on requirements of the measuring site. For further detailed information on data-collection practices, please refer to Chapter 3.

Success of the data collection is highly dependent on local conditions of the measurement location. Ideally, the river reach to be measured should be between 200 and 300 m in length to guarantee a representable average cross-section. In principle counts: the longer the better, but longer segments usually come with limitation on the practicality of data collection. Location suitability basically relates to two aspects:

1. Ground visibility from the sky. This is influenced by vegetation in and around the channel area, and the presence of water in the river.

2. To what extend uniform flow conditions can reasonably be assumed. This is mostly influenced by back-water effect from downstream conditions.

Relating to point 1, the researcher should make sure the reach does not contain too much (high) vegetation on either the main channel (e.g. Figure 4.2c) or the banks/floodplain (e.g. Figure 4.2a). Vegetation obscures the riverbed from the aerial photos, thereby increasing errors in the DEM. Vegetation can be manually removed from the DPC, creating holes in the 3D model that can then be filled by interpolation. However, too much of this naturally decreases accuracy of the 3D model. Water that is still flowing in the river has a similar influence as it obscures the riverbed from the photos. In this case the researcher needs to measure the bed-profile of the submerged channel area in order to compute an accurate DEM. Ideally this should be done at multiple locations within the reach. In addition, water can pose difficulties for photo alignment as the appearance of the water surface is constantly changing due to waves and reflection of the sun.

Relating to point 2, one should measure as far away from downstream disturbances as possible. Some examples of these disturbances are:

- Confluences with other rivers or lakes.
- Sharp turns or big obstacles such as rock formations.
- Big changes in river geometry or slope.

The presence of water in the river has some pros and cons. The cons are already mentioned and concern both the need for additional measurements (and equipment) as well as complicating DEM computation. The pros are that it can allow for the researcher to conduct a measurement of the water-slope, one of the needed parameters for computing a_1. In addition, it can allow for a flow-measurement which can be used to calibrate the roughness coefficient n (or a_1).

Just to paint a picture, the ideal measurement location would have the following characteristics:

- A straight section of about 300 meters long.
- No (or very little) vegetation on both the main channel and the flood-plains.
- Not (or negligibly) influenced by back-water during high flows.
- A relatively small (i.e. relative to the main channel) stream of flowing water to measure the water slope and flow but still allows for easy cross-sectional measurements.

  Note: A dry river is best for geometry measurements. A flowing river is best for computation of remaining parameters. Dual measurements would benefit each the most.

4.5. Challenges and Lessons Learned

As can be expected when doing fieldwork, a range of challenges were encountered both in general and during both phases of data collection. Relating to testing the applicability of the method, this is also an important part of the learning process. The main challenges are mentioned in a categorised manner below.

Organisational

As in any endeavour, proper planning and organisation will benefit the outcome. When working in a cooperative environment with multiple parties, a big part of this can be linked to communication. A mix of formal (MoU) and informal agreements, combined with some misplaced assumptions are likely to negatively effect a smooth transition of the envisioned proceedings for all parties involved.

Lessons Learned:
First and foremost it is important that clear lines of communication are established. Secondly, explicit agreements should be made that determine the roles and responsibilities (both financial and organisational) of all parties involved. It is important to safeguard enough preparation time as these things are usually very time consuming. Also referring to organisation, the researcher(s) needs to determine whether any additional licences or other official agreements are needed to conduct the required measurements and make sure these can be obtained in a timely manner.

Communication

Obviously any success depends on good communication. Firstly, the language barrier that existed between the writer and the rest of the fieldwork participants proved to be a hampering force on some occasions. Being able to discuss about for example how certain measurements should be taken and how to optimize collaboration will highly improve effectiveness and efficiency of the data collection. Secondly, the local languages that are spoken by the inhabitants of the villages on the various measuring sites can provide difficulties even for native Mozambicans. Communication with them is essential to achieve compliance and permission to perform measurements in their backyard.

Lessons Learned:
The best solution is of course to master a common language with the people you are working with. This however is in many situations not a feasible solution due to obvious reasons. As communication was less of a problem at the office in Songo due to the presence of English speaking staff, it would have been better to have a detailed briefing on fieldwork activities with the participatory crew there in advance. This would allow for the possibility of help with translations and to make sure everyone is on the same level of understanding concerning relevant matters. It is also essential to have at least one person in your team who speaks the local language and/or dialect present at the planned measuring site.

Knowledge and skills

The knowledge and skill that are necessary to secure sufficient quality and quantity of the collected data also provided some challenges. However, acquiring these skills and knowledge is also part of the process of doing fieldwork of course. One clear example is when during phase one, insufficient location-data of the GCPs was collected to set up a local grid involving all of the GCPs. This was caused by a lack of experience in doing so by means of a dumpy levelling device.

Lessons Learned:
It would be good to go through the whole procedure on a nearby test location in advance. The test-run should be done by using the exact same equipment as will be used during actual data collection and should also include processing of the test-data. This way the researcher(s) will be familiar with operating the equipment and the needed proceedings for securing sufficient data.

Environment

Environmental constraints are hard to avoid. The main environmental constraint encountered during this research concerns the amount of vegetation on the measuring site. As also explained in Section 4.4, the presence of vegetation blocks the UAV's view on the riverbed, which is what we are interested in. On certain sites, such as that of Rio Mucanha (Figure 4.2a), vegetation cover was of such a degree that only a section of only about two meters in length was attempted to be measured. At the site of Rio Tongoé (Figure 4.2c) the abundantly present high reeds will likely prevent any photos from being useful for DEM computation.

Another challenge enforced by environment relates to the presence of water, either flowing or stagnant. The lack of flowing water prevented the researcher from being able to perform both slope- and discharge measurements. An issue that arose when water was present, e.g. Rio Muze (Figure 4.2b) and Rio Aruãngua (Figure 4.2h), was that of the presence of dangerous wildlife such as crocodiles and hippopotamuses.

Lessons Learned:
With regards to the presence of abundant vegetation, it would be beneficial to scout the measuring river in advance in order to determine whether a suitable cross-section can be found. Bringing along some equipment to cut some reeds away when wanted can also be of help.

Climate

Just like environmental ones, challenges induced by climatic circumstances are unavoidable. Luckily regions such as Tete have a quite well defined rain- and dry-season. So in certain months the risk of precipitation can we estimated quite well. Temperature can also be of an issue. Not only do high temperatures increase efforts for physical labour, also can it have a serious impact on equipment.

As an example, during phase two of this research, temperatures occasionally rose to a level where smart-phones stopped working, rendering the U.A.V. uncontrollable for continuing the flight plan. High temperatures also make it hard to perform level-readings on relatively long distance due to vibrations of the rising air.

Lessons Learned:
The only thing one can do is to keep track of the forecast and make sure sufficient drinking water is available (be aware this is not always a given). Obviously protective clothing is an important consideration.

(a) Mucanha

(b) Muze

(c) Tongoé

(d) Duângua

(e) Cherisse

(f) Capoche

(g) Luia

(h) Aruãngua (Luangwa)

Figure 4.2: Photos of the 8 different measuring locations ordered in increasing channel size.

5

Results and Discussion

In two phases of fieldwork, eight measurement sites have been visited in total (Chapter 4). Two of the measured rivers have been left out of this analysis completely as the collected data for those sites did not meet the standards for further processing (Section 4.4). The two sites that have been left out are Rio Aruãngua (Luangwa River) and Rio Tongoé. For the prior river, insufficient images and complementary data could be collected to compute a cross-section. For the latter, abundant vegetation in the form of high reeds resulted in too much of the section to be invisible to the camera.

Results will be presented (and discussed) in a separate manner, thereby making a division between the river reach that is used for assessing the performance of the proposed method (Section 5.2) and the remaining rivers (Section 5.3). As Q-h data was only available for Rio Luia, only this tributary is used for performance assessment and results for this river will be discussed first. Secondly, results will be presented for Rio- Duângua, Mucanha, Muze, Cherisse, and Capoche.

5.1. Digital Elevation Models

A general overview of information on both input and output of the computed elevation models is provided in Table 5.1. Figure 5.1 shows the orthomosiac and DEM of Rio Luia (remaining tributaries in Appendix D). When looking at the images in Figure 5.1, one immediately notices the (white coloured) data gaps in the corners of the orthophotos and elevation models. This is caused by one of two reasons, the first is not enough overlapping images being available for computation of the DPC in these areas. The second option is that the overlapping images show too little similarity to be matched. This can be the case when the photographed surface is constantly changing, for example with flowing water or tall vegetation when it's windy. Another thing that can be noticed are the faded areas in the DEMs. These are the result of manual alterations to the DPC, mainly to remove disruptive vegetation such as trees and large bushes. In DEM computation, the holes that thereby appear in the DPC are filled by means of interpolation. The used programme is not able to fill the data gaps in the corners. Appendix F presents more detailed information on individual GCP errors per analysed river reach.

Table 5.1 displays both the absolute and relative overall RMSE-values for each of the measuring sites. Note that mentioned errors are referred to as reflecting DEM-accuracy in its entirety but they actually only reflect the accuracy of the GCPs within a DEM. However, this is the only available measure for DEM-accuracy and is assumed to be representative for the entire DEM. For the RMSE, a separation is made between the error in the horizontal and the vertical plane, depending on the error in XY and Z locations of the GCPs respectively. The relative errors are the absolute errors presented as a percentage of the diagonal distance of the DEM for the horizontal plane ($\varepsilon_{XY,R}$) and the maximum elevation difference within the DEM for the vertical plane ($\varepsilon_{Z,R}$).

DEM accuracy in the XY-plane is seen to be very good with all but one values of $\varepsilon_{XY,R}$ being below $1.0\ \%$. Only Rio Muze shows a higher error but this can be expected due to the relatively high amounts of noise present in the photographs induced by vegetation and stagnant water (Figure D.1e). This is also reflected in the high value for $\varepsilon_{Z,R}$. Although less so than Rio Muze, the data from Rio Mucanha also suffers from vegetation but has an additional negative effect from shadow (Figure D.1c). $\varepsilon_{Z,R}$ of Rios

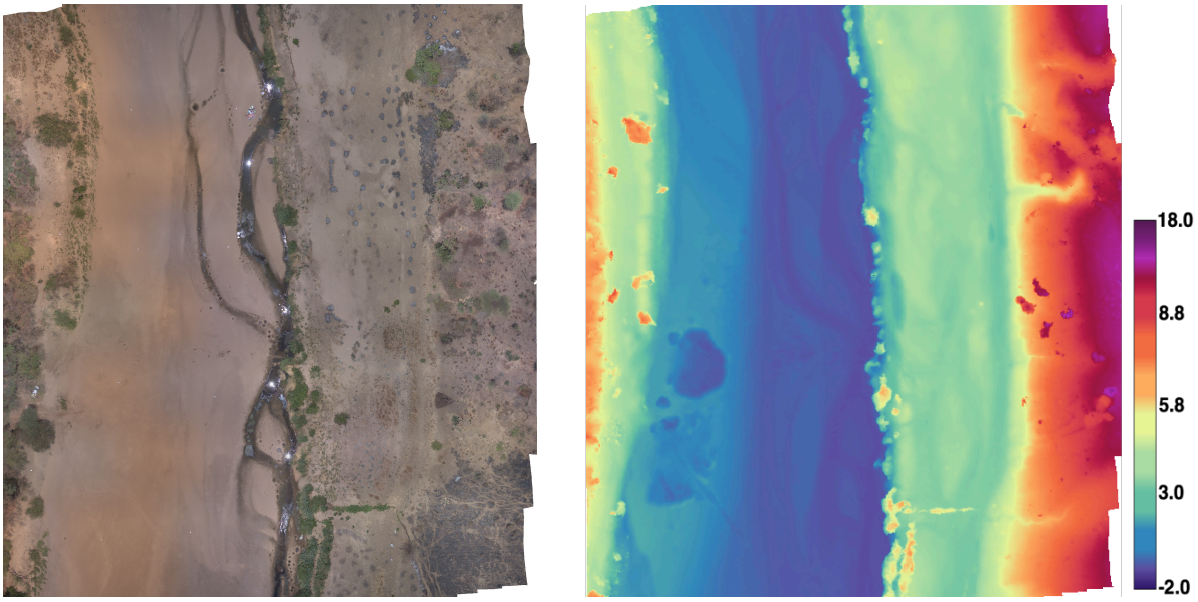

(a) Orthomosaic Rio Luia (b) DEM Rio Luia

Figure 5.1: Photogrammetry output images of Rio Luia with downstream direction facing downwards (colour-scale in meters).
Output of remaining tributaries in Appendix D.

Duângua, Cherisse and Luia can be seen to be very low with values between 0.03 and 0.13 %. That of Rio Capoche is slightly higher (1.34 %). This is likely to be caused by the fact that local conditions did not allow for optimal positioning of the GCPs which resulted in the control points being spread out over only half of the measured area.

Section	Length $[m]$	Width $[m]$	D_{XY} $[m]$[1]	$D_{Z,Max}$ $[m]$	GCPs	Photos	ε_{XY} $[m]$	$\varepsilon_{XY,R}$ [%][2]	ε_{Z} $[m]$	$\varepsilon_{Z,R}$ [%][3]	Comments
Duângua	153.79	103.39	185.31	12.87	12	57	0.466	0.25	0.015	0.12	3 GCPs excluded[4]
Muchanha	6.66	28.16	28.94	6.51	7	38	0.162	0.56	0.170	2.61	2 GCPs not used[5]
Muze	10.80	44.94	46.22	8.24	10	28	0.879	1.90	0.301	3.65	3 GCPs not used[6]
Cherisse	263.40	95.50	280.18	19.88	14	113	1.679	0.60	0.023	0.13	
Capoche	220.00	204.00	300.03	14.15	14	150	2.565	0.85	0.190	1.34	
Luia	246.90	224.70	333.84	15.27	14	130	1.262	0.38	0.005	0.03	

Table 5.1: DEM specifications for the processed river reaches (ε = RMSE). Ordered chronologically by time of measurement.

5.2. Method Performance: Rio Luia

5.2.1. Rating Curve Computation

This section will show the results of the individual steps leading to computation of the final (compound) rating curve as described in Section 3.2.6.

A best estimate for the maximum stage at zero flow (h_0) is set to be equal to the lowest point in the reach average cross-section because (1) insufficient data is available to determine h_0 for established local grid system and (2) the level of deepest point is deemed to be a good indication of h_0 for a channel controlled section [10] (also see Section 3.2.6). As can be seen in Figure 5.2 (TL), a clear geometrical separation between the main channel and the floodplains can be distinguished. For this reason it makes sense to compute a compound rating curve, splitting up the equation that relates the geometry to the water level. As also indicated in the same figure, the level at which this separation occurs (h_{sep})

[1] $D_{XY} = \sqrt{L^2 + W^2}$.
[2] Error relative to D_{XY}
[3] Error relative to $D_{Z,Max}$
[4] 3 out of 12 GCPs excluded from the process of DEM computation due to large errors in their coordinates (Section 5.3).
[5] 2 out of 7 GCPs could not be used because insufficient measurements prohibited their location to be calculated (Section 5.3).
[6] 3 out of 10 GCPs could not be used because insufficient measurements prohibited their location to be calculated (Section 5.3).

is equal to the stage at which the floodplain start to participate.

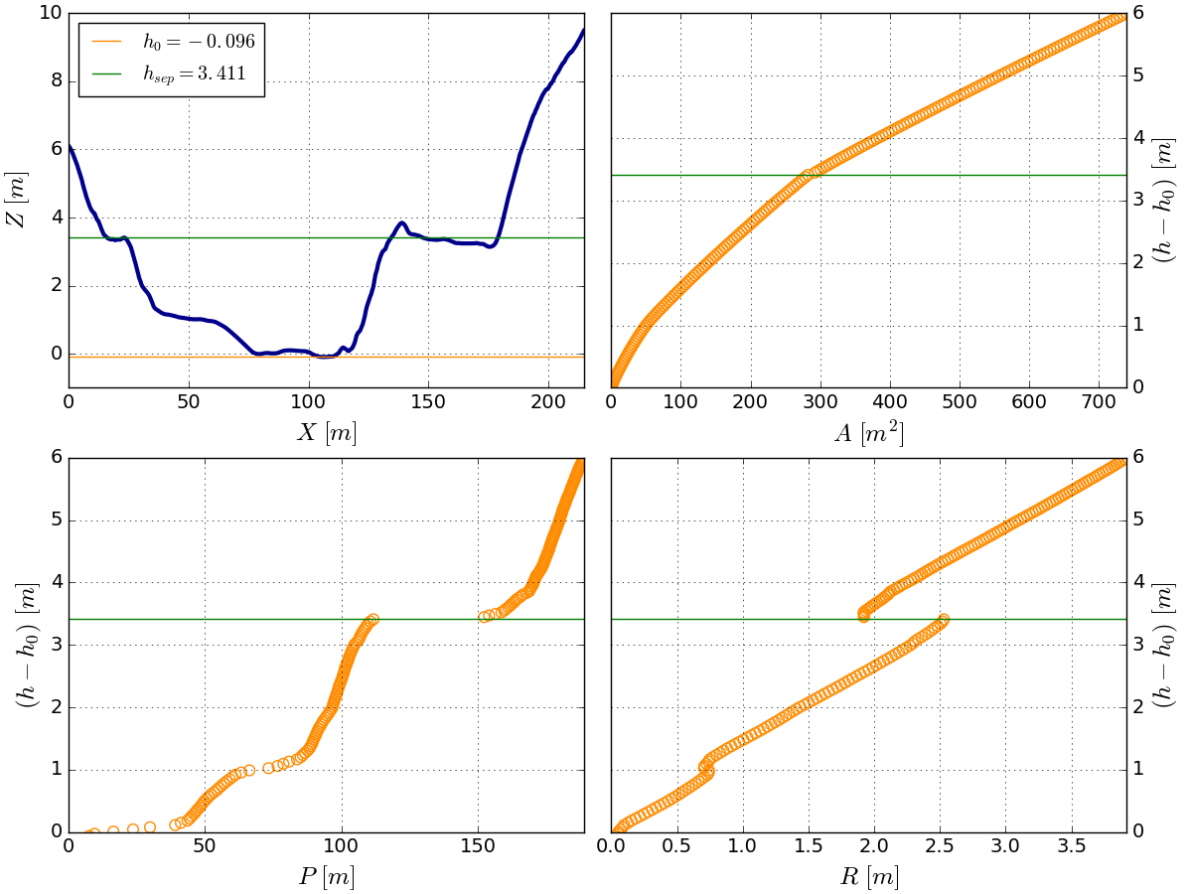

Figure 5.2: Geometrical parameter calculation for the reach average cross-section of Rio Luia. From top left (TL) to bottom right (BR): Reach average cross-section, Area (A), Wetted Perimeter (P) and Hydraulic Radius (R)

Another justification of this decision can be found in the reach average relations between the effective water level $(h-h_0)$ and the hydraulic parameters A, P and R (TR to BR in Figure 5.2). A very clear upwards jump in the wetted perimeter can be seen as soon as the floodplains come into play. This jump is also reflected by a drop in the hydraulic radius as temporarily P increases more rapidly than A ($R = \frac{A}{P}$).

Determination of the a_2 $[m^{8/3-b}]$ and b [-] parameters is done by using non-linear regression to fit a power-function to the relation between $AR^{\frac{2}{3}}$ and the effective stage. The results can be seen in Figure 5.3. For Rio Luia, values for a_2 and b are calculated to be $35.405\ m^{8/3-b}$ and 2.167 respectively for the main channel and 315.050 and 1.511 for the floodplains. When looking at the magnitude of the b values this corresponds to what can be expected given the shape of the section, where the flood plain has a very rectangular shape and the main channel approached a slightly more parabolic shape (Figure 2.3). The constant in the equation for the upper segment relates to: $AR^{\frac{2}{3}} = 35.405(h_{sep}-h_0)^{2.167} = 537.068$ How a different value for h_0 would have influenced these parameter values will be addressed in Section 5.2.3.

Computation of the a_1 parameter is divided in determination of the slope (i) and Manning's roughness coefficient (n). As explained in Section 3.2.6, n is preferred to be calibrated due to its complex nature. However, this requires discharge data. As no discharge data could be collected in the dry season and the discharge data from ARA-Zambeze can not be linked to own measurement due to an unknown difference in elevation scales, calibration of the roughness coefficient is not possible.

Figure 5.4 shows (a) the increase of the conveyance (C or $AR^{2/3}$) in downstream direction (Y) of the

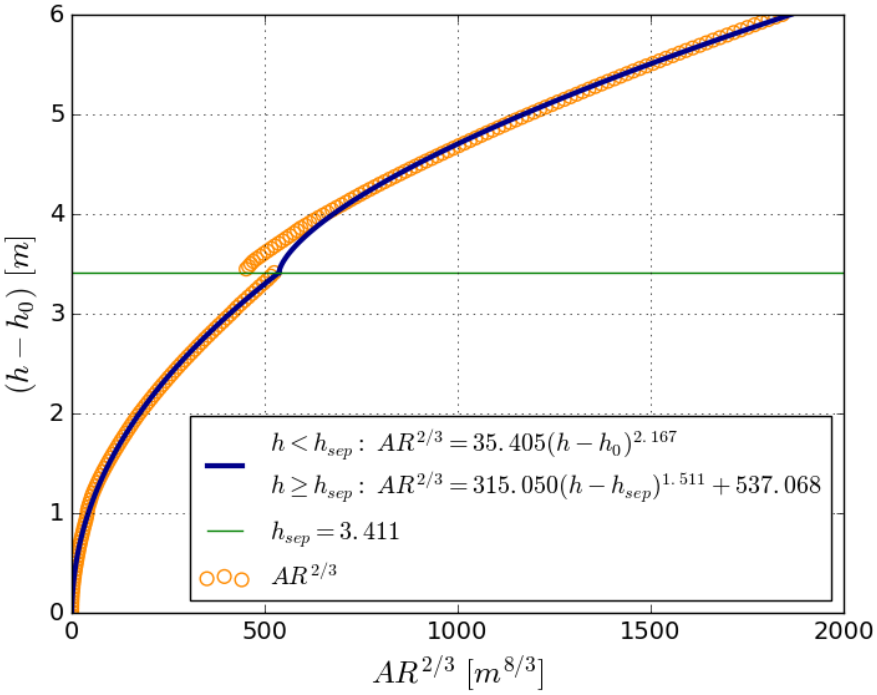

Figure 5.3: Compound curve for the conveyance

river reach when a constant water level, i.e. $i = 0$, is assumed ($^{dC}/_{dY} = 0.659\ m^{5/3}$) and (b) the needed slope to 'stabilise' this for uniform flow conditions. Linear regression has been applied to form a straight line fit through the $AR^{\frac{2}{3}}$ data to determine $^{dC}/_{dY}$. Naturally, the calculated value of $^{dC}/_{dY}$ (Figure 5.4a) depends on which value for the constant water level is chosen. It therefore has to be noted that the slope is adjusted to the main channel of the section. The calculated slope has a value of $i = 2.23 \cdot 10^{-3}\ {}^{m}/_{m}$ (Figure 5.4b).

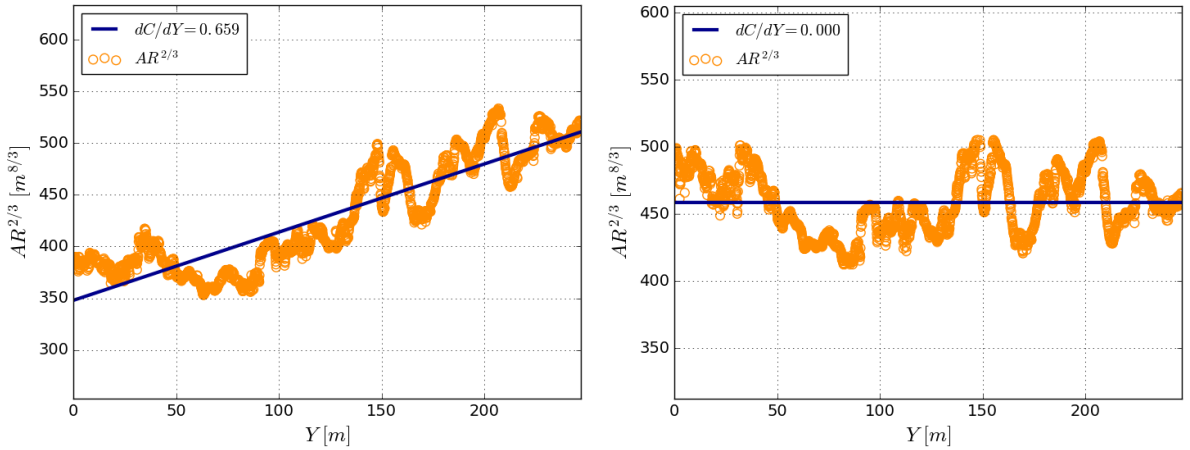

(a) Constant water-level ($i = 0$)

(b) Induced slope $i = 2.23 \cdot 10^{-3}$

Figure 5.4: Slope calculation for Rio Luia

Data from the ASTGDEM is used to form a comparative measure for the calculated slope. Figure 5.5 shows the elevation profile of the full river and the slope in a section of $20\ km$ around the measuring site ($10\ km$ up- and downstream). With a derived slope of $i = 1.32 \cdot 10^{-3}$, the graphs show that the uncertainty of the slope calculations can easily be a factor two. In this case for Rio Luia, the graph in Figure 5.5b clearly shows a locally steeper slope around the measuring site, coinciding more with the

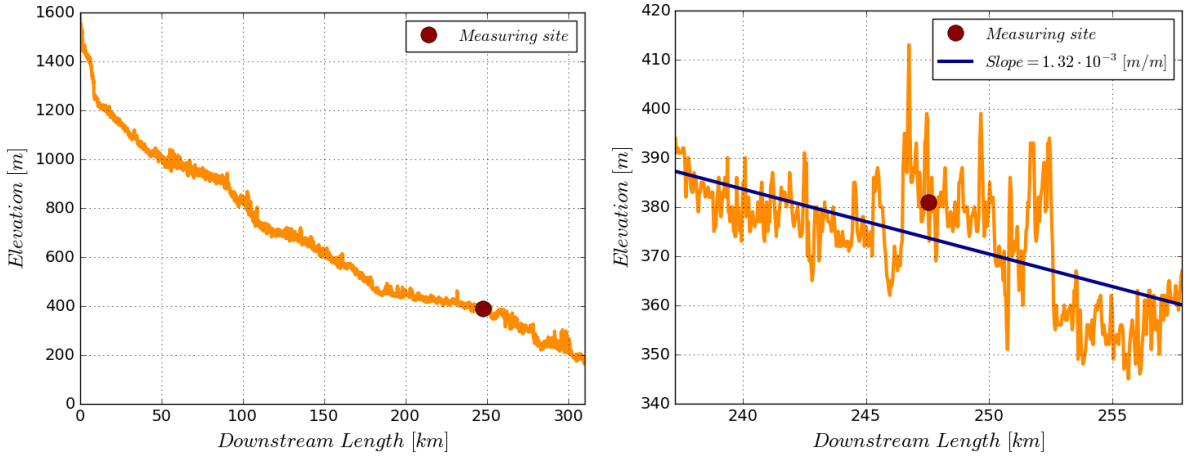

(a) Full length of the river.

(b) $\pm 20\ km$ around the measuring site

Figure 5.5: Elevation profile of Rio Luia based on ASTGDEM and local slope around measuring site.

other higher calculated slope of $i = 2.23 \cdot 10^{-3}$. The high outliers are assumed to be faulty and are likely caused by inaccuracies in the GDEM which has a vertical accuracy (RMSE) that generally lies between 10 and $25\ m$ according to [21] and showed an RMSE of about $7\ m$ by [3]. Another source of inaccuracy in the elevation profile comes from the course of the river's shapefile that is likely to not be exactly accurate due to changes in river morphology and the discrete nature of the river's representation by a polyline. The locally higher slope around the measuring site is likely to be more in effect during lower flows, while the regionally lower slope ($1.32 \cdot 10^{-3}$) is likely to be more in effect during higher flows.

The overall elevation profile from the GDEM (Figure 5.5a) very nicely shows the changing slope-regimes with rapids and flatter areas. From here it can be seen that the measuring site seems to be very close to a transitional area of a lower slope going into a higher slope. This can also be of influence on the higher local slope at the measuring site. Regional GDEM-based slope calculations for the five additional rives can be found in Appendix E.

As has been explained, using the computed DEM of the reach for direct slope calculations is problematic due to the river's flow paths not following a straight line. However, because the measured reach for this river shows a pretty straight pattern (Figure 5.1b), an attempt is done to form an additional comparative measure for the calculated slope. Over the width of the main channel, the downstream elevation is subtracted form the upstream elevation and the result is divided by the length of the reach. This resulted in a slope with a value of $i = 2.28 \cdot 10^{-3}\ {}^{m}/_{m}$ for the main channel, thereby complementing the reliability of the calculated slope of $i = 2.23 \cdot 10^{-3}\ {}^{m}/_{m}$.

In addition, Equation 3.13 can be used to estimate i based on an analytically derived formula. In doing so ${}^{\mathrm{d}C}/_{\mathrm{d}Y}$ from figure 5.4a can be used. The values for C and R corresponding to the same water level are found through the relations established in Figure 5.2. When doing so, a slope of $i = 5.93 \cdot 10^{-3}\ {}^{m}/_{m}$ is established, being about 2.5 times bigger than the previously calculated value. The difference in the slope is possibly caused by the assumptions underlying the derived formula such as $A = B \cdot d$ and $R \approx d$. In addition, the value of ${}^{\mathrm{d}C}/_{\mathrm{d}y}$ is derived over the length of the river reach, while those of C and R are derived from one reach-average cross-section. Discrepancies in the geometry, such as tall vegetation, can be seen in Figure 5.4a by the fluctuations in $AR^{\frac{2}{3}}$ and obviously influence the slope of the regression line that is used as an overall value for ${}^{\mathrm{d}C}/_{\mathrm{d}y}$. The influence of combining these values of which the geometrical base they are derived from slightly differ is not investigated here. Of course the same geometrical discrepancies are also influencing the slope calculated in Figure 5.4b, but as this is a more direct way that does not involve additional variables, this is considered to be more reliable.

Manning's roughness coefficient is estimated based on literature. As proposed by [6] and [9], factors that influence n can be combined to form an overall estimate of the roughness coefficient (Equation 5.1):

$$n = (n_b + n_1 + n_2 + n_3 + n_4)m \tag{5.1}$$

where

n_b = a base value of n for a straight, uniform, smooth channel in natural materials $[sm^{-1/3}]$
n_1 = a correction factor for the effect of surface irragularities $[sm^{-1/3}]$
n_2 = a value for variations in shape and size of the channel cross-section $[sm^{-1/3}]$
n_3 = a value for obstructions $[sm^{-1/3}]$
n_4 = a value for vegetation and flow conditions $[sm^{-1/3}]$
m = a correction factor for meandering of the channel $[-]$

The respective parameter values are selected from a collection of tables from [6]. The base value has been estimated to be $0.030\ sm^{-1/3}$ (coarse sand channel). Corrective values n_1 to n_4 and m have been estimated to be $0.005,\ 0.000,\ 0.01,\ 0.01\ sm^{-1/3}$ and 1.0 respectively, resulting in an estimated n-value of $n = 0.055\ sm^{-1/3}$. When looking at [25], the coefficient value for a clean winding natural channel with some pools and weeds, lies in the range of $n = 0.035$ to $n = 0.050\ sm^{-1/3}$. [3] calibrated the Manning's roughness coefficient for the Johor river in Malaysia using five different model set-ups. The results where values in the range between 0.042 and $0.055\ sm^{-1/3}$ for the main channel and between 0.051 and $0.081\ sm^{-1/3}$ for the floodplain. As becomes clear from this variety of values, there is not one straight forward way to determine a very accurate value for the roughness coefficient from literature. The truth is likely to lie somewhere within the range of mentioned estimates. For further proceedings, the magnitude of the roughness coefficient is estimated to be $n = 0.050\ sm^{-1/3}$. It has to be noted that for this analysis one value for n is assumed to hold for the entire cross-section. In real-life this is unlikely to be the case and generally the floodplains display a higher roughness than the main channel. However, [25] showed that a uniform Manning's coefficient can be used for the entire river profile due to parameter compensation (Section 5.4). Sensitivity to n is analysed in the following sections.

5.2.2. Rating Curve Performance

Figure 5.6 shows the final result of the physically-based compound rating curve for Rio Luia. As elaborated upon in the previous section, $n = 0.05\ sm^{-1/3}$ and $i = 2.23 \cdot 10^{-3}\ m/m$. The rating curve is plotted together with the Q-h data from ARA-Zambeze and the rating curve corresponding to that data. Note that, even though they appear to match, the curves are plotted on different Y-axis as they each maintain a different level-scale. This is because insufficient data was collected to link the elevation scales of the two different data sets. For this study, a local grid was set up based on the calculated locations of the ground control points. The datum for elevation (z) was set equal to the lowest measured GCP. During the infield measurements, the researcher failed to include the staff-gauge from ARA-Zambeze in the surveying-measurements, thereby not being able to link local grid elevation to ARA-Zambeze's elevations. This means that in Figure 5.6, e.g. h-$h_0 = 3\ m$ on the TU-computed curve (blue) does not necessarily translate to the same real-life water height for h-$h_0 = 3\ m$ on the ARA-computed curve (red).

For this reason, actual quantification of the performance is not possible because the Q-h measurements are referenced to the scale of ARA-Zambeze. Therefore, performance of the computed rating curve must be done qualitatively by means of visual analysis and expert judgement.

First and foremost, an important observation is that it is definitely possible to compute a physically-based compound rating curve based on aerial imagery. Even though the water levels can not be matched exactly, it is unlikely that h_0 differs enormously. Especially given the parameter-uncertainties in h_0, i and n, it is not a bad first approximation of ARA-Zambeze's curve. In addition, the compound rating curve computed in this study does not refer to the exact same control-section (and corresponding data) as that of ARA-Zambeze's does. The cross-section used in this study is an average section based on a reach of about $250\ m$ upstream of a bridge. Although their staff-gauge at this particular river was located on a pillar on the upstream side of that same bridge, it is not known at which distances from the bridge the flow-measurements were performed. If their discharge measurements have been performed directly upstream of the bridge at the same section as the staff-gauge, it is very possible that some backwater effects have influences their measurements. This could mean that indeed a smaller Q is found for the same h, resulting in a leftwards shift of the rating curve compared to a reach-average cross section more upstream of the bridge. In addition, the set of 17 Q-h measurements range from

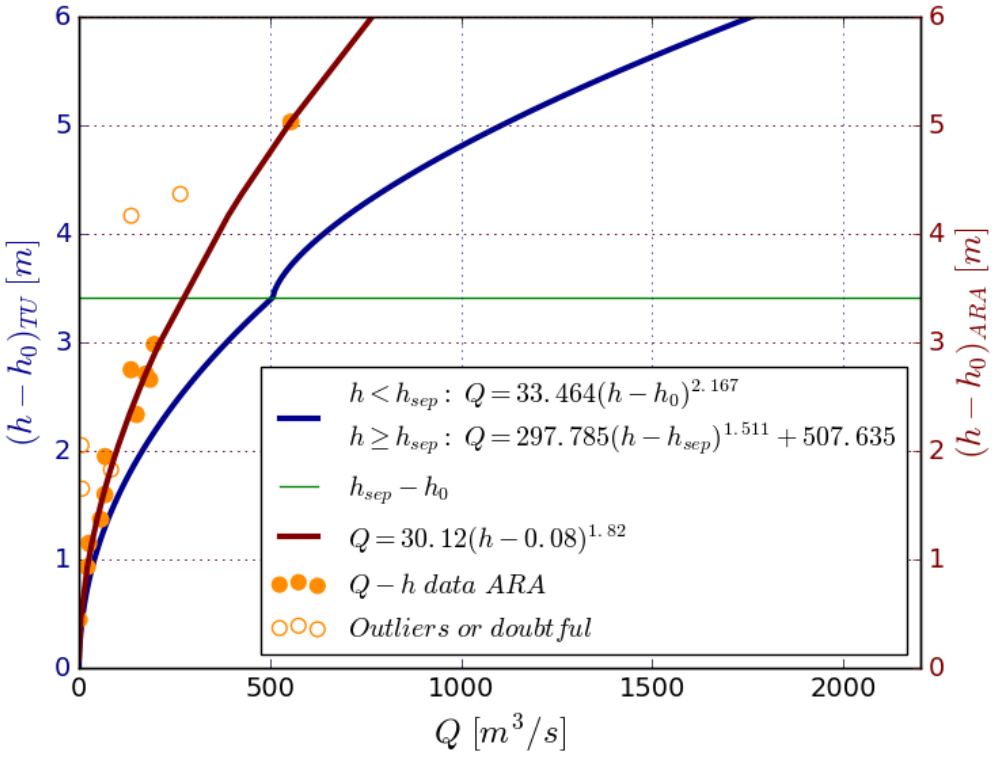

Figure 5.6: Rating curve for Rio Luia; blue: computed by TU, red: computed by ARA-Zambeze. $n = 0.05\ sm^{-1/3}$ and $i = 2.23 \cdot 10^{-3}\ m/m$.

2008 to 2015 (with one dating from 1999). Therefore it is possible, that since the first flow-measurement, the geometry of the section has slightly changed due to scouring and deposition of sandy bed-material.

Note that even though the difference between the h-scales (i.e. h_0), can not be quantified, it is deemed unlikely that ARA-Zambeze's differs greatly from TU Delft's as their value for h_0 also lies close to zero. Therefore the rating curve is expected to follow the pattern of the Q-h data. The previous section showed that the calculated i-value is not without uncertainties. In addition, it is likely to depend on water level. It was made clearly evident that n-estimates based on literature carry a lot of uncertainty as well. Therefore, these parameter are expected to be of most influence to the mismatch between the computed rating curve and the Q-h data. Figure 5.7 shows a set of graphs where the computed rating curve has been fit to the data of ARA-Zambeze by (1) adjusting the combined influence of slope and roughness (Figures 5.7a and 5.7b), (2) adjusting the roughness individually (Figure 5.7c), and (3) adjusting both the slope and the roughness individually (Figure 5.7d). For Figures 5.7b to 5.7d, parameters have been adjusted in a separative manner by differentiating between the lower- and the upper segment of the rating curve.

As the relative influence of the uncertainties in n and i have not been quantified yet, it makes sense to look at their combined influence as a_1 ($= n^{-1}\sqrt{i}$). Parameter a_1 as initially estimated has a value of $0.95\ m^{1/3}/s$ for both segments in the compound rating curve. In Figure 5.7a it can be seen that this needs to drop to a value of $0.53\ m^{1/3}/s$ to match the Q-h data of the main channel. When the one data point in the upper segment is to be included, a_1 for the floodplain needs to be decreased further to a value of $0.42\ m^{1/3}/s$ (Figure 5.7b). This would result from both an increase in the roughness coefficient and a decrease of the surface slope, both of which scenarios are likely to be the case.

When assuming the computed slope is more or less correct, the needed adjustments in n can be seen to be an increase from 0.05 to 0.090 and $0.110\ s/m^{1/3}$ for the main channel and floodplain respectively. This would indicate a very large underestimation of the estimated range of the roughness coefficient based on literature. So much actually that this seems to be unlikely. This means that the calculated slope need to be used with care and stipulates the need for further verification of used method for slope calculation. When a lower slope is assumed, such as the one derived from the GDEM, it can

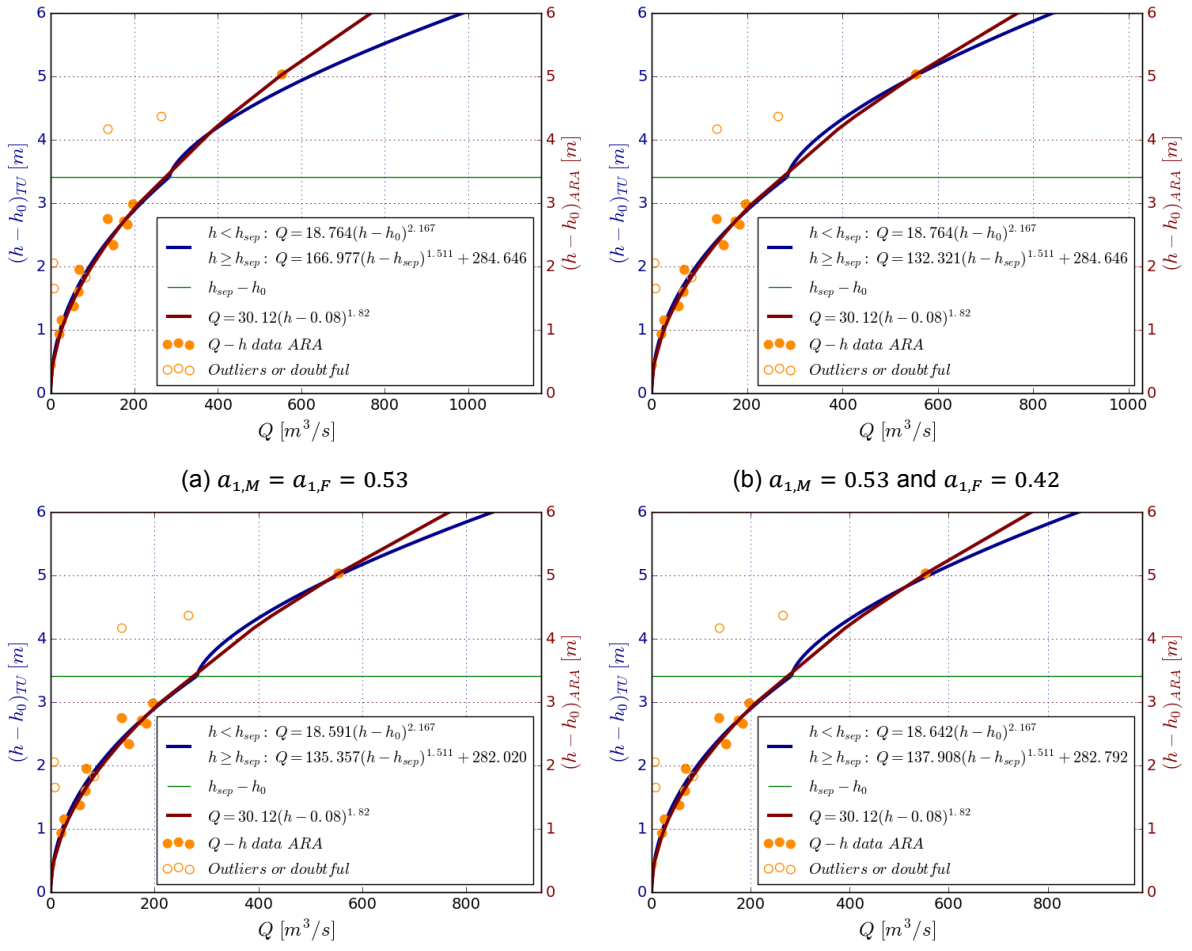

(a) $a_{1,M} = a_{1,F} = 0.53$ (b) $a_{1,M} = 0.53$ and $a_{1,F} = 0.42$

(c) $i = 2.23 \cdot 10^{-3}$, $n_M = 0.090$ and $n_F = 0.110$ (d) $i = 1.32 \cdot 10^{-3}$, $n_M = 0.069$ and $n_F = 0.083$

Figure 5.7: Adjusting i and n to match the rating curve to the Q-h data.

be seen that the required values for n correspond to 0.069 and 0.083 $s/m^{1/3}$ (Figure 5.7d). This would still indicate an underestimation of the estimated roughness coefficient but to a more reasonable extend.

It can be noticed that the exponent value for the TU-computed rating curve is a fair bit higher than that of ARA-Zambeze (2.17 vs. 1.82). Because b [-] depends on the geometry of the control-section, it is possible that this is caused by either the use of a different cross-section or a misrepresentation of the geometry due to errors in the DEM. Therefore, an additional analysis is done to see how a_2 and b vary over the length of the entire reach. Figure 5.8 shows the spread of both parameter values of the lower segment of the rating curve for each of the 2469 cross-sections that are incorporated in the reach average cross-section. As can be seen the b-value as computed in the previous section (2.167) lies around the median. It can be seen that there is not much spread with a standard deviation of 0.07 and a minimum and maximum value of about 2.025 and 2.300 respectively (excluding outliers). a_2 shows to be somewhat more variant with a standard deviation of 4.02 $m^{8/3-b}$. This tells us that in that particular part of the river, the value of b is quite steady, thereby not really enforcing stated suspicion. In addition, the very small relative errors of the elevation model (Table 5.1: $\varepsilon_{XY,R} = 0.38\%$ and $\varepsilon_{Z,R} = 0.03\%$) do not suggest significant misrepresentation of the cross-section due to errors in the DEM.

Therefore, a different hypothesis is tested by looking at the way the relation between $AR^{\frac{2}{3}}$ and h is determined. As mentioned in Section 3.2.6, the classic and most common way to compute rating curves is through the process of linear regression of double-logarithmic Q-h data. However, in this study, fitting of the power-function to the geometry of the section is done by non-linear regression as the Q-h relation is obviously non-linear for $b \neq 1$. In order to investigate the influence of using the dif-

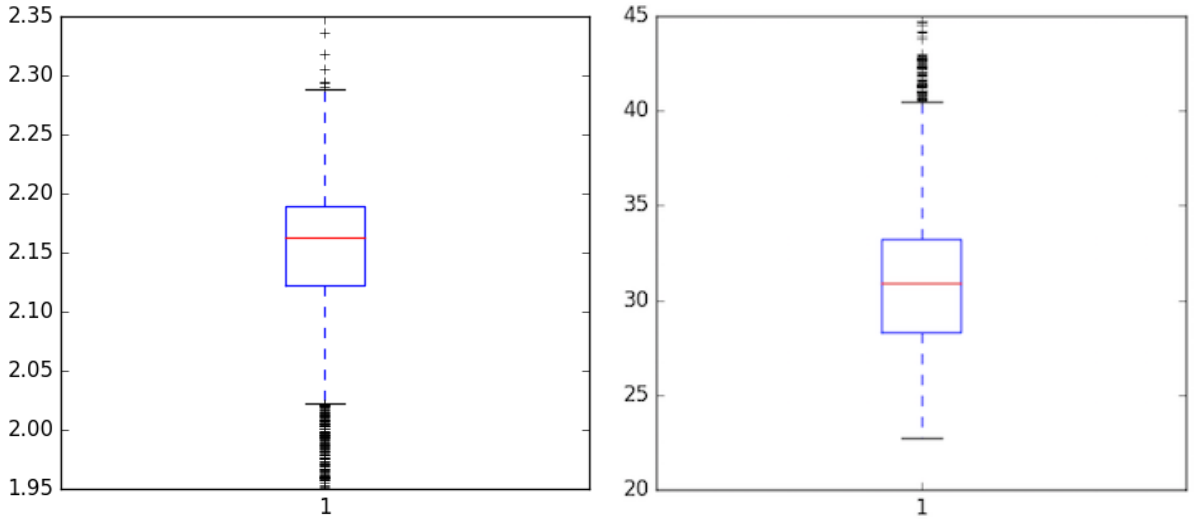

(a) b: $\sigma^2 = 0.0042$ and $\sigma = 0.0650$ (b) a_2: $\sigma^2 = 16.1272$ and $\sigma = 4.0159$

Figure 5.8: Variability of b and a_2 along the length of the main channel

ferent techniques, the relation between $AR^{\frac{2}{3}}$ and stage is also established through linear regression on the logarithm of Q and $(h\text{-}h_0)$. Figure 5.9 and Table 5.2 show the results of comparing b-computation through linear regression and non-linear regression. Hereby a separation is made between the lower segment of the rating curve (main channel) and the full channel. For the prior, the equation from the lower segment of Figure 5.3 is used for the non-linear fit. For the latter, a single curve is fitted to the entire section (also see Table 5.2). What can be noticed is that linear regression results in a much lower b-value, very much in the same range as that of ARA-Zambeze's rating curve. However, from Figures 5.9b and 5.9d it can be concluded that in both cases the relation computed through non-linear regression performs better in mimicking the geometry of the control-section.

	Linear Regression	Non-linear Regression
Main channel	1.733	2.167
Full section	1.887	2.364

Table 5.2: Computed values for exponent b [-] (single curve)

Another observation of note, is the difference between the use of a single rating curve (ARA-Zambeze) or a compound rating curve (TU). Even though it is surely possible that ARA-Zambeze's single curve correctly relates discharge to the whole range of water-levels, this is difficult to verify as there is only one measurement in the high-flow regime, also stipulating the difficulty of obtaining high-flow measurements. As a significant change in geometry can be seen in the computed elevation model, the researcher argues that the increased feasibility of computing a compound rating curve without high-flow measurements is already a big step forward.

5.2.3. Parameter Sensitivity

As addressed in the previous sections, uncertainty of parameter-values has a direct influence on the shape of the final (compound) rating curve. This section will elaborate on those effects and thereby give more insight in the underlying challenges.

Figures 5.10a and 5.10c show the sensitivity of the rating curve to the parameters n, i, a_2, b, and h_0 by displaying the effect of an equal percent change in magnitude ($\pm\ 10\%$) of the different parameters. Here, the rating curve as computed in the previous section (Figure 5.6) is taken as the reference. As can be seen, h_0 is excluded from this graph as decreasing its value with 10% is physically impossible. Also, because its value is close to zero, a 10% increase will not show any difference. Therefore, Figure 5.10b is added to show the effect of increasing h_0 with absolute values. The range of h_0 used in the plot

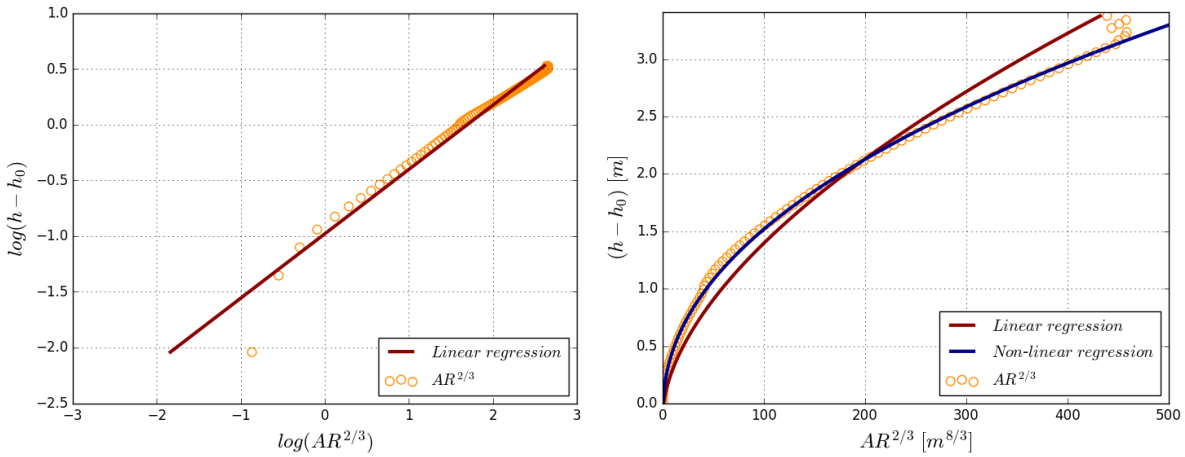

(a) $b = 1.733$ $(R^2 = 0.987)$

(b) $R^2_{LR} = 0.969$ $R^2_{NLR} = 0.992$

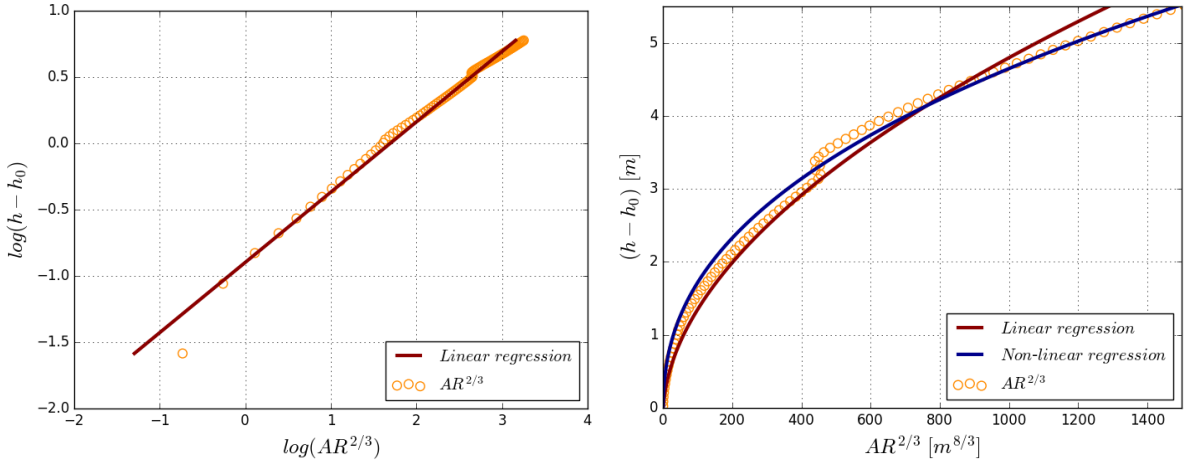

(c) $b = 1.887$ $(R^2 = 0.996)$

(d) $R^2_{LR} = 0.966$ $R^2_{NLR} = 0.996$

Figure 5.9: Comparing computation of geometry parameters by linear- and non linear regression for the main channel (a and b) and the entire section (c and d).

is arbitrarily chosen. From Figure 5.10a (and 5.10c) it can be concluded that relatively, the rating curve is most sensitive to the values of parameter b. Interesting to see is that decreasing n has a slightly bigger effect than an increase in a_2, but the opposite does not hold, i.e. a decrease in a_2 causes a bigger change than an increase in n. This might indicate a dependency between the two parameters. However, the influence of n and h_0 can be seen to be almost equal. Compared to n, a_2 and b, a relatively equal change in i is of little influence.

The rating curve can be seen to be very sensitive to the value of b, a change of plus or minus 10% results in a relatively large change in the shape of the curve. Obviously an increase in the exponent-value leads to a higher rising speed for the magnitude of Q. From a physical perspective this also makes sense. As can be seen in Figure 2.3, a higher b value relates to a more triangular shape of the cross-section. With a more triangular shape, the added conveyance area for increasing water depth is larger than for a section with a more parabolic or rectangular shape.

The a_2 parameter can not be linked to a clear physical characteristic of the geometry the same way b can. However, an increase in a_2 equates to an increase in the conveyance and therefore also an increase in the discharge, as is seen in the graph.

The effect of the roughness coefficient is also as can be expected. An increase in roughness translates into a decrease in flow for the same stage due to an increasing flow resistance.

The effect of slope is also as expected. An increasing slope results in an increase in discharge. It can be seen that the rating curve is less sensitive to the i parameter as it is to other parameters, a 10% in- or decrease of the slope does not significantly influence the Q-h relation.

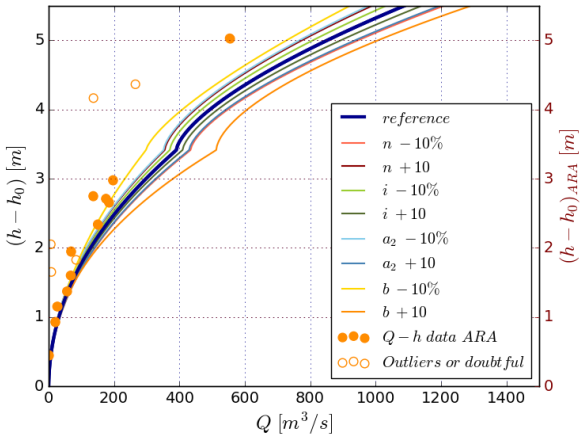

(a) Influence of n, i, a_2 and b.

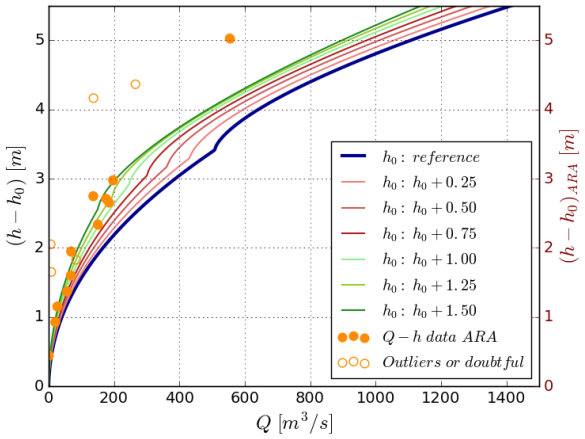

(b) Influence of h_0

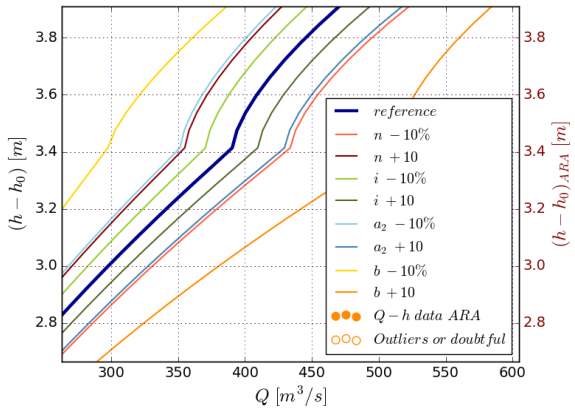

(c) As (a) but zoomed in.

Figure 5.10: Relative sensitivity of the rating curve to parameters n, i, a_2, b and h_0

Increasing the value of h_0 can be seen to shift the rating curve towards the left, thereby better approaching the shape of ARA-Zambeze's rating curve. This shift to the left makes sense, with a higher value for h_0 the effective stage decreases meaning less discharge is produced for the same water level. Note that a decrease of the parameter value is not possible as it was already set to the lowest elevation value of the cross-section.

The analysis above provides a sense of how the rating curve reacts to changes in the parameter values. This gives a good first impression of how errors in the parameter values have had an influence on the computed rating curve. However, this does not take into account the actual uncertainty of established parameter values, and therefore does not provide the full picture. In order to quantify the relative influence of the individual parameters on the error of the resulting rating curve, i.e. discharge, the theory of propagation of errors is applied in this sensitivity analysis (also see Section 3.2.8). For the sake of simplicity, covariance between the parameters will not be investigated and is therefore not included in this analysis.

To aid in understanding the following derivation, the mathematical formula for physically-based rating curve computation, as used in this study, is once again stated in Equation (5.2).

$$Q = n^{-1} i^{\frac{1}{2}} a_2 (h - h_0)^b \tag{5.2}$$

By making use of (3.14), the standard error (variance) in the computed discharge Q can then be written to be:

$$\sigma_Q^2 = \left(\frac{\partial Q}{\partial n}\right)^2 \sigma_n^2 + \left(\frac{\partial Q}{\partial i}\right)^2 \sigma_i^2 + \left(\frac{\partial Q}{\partial a_2}\right)^2 \sigma_{a_2}^2 + \left(\frac{\partial Q}{\partial (h-h_0)}\right)^2 \sigma_{(h-h_0)}^2 + \left(\frac{\partial Q}{\partial b}\right)^2 \sigma_b^2 \tag{5.3}$$

Where the individual partial derivatives are derived to be:

$$\frac{\partial Q}{\partial n} = -n^{-2} i^{\frac{1}{2}} a_2 (h - h_0)^b \tag{5.4}$$

$$\frac{\partial Q}{\partial i} = \frac{1}{2} n^{-1} i^{-\frac{1}{2}} a_2 (h - h_0)^b \tag{5.5}$$

$$\frac{\partial Q}{\partial a_2} = n^{-1} i^{\frac{1}{2}} (h - h_0)^b \tag{5.6}$$

$$\frac{\partial Q}{\partial (h - h_0)} = b(h - h_0)^{-1} n^{-1} i^{\frac{1}{2}} a_2 (h - h_0)^b \tag{5.7}$$

$$\frac{\partial Q}{\partial b} = \ln (h - h_0) n^{-1} i^{\frac{1}{2}} a_2 (h - h_0)^b \tag{5.8}$$

When (5.4) to (5.8) are substituted into (5.3) and then divided by (5.2), the following equation is obtained showing the relative influence of the parameter-errors on the error in Q:

$$\frac{\sigma_Q^2}{\overline{Q}^2} = \frac{\sigma_n^2}{\overline{n}^2} + \frac{1}{4}\frac{\sigma_i^2}{\overline{i}^2} + \frac{\sigma_{a_2}^2}{\overline{a_2}^2} + b^2 \frac{\sigma_{(h-h_0)}^2}{\overline{(h - h_0)}^2} + \ln (h - h_0)^2 \sigma_b^2 \tag{5.9}$$

Through defining the relative errors as follows,

$$\frac{\sigma_x^2}{\overline{x}^2} = r_x^2 \tag{5.10}$$

this can be written as:

$$r_Q^2 = r_n^2 + \frac{1}{4} r_i^2 + r_{a_2}^2 + b^2 r_{(h-h_0)}^2 + \ln (h - h_0)^2 \sigma_b^2 \tag{5.11}$$

Using the derived equation in (5.11), two different analysis of error propagation are performed. One is to show the relative error induced by parameter uncertainty for the case when n is estimated based on literature, and the other is to show the case for when n is calibrated. Note that for the latter case, calibration refers to adjustment of the n value to match the shape of ARA-Zambeze's Q and h data, as done in Figure 5.7.

Application of the theory of error propagation requires establishment of the mean (μ) and standard deviations (σ) of the individual parameters. For the slope, the value of i is assumed to lie within the range between the calculated slope and the slope derived from the ASTGDEM. The mean and standard deviations for the parameters a_2 and b are determined by looking at the spread in the main channel of these parameters over the 2469 cross-sections of the reach. The uncertainty in h-h_0 obviously depends on h and the uncertainty in h_0. Therefore, in order to determine the uncertainty in h-h_0, an assumption regarding the uncertainty in h_0 had to be made. The stage at zero flow is estimated to lie between the used minimum elevation and $0.5\ m$. Three different water levels are evaluated, one in the low-flow regime ($h_1 = 1.6\ m$), one close to the limit of the main channel ($h_2 = 3.1\ m$) and one in the high flow-regime ($h_3 = 4.6\ m$). An overview of the used ranges of values, together with the corresponding μ's and σ's are presented in Table 5.3.

Table 5.4 presents the findings of the sensitivity analysis by error propagation. One conclusion that can be drawn, is that a calibrated n roughly doubles the accuracy of the computed discharge. The error in Q can be seen to lie between 67% and 30% for the non-calibrated case. This corresponds to what can be seen in Figure 5.6. The error decreases to values between 50% and 13% depending on water level. This brings us to the second important observation: the uncertainty of h_0 has a very big influence for low water levels (42% at h_1) and becomes significantly lower at higher water levels (4.2% at h_3). This decreasing effect of h_0 was expected to be the case. Both i, a_2 and b have a relatively low contribution to the uncertainty in Q where especially b has a very minor contribution. However, this does slightly increase for higher water levels, enforcing the stated need for an accurate representation of this geometrical parameter in the high-flow regimes.

	n	i $(\cdot 10^{-3})$	a_2	h-h_0	b
Range:	(1): 0.042 - 0.081 (2): 0.069 - 0.090	1.320 - 2.233	22.653 - 40.513	h_1: 1.100 - 1.696 h_2: 2.600 - 3.196 h_3: 4.100 - 4.696	2.021 - 2.288
μ:	(1): 0.062 (2): 0.080	1.777	31.418	h_1: 1.398 h_2: 2.898 h_3: 4.398	2.151
σ:	(1): 0.028 (2): 0.015	0.646	4.015	h_1: 0.421 h_2: 0.421 h_3: 0.421	0.065

Table 5.3: Used ranges and input values for the error propagation analysis. (1) and (2) respectively refer to the range of n for the case of estimated based on literature and the case of being calibrated.

This analysis shows that, in exception for very low-flows, accuracy of the physically based rating-curve will benefit most from decreasing uncertainty in n. For low flows, the major contribution to the error comes from uncertainty in h_0. Relative to the other parameters, h_0 remains to be of influence but this significantly decreases with increasing water level. The contribution of the error in $(h - h_0)$ is amplified by the b^2-term in Equation 5.11. It has to be noted that results of this error propagation analysis did not include the change of b for higher water levels. In reality, the exponent value is lower for the floodplain than it is for the main channel, which would result in an even bigger decrease of the relative error of $(h - h_0)$ for higher flows, and therefore also a decrease of the relative error in Q. Therefore, an important observation to make is that in contrast to conventional rating curve computational procedures, the physically based rating curve shows an increasing accuracy for increasing water levels due to the decreasing influence of the error in h_0. This resolves the biggest flaw in conventional rating curve computation, the decreasing predictive capability for high flows due to extrapolation of low flow data.

As mentioned, is has to be noted that in this analysis the range of the calibrated n values does not take correlation with uncertainty in i into account and could therefore still be improved by (1) decreasing inaccuracy in i and (2) determining the covariance between n and i.

Parameter:		n	i	a_2	$(h - h_0)$	b	Q
RCEC:*		r_n^2	$\frac{1}{2} r_i^2$	$r_{a_2}^2$	$b^2 r_{h-h_0}^2$	$\ln(h - h_0)^2 \sigma_b^2$	r_Q^2
h_1	(1):	0.204	0.033	0.016	0.420	0.001	0.674
	(2):	0.035					0.505
h_2	(1):	0.204	0.033	0.016	0.098	0.005	0.356
	(2):	0.035					0.187
h_3	(1):	0.204	0.033	0.016	0.042	0.009	0.304
	(2):	0.035					0.135

Table 5.4: Influence of the separate terms on the relative error of Q (also see Equations 5.9 and 5.11). *RCEC = Relative Contribution to Error is Calculated by:.

5.3. Additional Rivers

This section will present computed (compound) rating curves for the remaining five rivers: Rio- Duângua, Mucanha, Muze, Cherisse and Capoche. As no historical flow-records are available for these rivers, only the quality of the elevation models is discussed. Parameter calculation and estimation is done in the same way as for Rio Luia. Therefore, even though having a sound theoretical base, the presented rating curves present an estimation of the Q-h relation and are recommended to be perfected and validated before being used in further water resources planning activities.

An overview of both the computed and estimated parameter-values can be seen in Table 5.5. For all except Rio Capoche, a single rating curve proved sufficient to parametrise the section's geometry. For Rio Capoche a compound rating curve is established. Corresponding plots are found in Figures 5.11 to 5.15. The lighter blue bounds around the curves indicate a $\pm 30\%$ error-margin in Q.

	$n\ [sm^{-1/3}]$	$i\ [m/m]$	$h_0\ [m]$	$h_{sep}\ [m]$	$b_M\ [-]$	$b_F\ [-]$
Duângua:	0.056	$2.21 \cdot 10^{-3}$	-0.436	-	1.883	-
Mucanha:	0.120	$5.96 \cdot 10^{-3}$	-0.096	-	2.087	-
Muze:	0.125	$5.96 \cdot 10^{-3}$	-0.575	-	2.155	-
Cherisse:	0.110	$6.07 \cdot 10^{-3}$	0.279	-	2.088	-
Capoche:	0.055	$1.09 \cdot 10^{-3}$	0.063	3.235	1.803	1.312
Luia[1]:	0.050	$2.23 \cdot 10^{-3}$	0.063	3.411	2.167	1.512

Table 5.5: Parameter-values for physically-based (compound) rating curves of stated rivers. Subscripts 'M' and 'F' relate to 'Main channel' and 'Flood Plain' respectively.
[1]Added for comparison.

Figure 5.11 shows the computed rating curve for Rio Duângua. This being the first measurement site, the whole measuring process was still heavily subdue to teething troubles. This led to less precise ground-surveying measurements and a very inefficient flight-plan for the UAV. Because three out of twelve GCPs were located too close to high vegetation, they induced large errors in the DEM and were therefore not used in DEM computation.

Apart from being somewhat smaller and not having a clear separation between flood plain and main channel, this river showed many similarities with Rio Luia on both vegetative cover and composition of bed-material. As can be seen in Figure D.1b, the reach that was mapped shows a bit of a curve and widening of the river in the downstream part. To minimize the influence this has on the reach-average cross-section, the lower quarter of the DEM was not used in rating curve computation.

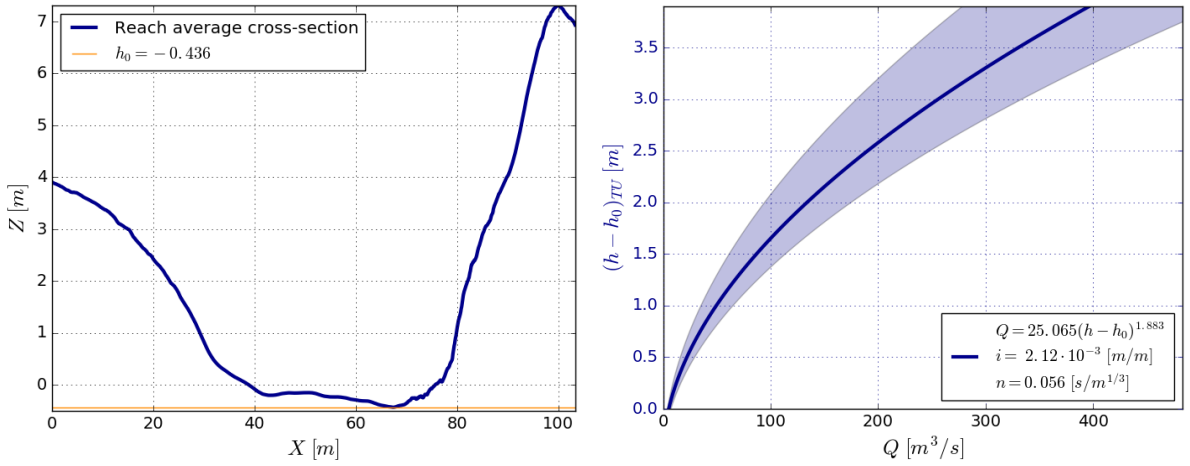

(a) Average cross-section

(b) Rating curve

Figure 5.11: Rating curve computation for Rio Duângua. The lighter blue band around the curve shows a $\pm$ 30% accuracy range.

As also mentioned in Chapter 4, Rio Mucanha (Figure 5.12) was a very difficult river to map due to the heavy overgrowth from trees on the riverbanks. Only a very small stretch of about $6.5\ m$ directly downstream of a bridge was suitable to take pictures of and even this was a difficult task due to the presence of an electricity line on that side. Due to errors in the measuring procedure, two out of seven GCPs could not be used in DEM computation.

The short reach was expected to not be long enough to see any difference in the conveyance in downstream direction ($^{dC}/_{dy}$) which is used for slope-estimation. The reason $^{dC}/_{dy}$ has been established is likely to be caused by the widening of the section as it is directly downstream of a bridge (and not by an increase in water depth). For this reason the calculated slope should not be considered to be very trustworthy. For this reason, the regional slope derived from ASTGDEM (Appendix E: $i = 2.40 \cdot 10^{-3}$) is considered to be a better approximation, and is therefore used in the displayed rating curve. In addition, this can not be considered to be a good section to establish a rating curve as the widening in the section at this location counteracts the liability of the uniform flow assumption.

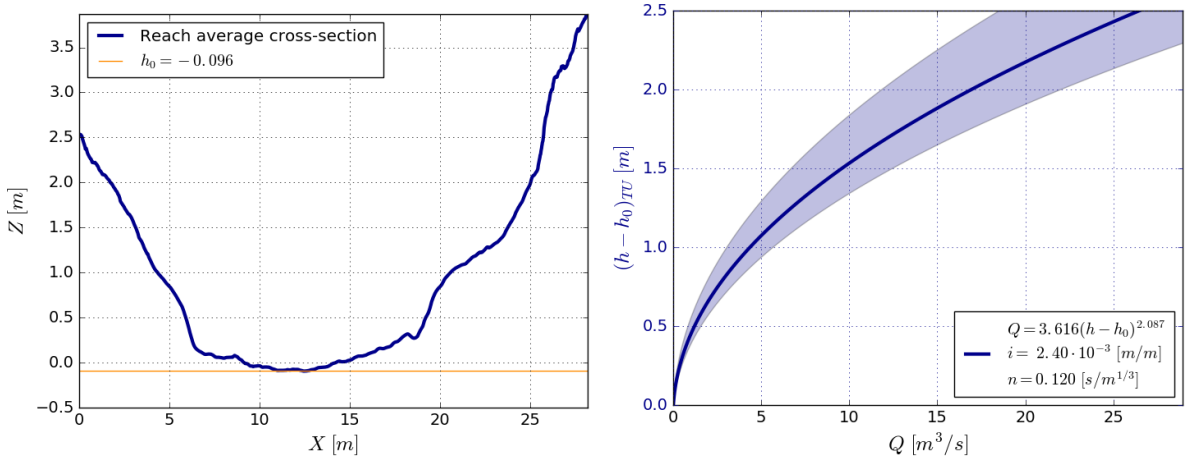

(a) Average cross-section (b) Rating curve

Figure 5.12: Rating curve computation for Rio Mucanha. The lighter blue band around the curve shows a $\pm$ 30% accuracy range.

Figure 5.13 shows results for Rio Muze. Similar to Rio Mucanha, vegetative cover was of an issue here. A stretch of about $10\ m$ directly upstream from a bridge was the only nearby location without too much overhanging trees. However, as can be seen on Figure D.1c, this could not be entirely avoided as the banks were still covered with high bushes. Removal of these disturbances for DEM computation has led to significant interpolation of data-gaps in the 3D model, thereby negatively influencing its accuracy.

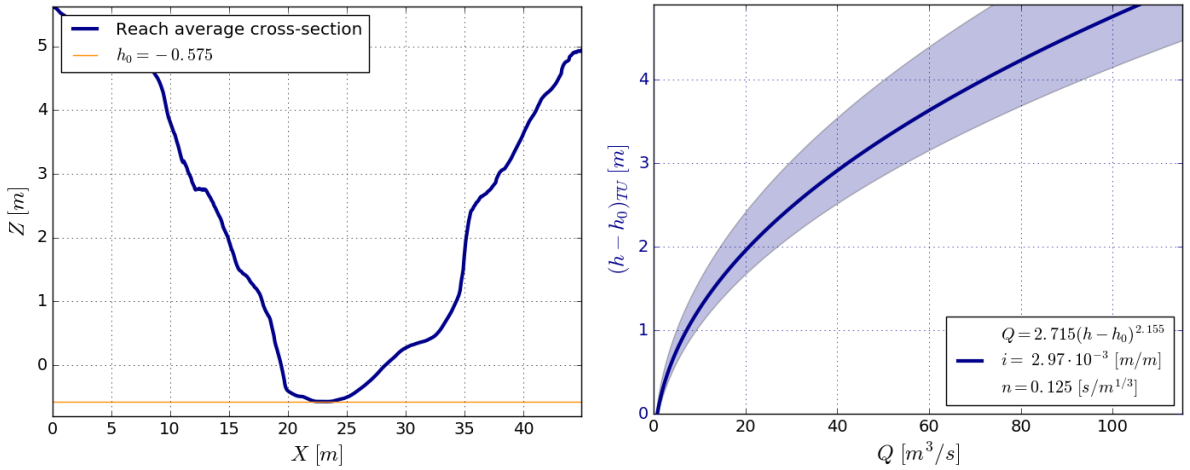

(a) Average cross-section (b) Rating curve

Figure 5.13: Rating curve computation for Rio Muze. The lighter blue band around the curve shows a $\pm$ 30% accuracy range.

As the same image also shows, still some water was present at the time of measuring. The depth-profile could not be captured due to the possible presence of crocodiles. However, on-site observation showed the water to be extremely close to stagnant and the profile was estimated to have a triangular shape towards the middle with a maximum depth of around $0.5\ m$. It is important to note the inundated area is not incorporated in the 3D model and that the processed results are based on the water-surface being the lowest point. Due to errors in the measuring procedure, three out of ten GCP's could not be used in DEM computation.

The analysed reach is not long enough to see any difference in the conveyance ($^{dC}/_{dy}$) which is used

for slope-estimation. Therefore, the regional slope derived from ASTGDEM (Appendix E: $i = 2.97{\cdot}10^{-3}$) is used.

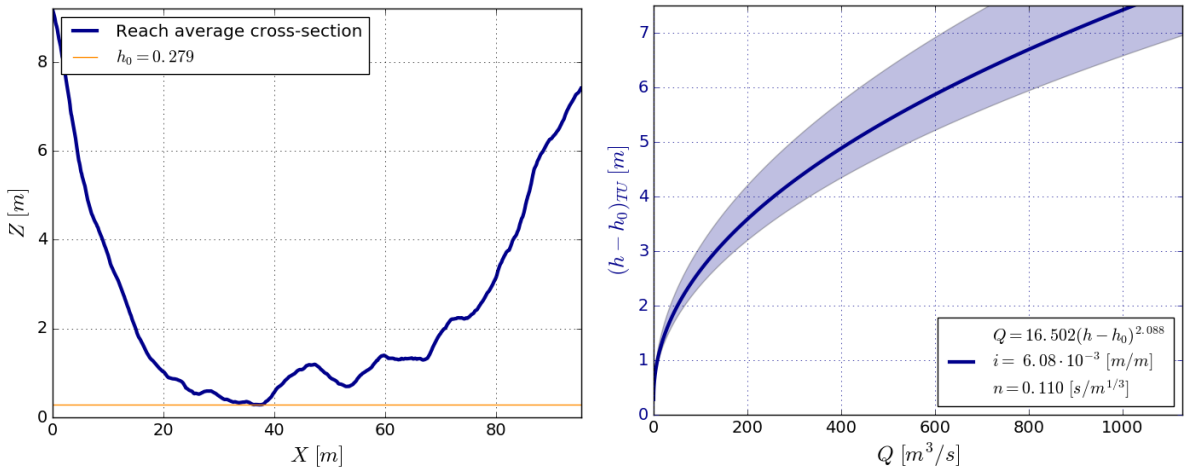

(a) Average cross-section (b) Rating curve

Figure 5.14: Rating curve computation for Rio Cherisse. The lighter blue band around the curve shows a $\pm$ 30% accuracy range.

Being the first river to be measured during the second phase of fieldwork, Rio Cherisse proved to be extra challenging due to its variable terrain and surplus of vegetation (high reeds) in the middle of the channel (Figure D.1g). As can be seen, there was still some water in the channel. However, this was flowing so slow it was hard to say if it was flowing at all. This, in combination with the fact of it being only a very small and shallow (10 to $20\ cm$) stream led to the decision to consider this to be negligible.

A long reach was chosen to minimise the impact of the vegetation in the main channel. The combination of big boulders and parts with dense vegetation made the ground-surveying to be a very tedious performance. The data-gaps that are visible in the lower right corner of the DEM (Figure D.1h) are the result of the images not being usable due to trees in that area. The resulting rating curve can be seen in Figure 5.14.

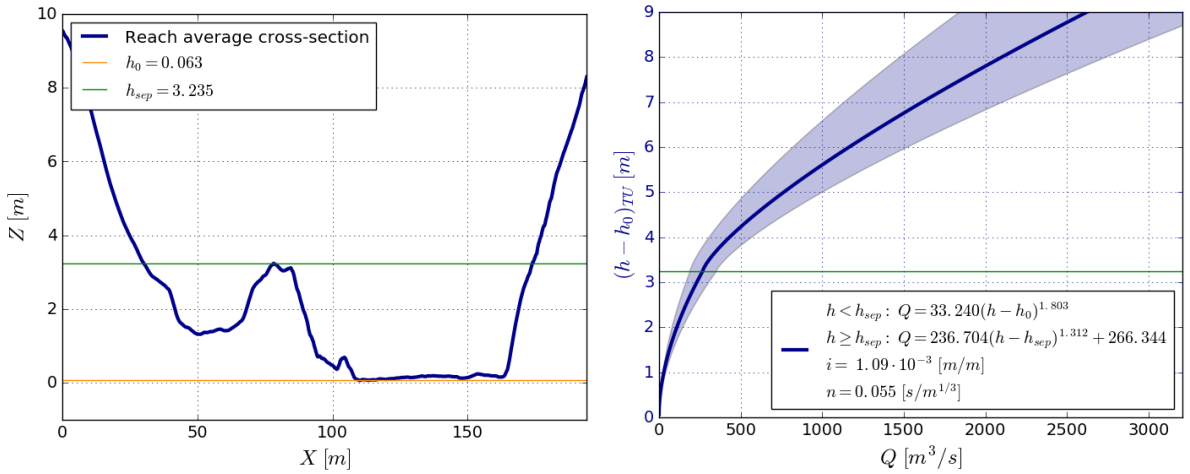

(a) Average cross-section (b) Rating curve

Figure 5.15: Rating curve computation for Rio Capoche. The lighter blue band around the curve shows a $\pm$ 30% accuracy range.

Even more so than others, the measurements at Rio Capoche suffered greatly from extreme heat

during that day. This resulted in the smart-phone (used to control the drone) to shut down to prevent from overheating as well as increasing inefficiency of the drone-battery. In addition, the size of the area limited options to cover the area with the ground control points, which were only used on the main channel and the western bank (left on Figure D.1j). The high separative bank also made it practically unfeasable to incorporate the floodplain in the ground-surveying. The effects of the floodplain can clearly be seen from the results in Figure 5.15.

In Table 5.1 it can be seen that Rio Capoche's elevation model shows a relatively large error compared to the other reaches. This is expected to be caused by (1) the fact that a large (almost halve) part of the reach is not covered by ground control points due to above-mentioned reasons, (2) due to the very uneven rocky riverbed where most of the GCPs lay on, and (3) due to local climatic conditions that complicated ground measurements.

5.4. Additional Discussion

The results have been discussed primarily in the preceding sections of this chapter. This section will elaborate on more general biases and limitations of this research and the proposed method for physically-based rating curve computation.

Probably the most important thing to note is that the proposed method for computation of a physically-based rating curve through UAV-made aerial images shows a lot of potential. However, one of the major limitations is that it does not completely exclude the need for stage-discharge measurements. It does reduce it however. At least one Q-h measurement is still needed to calibrate Manning's roughness coefficient n (and perhaps i) when a uniform n is assumed. Ideally this measurement is performed around the same time as the aerial-survey is performed in order to safeguard no significant changes in section geometry have taken place. This obviously means that enough water needs to be flowing through the river to perform accurate flow-measurements. The presence of flowing water would also provide the benefit of being able to measure the slope of the water surface. Multiple discharge measurements would provide the additional options of determination of h_0 and possibly differentiate multiple values for the roughness coefficient.

The next limitation in this research concerns the slope calculations based on $^{\mathrm{d}C}/_{\mathrm{d}y}$. Although having roughly the same order of magnitude, some difference was found in the slopes computed through the two different ways as explained in Section 3.2.6 even though they are based on the same principle: under uniform flow conditions the conveyance is constant over the length of a channel reach. Slope calculation based on the derivation (Equation (3.13)) is subjected to a set of assumptions that are a possible explanation for the different outcomes. The derivation assumes that $A = Bd$ and $R = d$. Even though, this is not an unrealistic approximation as $B \approx 180\ m$ for $d \approx 6\ m$ it is exactly that, an approximation. Another discrepancy in calculating the slope by means of Equation (3.13) is that the value for $^{\mathrm{d}C}/_{\mathrm{d}y}$ is determined in a slightly different manner than those for C and R.

In addition, another assumption that does not only influence slope calculations, is that of uniform flow. When the slope is calculated by means of levelling out $\frac{\mathrm{d}C}{\mathrm{d}y}$, this basically comes down to the attempt of making non-uniform flow ($\frac{\mathrm{d}h}{\mathrm{d}y} = 0$ and $\frac{\mathrm{d}C}{\mathrm{d}y} > 0$) uniform again ($\frac{\mathrm{d}h}{\mathrm{d}y} > 0$ and $\frac{\mathrm{d}C}{\mathrm{d}y} = 0$). The influence this assumption has on the reliability of the slope calculations does not lie within the scope of this study and it is important to note that proposed method for slope calculation has not been tested and verified with ground-data. Therefore, the method should be accepted with caution until definitively proved to hold up in further research.

Assuming uniform flow is obviously a very important assumption. It is the foundation of the physically-based rating curve (Chapter 2). However, up till which extend this is a reasonable assumption for the measured control-sections is difficult to say as this would require more knowledge on the entire downstream parts of the rivers. Even though most of the measurement were done in fairly straight river reaches, no investigation is performed to downstream obstructions that might cause significant backwater effects at certain water levels.

Another set of limitations can be assigned to the completeness of which underlying theory for rating curve and parameter computation is applied. One of such limitations is induced by using a single roughness coefficient for the entire section. In reality, n will most likely be higher for the floodplains than it is for the main channel, thereby making the roughness coefficient a function of water level. This is not incorporated in rating curve computation in this study. However, [25] showed that a uniform Manning's

coefficient can be used for the entire river profile due to parameter compensation. Floodplains usually have a higher roughness than the main channel due to vegetation, but this is compensated by the decrease in roughness caused by a higher water level.

Another limitation of note is that the proposed method does yet only focuses on computation on a 'simple' (compound) rating curve. As described by [10], rating curves can be separated into simple rating curves that are applied to uniform flow conditions, and more complex rating curves to account for:

- Backwater corrections
- Unsteady flow corrections
- Shift adjustment

A final point of discussion should be devoted to the use of (stereo-) photogrammetry software and GCPs for DEM computation. A lot of uncertainty still exists as to what the ideal data-properties and procedures for data collection are. Important properties of aerial surveying such as:

- Flying a single grid (flight-lines either normal or parallel to flow direction) or a double grid (flight-lines in both directions)
- The angle of the camera
- Optimal altitude and flight speed
- Optimal amount and positioning of ground control points

are based on personal experience and information gained from online forums and software manuals. However, scientific literature on such topics is still lacking. In addition, as also mentioned in Chapter 3, Agisoft Photoscan is a so-called black-box program as there is no detailed information on how the software exactly functions. This makes it difficult to pinpoint the cause of certain errors in the DEMs.

6

Recommendations

This research focussed on the applicability and feasibility of a newly proposed method for computation of a physically-based rating curve by using UAV-made aerial imagery in a part of the Zambezi catchment. In our view, the proposed method has the possibility to form an important step towards a more accurate procedure for off-site remote river rating than currently used methods. Being able to more accurately quantify river-flow from satellite products would mean a big step forward in the field of hydrological modelling of ungauged (or poorly gauged) basins.

Given the exploratory nature of this study (also see Section 1.2), it only makes sense that this thesis takes on an advisory perspective as well. Therefore, this chapter will discuss a set of recommendations on moving forward with this research. In doing so, a separation will be made between (1) recommendations that in the view of the researcher will benefit proposed method in general, (2) recommendations that will thereby help achieve the above mentioned goal of remote river rating and (3), both the feasibility of proposed method and the applicability of obtained results for the supporting parties in the study area of Tete, Mozambique: HCB and ARA-Zambeze.

6.1. Method in General

As discussed in Section 5.4, many uncertainties still exist with respect to the best method of aerial data collection for DEM computation. Therefore, a first step forward would be to reduce these uncertainties. Starting at the base, the following topics could highly improve data collection for DEM computation:

Flight Planning and Drone Control

Making a flight plan is essential to ensure that (1) enough pictures are collected, (2) the pictures contain sufficient overlap, (3) the pictures are of sufficient quality and (4) battery-life of the UAV is used efficiently. Made flight plans in this study are mostly based on personal experience and information gathered from online forums and manuals. Therefore it is recommended to conduct further research to the effect of different flight plan settings on the accuracy of the DEM. These settings involve: camera angle, flight-paths configuration (normal vs. parallel to flow direction) and flight speed.

One can imagine that adjusting the angle of the camera could increase the camera's ability to capture objects from the side. In this study, an angle of $80°$ ($90°$ being the camera pointing straight down) was applied in all flight plans. This decision was based on expert knowledge. However, the effect of using different camera angles in different types of landscapes has not yet been properly documented.

The same goes for using a single- or double grid flight plan, a single grid flight plan being to fly only in lines parallel or perpendicular to the flow direction and a double grid being to fly in both directions. One can easily argue that flying in both directions would yield a better view on the area of interest from different angles and is therefore preferred. However, this results in the collection of significantly more photographs and will therefore highly increase processing time which can be considered to be a negative side effect. In this study, all DEMs are based on flight plans only containing flight paths normal to the general flow direction (single grid). As the resulting elevation models are certainly not unsatisfactory it would be very interesting to investigate the added value of using double grid flight plans.

Investigating the influence of flight speed is of relevance in order to optimize the area that can be covered by the UAV as this obviously directly relates to the distance of a flight plan. This was actually considered to be one of the main limiting factors during the fieldwork in this study. As increasing flight speed could negatively influence photo quality, a trade-off has to be made between quality and maximum flight distance. Further research should investigate (1) the influence of flight speed on photo (and DEM) quality and (2) the influence of flight speed on UAV battery life and maximum flight distance.

Something that could help in all these matters is the use of appropriate software for flight planning and drone control. The researcher's decision to use Litchi was based on personal experience with this application. However, as drone's are being applied in more and more different fields of research and business, the availability and quality of these flight planning applications is increasing as well. Pix4dCapture is just one example that might have much better all-inclusive planning capabilities than Litchi. Obviously there are other options out there and it is recommended to further look into the available options for application in this field of study.

Photogrammetry Software

The pro's and con's of the used photogrammetry software, Agisoft Photoscan, have been addressed on multiple occasions. The main advantages are being user friendly and providing a wide range of options including error-calculation of the ground control points, and the main disadvantages being its high license-prices and the fact that it is a black-box program. Just like with the flight planning software, Photoscan was chosen to be used based on personal experience, but surely this is not the only option. More insight in the presence and capabilities of similar software should be obtained to conclude whether Photoscan is actually the most suitable photogrammetry software for the application of proposed method. The researcher would like to draw some extra attention to the use of an open-source software called OpenDroneMap (ODM). One advantage of using an open source software is the increasing transparency of program functionality. In addition, when working well, they tend to create a big online community that can be consulted for any type of issues. The most obvious asset is of course the financial benefit. This also increases the applicability of this method for those areas who are likely to be limited by available funding for water-resources research and related fieldwork, which is of importance to this study (Chapter 1).

GCPs

Mainly mentioned for the sake of completeness, DEM accuracy will obviously benefit from more accurate data on GCP- location and elevation. Even though sufficiently accurate elevation data can be obtained with a simple (dumpy) levelling device, this can be a very tedious job. In general it can be said that ease of the proceeding would greatly benefit from a more automated method of obtaining GCP data such as by means of using a DGPS. However, availability of equipment and accuracy of the data (especially altitude) can be of an issue. Perhaps, a composite approach can be used whereby locations are recorded with GPS and elevations are measured with a levelling device. This would save time and provide the advantage of being able to geo-reference the elevation model. When the accuracy of GPS-coordinates is doubtful, it is possible to for example, anchor the GCPs and conduct multiple GPS measurements over time, thereby increasing the likeliness of averaging out coordinate-errors. Further investigation will have to prove if this could lead to sufficiently accurate results. When available, the use of a total-station could also highly ease ground surveying practises and improve results.

In case using a dumpy level (with or without degree-circle) and a measuring tape is preferred to collect GCP data (as was the case in this study), DEM computation could be improved by allowing for GCP-specific error calculations instead of using overall values as was done here. This would require collecting more information on possible errors in the collected data induced, for example, by obstacles between GCPs.

Rating Curve Computation

Next to possible improvements for data collection and DEM computation, some recommendations should be devoted to improvement of rating curve computation. The most important of which concerns an issue that has been stipulated many times in this thesis: the need for discharge measurements. It is highly recommended to collect data when there is still water flowing through the river. This is of course, when the researcher also has the ability to actually perform Q-h measurements. This allows for

measurements of the slope and calibration of the roughness coefficient (or calibration of both) which is considered to be the biggest source of uncertainty for the high-flow regimes of the rating curves computed in this study. Multiple discharge measurements over time would improve the curve even more by (1) increasing accuracy of calibrated n and (2) allows for calibration of h_0 which is the seconds biggest source of rating curve inaccuracy, especially for low flows.

Maybe even more ideal, for rating curve computation of an intermittent river, would be to perform discharge measurements at the end of a wet-season, and perform UAV measurements somewhere in the dry-season. This way, the discharge measurements (and corresponding roughness) are still representable for that river(geometry) during the dry-season and the UAV measurements don't suffer from a partly inundated riverbed. This does however require a trade-off to be made with both logistical and financial means.

Another very interesting topic for further research would of course be the verification of the suggested method for slope calculation. Again, this would require more measurements during the wet-season or early dry-season when the rivers haven't dried up yet. The ability to calculate the (theoretical) slope of the water surface based on a detailed description of river geometry could provide a very useful tool in rating curve computation for ungauged rivers.

6.2. Towards Remote River Rating

With the current advancements in the field of remote sensing (both big-and small scale), the researchers see a lot of potential for an increased accuracy and applicability in using remotely sensed images to collect flow-data in ungauged river basins in an off-site setting. This study has aimed to provide one step in this direction, but there are definitely some more steps left. In this study, the researcher showed the potential of using aerial photography from a simple commercial drone for rating curve computation through a detailed mapping of the river's geometry. Using this detailed representation of geometry, it should be possible to establish the relation between the inundated area in the river reach and the corresponding discharge through that reach. Once this relation is known, satellite products that reveal the inundated area of a reach can then directly be transformed into discharge values. Another option is to use satellite data not to determine the inundated area, but to establish the water level at a certain cross-section [8] [16]. This can then directly be linked to the rating curve for quantification of discharge.

Further research is needed to (1) link the theoretical discharge to the inundated area of a river reach and, (2) determine which satellite products are best suitable for this specific application. Satellite images can basically be distinguished in four different classes: optical, thermal, microwave and radar. Optical images can distinguish water by its darker color. The advantages are fairly high resolutions but a big disadvantage is its dependency on clear skies (i.e. no clouds). Thermal images that can detect water by a lower temperature have the advantage of being available on small time-scales but generally have a bigger resolution than optical images do. Resolution of microwave images are coarser even still. Radar has potential as well, SAR (Synthetic Aperture Radar) in particular. The advantage of radar is that it does not care about cloud cover and therefore it always produces useful data. Another good thing is that SAR can be used to determine actual water levels as opposed to just a picture showing where there is water and where is not. The disadvantage is that SAR imagery contains a lot of noise that needs to be filtered out. However, algorithms are available for this purpose. Another downside is that altimetry with SAR is made up out of local points and therefore needs to be averaged out over larger areas. Therefore, SAR is proven to be useful for water levels on lakes and seas but might be hard to use for (smaller) rivers. Also, the satellite trajectories need to cover the area of interest which might not always be the case.

In general, it has to be investigated if the spatial scale of the available data matches what is requested. SAR and optical are likely to have a higher resolution than thermal and definitely microwave.

Another option is of course to use different sensory technologies on smaller UAVs. The most obvious (cheapest) way is to use an optical sensor as is done in this study, but UAVs can obviously be equipped with other sensors as well. This would however mean that one still has to go to the site to fly the UAV.

6.3. Supporting Parties

The objectives of the two-month period in north-western Mozambique were to (1) collect data to test proposed method for physically-based rating curve computation, (2) introduce the proposed method to local business (HCB) and water authorities (ARA-Zambeze) and (3) test and advice on applicability on proposed method in the (Mozambican) Zambezi basin. As discussed at length in Chapters 4 and 5, data collection did not go without mistakes, but the whole process both during and after these two months have created valuable insights to above-mentioned objectives. Additional to Section 6.1, a set of recommendations for the supporting parties will be discussed here. A general description of the procedures as implemented was shared with HCB staff during fieldwork. This has been improved to contain the findings of this study an can be found in Appendix B.

First and foremost, even though the results could not be validated quantitatively, the potential of applying this method has surely been demonstrated. As both parties seem to be on good collaborative terms, the researcher suggests the acquisition of a commercial drone (such as the DJI Phantom 3 Advanced/Professional or the DJI Phantom 4) by either one or both of the parties. This would allow for further validation of the method and application in future rating curve computation. Note that a drone obviously can also be of use in other applications such as basic inspection of structures. Ideally, the measurements at Rio Luia are redone but this time with inclusion of ARA-Zambeze's staff gauge in order to link elevation scales and allow for both calibration of the roughness coefficient, the stage at zero flow and further validation of the results. One thing of importance (and in this case learned the hard way) is to always include the zero of the staff gauge, if present, in the topographical survey. If there is no gauge, install a fixed reference point that can be used to link future measurements and possible connect a future gauge to.

Ones this is achieved, probably the most interesting addition would be gained by performing measurements at Rio Aruãngua. However, as infrastructural limitations make it difficult to travel upstream from the confluence with the Zambezi river, additional research is needed to establish the reliability of the rating curve for increasing water levels of the Zambezi due to backwater effects. This additional research should determine whether or not it is useful to compute a rating curve for a section so near to a big confluence point. It is likely that if a rating curve would be computed, the accuracy of the curve is highly dependent on the water level of both the Zambezi and Aruãngua itself. Because the discharge of the Zambezi is largely controlled by dams, flow of the Aruãngua can surpass that of the Zambezi during the wet-season. This has also been confirmed by local staff. In that case, the physically-based rating curve could still provide a significant improvement on high-flow river rating. Very important, especially when measuring a big site like Rio Aruãngua, is to ensure one has enough time. It is recommended to plan for at least one whole day at the site in order to collect all the required data with sufficient accuracy and precision. If not yet completely familiar with the proceedings, even more time could be needed. In addition, in this particular case it is highly recommended to ensure one has the required permissions to fly a drone over the border area. This might also increase the time needed at the location.

As not all tributaries are of direct interest to HCB due to their confluence points being downstream of the dam, some additional attention will be paid to the visited tributaries upstream of the dam. The measuring site at Duângua proved to be a very suitable place for the measurements. However, as is the case for all visited upstream-tributaries except for Aruãngua, no flow data is available there. A rerun of data-collection at the site of Duângua could proof to be useful as some beginner's mistakes were made during data collection there (Section 5.3). For the other tributaries (i.e. Rio- Mucanha, Muze and Tongoé) it would be advisable to look for better locations, as measurements for all these rivers were significantly influenced by a surplus of vegetation. This is of course a trade-off one has to make between having a suitable cross-section and the effort it takes to reach that cross-section. In any case, in the absence of better alternatives and/or discharge data, the physically-based rating curve can successfully provide a rough estimate of the relation between discharge and water level for these tributaries.

7

Summarizing Conclusions

This thesis study aimed to provide a solution for the shortcomings concerning conventional rating curve computation. In a response to the many limitations and uncertainties in discharge monitoring in general, but especially for ungauged catchments, the researchers see big potential in the use of state-of-the-art remote sensing technologies such as the use of an unmanned aerial vehicle (UAV). A vision of an improved manner of off-site remote river rating, where satellite images are used for accurate discharge monitoring of (ungauged) river catchments, is the main driver behind this research. This study has presented a step towards this concept of remote river rating by using a simple commercial UAV in the improved computation of rating curves.

Conventional rating curve computation struggles with the issues of being data-intensive, inaccurate in high-flow regimes and susceptibility to changes in cross-sectional geometry. In the view of the researchers, an answer can be found in a more physically-based rating curve that allows for substantiation through a detailed representation of the river's geometry. Apart from (1) increasing accuracy by removing the need for extrapolation to high-flow regimes, the physically-based rating curve would (2) be less susceptible to changes in geometrical changes due to scouring and sediment-deposition, (3) be more easily to update if geometrical changes do occur, and (4) would require much less data and is therefore likely to be cheaper to establish. The physically-based rating curve is based on Manning's formula for steady uniform flow (Equation 2.3). In order to make a comparison to conventional rating curves, Manning's formula can be rewritten to a power-law function (Equation 2.4) whereby a separation is made between a part that captures the geometry of the river ($a_2(h-h_0)^b$) and a part that accounts for slope and roughness (a_1).

In order to test the hypotheses and fulfil the supporting objectives (Section 1.2), the research included two months of fieldwork in the north-western Tete province of Mozambique. Here, as a guest of HCB in Songo, the researcher collaborated with local parties HCB and ARA-Zambeze to perform measurements on a set of tributaries to the Zambezi river. Eight rivers were visited in total of which two the data was of insufficient quality and quantity to be used in further analysis (Chapters 4 and 5). In addition, the visit to Songo was also meant to provide local staff with introductory training in the proposed method for physically-based rating curve computation and the corresponding data collection (Section 4.2).

A DJI Phantom 4 was used in combination with a third-party flight-planning software called Litchi to collect the aerial imagery. Square wooden plates of $50 \times 50\ cm$ with a 2 by 2 black and white chessboard pattern were used as markers for the ground control points (GCPs). Litchi provides many options for detailed flight-planning but its non-automated way-point based structure can be considered to be somewhat cumbersome. In addition, when in a flight-mission, all manual control will be overruled making it impossible to perform small manual adjustments without aborting the mission. The markers were very clearly visible from high altitudes and could have even been a bit smaller to ease transportation.

A single grid flight path was flown perpendicular to the flow direction. Attempted image overlap was 80% in the forward direction, 60% in the sideways direction and the photogrammetry software Agisoft Photoscan was used for digital elevation model (DEM) computation. All further analysis was done in Python.

The fieldwork was divided into two phases. During the first phase, a dumpy level with degree-circle was used to set up a local grid-system (XYZ) of GCP locations and elevations. A lack of experience resulted in insufficient measurements which led to some of the GCPs being excluded from further processing. For the same purpose, during the second phase a dumpy level without degree-circle was used for collection of elevation data and a $50\ m$ measuring tape was used to set up a system of triangles (Figure 3.6) for determination of GCP-location.

Both the two months in Mozambique and the preparative phase leading towards it have been a period full of challenges and valuable lessons and has therefore been a very important part of this study. The most important challenges and take-home messages include (also see Section 4.5):

1. Communication. Especially in the field, the language barrier proved to be a hampering force on some occasions. It would have been advisable to have a detailed briefing on fieldwork activities (before and after) in Songo/Tete where English-speaking personnel is able to help out.

2. Organisational. A mix of formal and informal agreements, combined with misplaced assumptions are likely to cause problems in general proceedings. Therefore, it is important to establish clear lines of communication and make explicit agreements on roles and responsibilities in the cooperative framework.

3. Knowledge and skills. Make sure to know which equipment is really available during the actual data collection and how to work with this equipment by doing test-runs.

4. Environment and climate. A reconnaissance to the measurement area will really benefit the assessment of environmental constraints such as dense vegetation or the presence of water and dangerous wildlife. Climatic constraint are obviously hard to avoid entirely but one can use seasonality to increase the change on favourable weather (and environmental) conditions.

Results have been produced for six different river-reaches: Rio- Duângua, Mucanha, Muze, Cherisse, Capoche and Luia. The measurable areas on the sites of Rio Mucanha and Muze were both heavily limited by dense vegetation on the riverbanks. Two factors seem to be of main influence to accuracy of the DEM: coverage of the area by GCPs and the presence of tall vegetation. Absolute errors range from $0.16\ m$ (Mucanha) to $2.57\ m$ (Capoche) in the XY direction and from $0.01\ m$ (Luia) to $0.30\ m$ (Muze) in the vertical direction (Z). The relatively high ε_{XY} for Rio Capoche is assumed to be caused by the low overall coverage of GCPs due to a high separative bank in the middle of the river (see Figure D.1j). See Table 5.1 for a complete overview of DEM specifications. It can be concluded that a high resolution elevation model can be computed showing very little relative error in both the horizontal plane (max 1.90%) and the vertical plane (max 3.65%). When Rio Muchanha and Muze are excluded due to their excessive disruption by vegetation, these values decrease to a maximum relative horizontal error of 0.85% and a maximum relative vertical error of 1.34% (both for Rio Capoche).

Rating curves have been computed for the six tributaries. Because historical Q-h data (from ARA-Zambeze) was only available for Rio Luia, only this river is used for analysing method performance. Figure 5.2 shows reach average cross-section and the relation between a set of geometrical parameters (A, P and R) with water level for this cross-section. The reach average cross-section is obtained by averaging 2469 (in the case for Rio Luia) individual cross-section contained in the DEM. It can be seen that non-uniformities are averaged out. The graphs show a clear separation between the main channel and the floodplains, which stipulates the need for a compound rating curve as opposed to one single Q-h relation. The relation between stage (h) and the conveyance (C or $AR^{2/3}$ $[m^{8/3}]$) is used to capture the geometry of the section in a power-law function (Equation 2.4 and Figure 5.3).

A lack of flowing water in the observed rivers gave rise to the need for an alternative way of quantifying the a_1 parameter depending on slope (i) and bed-roughness (n). When a constant water level ($i = 0$) is assumed in the downstream direction (Y) of the reach, the conveyance should increase due to an increasing water depth. Therefore, by plotting $AR^{2/3}$ against Y and applying linear regression, $\mathrm{d}C/\mathrm{d}Y$ can be determined for a certain constant stage. By enforcing a slope on the water surface, $\mathrm{d}C/\mathrm{d}Y$ can be brought down to zero, which in theory corresponds to the situation for uniform-flow. Through this iterative process, the theoretical 'local' slope corresponding to uniform flow in the measured reach can be established. For Rio Luia this resulted in slope of $i = 2.23 \cdot 10^{-3}\ m/m$. This corresponds to on-site observations and direct approximations based on the DEM. A compartive measure was formed

by deriving the 'regional' slope from ASTGDEM by looking at the elevation profile of a reach of $20\ km$ around the measuring location. Table E.1 shows that even though the local and regional slopes are in the same order of magnitude, the have about a factor two difference. This shows that the slope is likely to be influenced by the water level (i.e. local slope will dominate low flows and regional slope will dominate high flows) and stipulates the importance of (1) calibration or real time measurements of i and (2) the need to validate proposed method for slope calculation. Manning's roughness coefficient had to be calculated based on literature and was estimated to be $0.050\ sm^{-1/3}$. Insufficient data led to not being able to compute h_0 which is therefore equated to the lowest point of the cross-section, as is deemed to be a good approximation for a channel-controlled section [10]. The final resulting physically-based compound rating curve can be seen in Figure 5.6.

Due to a very unfortunate flaw in the obtained data, the elevation scale from the self-determined local grid at the measuring site could not be linked to the elevation scale used for ARA-Zambeze's Q-h data, thereby making it impossible to quantify rating curve performance based on the available historical data. Performance is therefore qualitatively assessed by means of visual analysis and expert judgement. However, as both h_0-values where close to zero, it is deemed unlikely that the scale-difference in elevation is very large. This gives reason to suggest the TU-computed rating curve should follow the same pattern as that of ARA-Zambeze. Especially in the the low flow regime as Q-h data in the high flow regime is very limited in quantity and therefore reliability. Additional analysis is performed to adapt the curve to the available discharge data by changing n, i, and their combined influence as a_1 ($n^{-1}\sqrt{i}$). The initially computed rating curve (Figure 5.6) shows to overestimate flow compared to that of ARA-Zambeze. However, taking into account parameter uncertainty, validity of the Q-h data and the fact that cross-sections do not completely match it can be concluded that the physically-based rating curve shows sufficient similarity with that of ARA-Zambeze's to assume the validity of the method for physically-based rating curve computation. Figure 5.7 shows the amount of change in n, i, and a_1 that is needed to fit the curve to the available Q-h data. When the computed slope is assumed correct, the required increase in the roughness coefficient shows a somewhat unrealistic underestimation of n. When the slope is decreased as well, the roughness shows to be underestimated by a value of about 0.02 for the main channel and $0.03\ s/m^{1/3}$ for the flood plain. A roughness coefficient of $0.07\ s/m^{1/3}$ for a fairly clean main channel can still considered to be on the high side, leading to suggest that the uncertainty in h_0 is also of significant influence. Overall, the fact that this method allowed for an easy extension to the high-flow regime in the form of a compound equation is deemed to be an improvement on a single curve as is used by ARA-Zambeze.

A sensitivity analysis is performed to quantify the influence of parameter uncertainty on rating curve performance. Not taking parameter uncertainty into account, the b exponent can be seem to have the biggest influence on the shape of the rating curve. A more or less equal impact can be subscribed to n and a_2, and changes in i have a relatively low impact. Theory of error propagation is used to quantify the relative contribution of the uncertainties in the parameter values (Table 5.4). The error in Q can be seen to lie between 67% and 30% for the non-calibrated case but this decreases to values between 50% and 13% depending on water level. An important observation is that the uncertainty of h_0 has a very big influence for low water levels (42% at h_1) and becomes significantly lower at higher water levels (4.2% at h_3). Both i, a_2 and b have a relatively low contribution to the uncertainty in Q where especially b has a very minor contribution. This analysis shows that, in exception for very low-flows, accuracy of the physically based rating-curve will benefit most from decreasing uncertainty in n. For low flows, the major contribution to the error comes from uncertainty in h_0. Relative to the other parameters, h_0 remains to be of influence but this significantly decreases with increasing water level. Therefore, another important observation to make is that in contrast to conventional rating curve computational procedures, the physically-based rating curve shows an increasing accuracy for increasing water levels due to the decreasing influence of the error in h_0. This resolves the biggest flaw in conventional rating curve computation, the decreasing predictive capability for high flows due to extrapolation of low flow data.

Referring to the aim of this study with the underlying objectives and hypotheses (Section 1.2), the overall conclusions are as follows. By means of using a simple commercial UAV and ground surveying equipment, an accurate high-resolution elevation model of a river reach can be made. This can however be tempered by extensive vegetation. The elevation model can successfully be used to compute a

physically-based (compound) rating curve that includes the high-flow regime. The ability to apply non-linear regression in capturing the relation between stage and section geometry performs better than applying linear regression on double-logarithmic Q-h data as is done in conventional methods. In addition, when there is no flowing water in the river, the DEM can be used to calculate the theoretical local slope corresponding to uniform flow conditions. The biggest overall limiting factor to accuracy is the need to calibrate n which requires at least one relevant flow measurement. For the low flows, inaccuracy in h_0 also has a big influence. When the roughness coefficient can be calibrated, the error in the physically based rating curve can be in the order of magnitude of 10% or less in the high flow regime of the river. This is considered to be a huge improvement compared to extrapolated high flow predictions in conventional rating curves. Updating of the rating curve can also be done with higher accuracy. As the method does not exclude the need for flow measurements, applicability of the proposed method is considered to have improved only slightly. However, the reduction of the needed amount of Q-h data is of course beneficial. As this study has shown, a rough approximation of the Q-h relation can be made without flow-measurements, which might be sufficient for some applications. Accessibility can not be considered to have improved as more equipment is needed when compared to conventional rating practises. However, it is of course possible that the benefits that a more accurate rating curve has on water resources planning, e.g. the ability to more accurately predict high flows, can make it financially attractive to invest in the needed equipment. Recommendations include:

1. Additional research to optimize flight planning. This includes research on both the use of other third-party software as well as specific characteristics like flight-speed, camera angle and flight-path configuration.

2. Look into the use of open-source photogrammetry software such as ODM and if possible, use more advanced surveying equipment to collect GCP data.

3. Collect discharge data at the end of the wet-season and collect the geometrical data somewhere along the following dry-season. This way collection and processing of the geometrical data is highly simplified and the discharge-measurement is still representable for the measured geometry. This of course only makes sense for intermittent rivers or rivers that have a significant difference in flow between wet and dry season.

4. Additional research to validate the proposed method for slope calculation based on $\mathrm{d}C/\mathrm{d}Y$.

5. Additional research to (1) use the measured geometry to link the inundated area of a river reach to discharge and (2) determine which satellite images are best suitable to accurately determine either the inundated area of a given reach or the cross-sectional water-depth profile.

For more elaborate documentation on all recommendations, please consult Chapter 6.

References

[1] Agisoft LLC. AgiSoft PhotoScan Professional (Version 1.4.0) (Software). Retrieved from http://www.agisoft.com/downloads/installer/, 2017.

[2] Agisoft LLC. Agisoft Photoscan Professional (version 1.3)(Software Manual), 2017.

[3] Anuar bin Md. Ali. *Flood Inundation Modeling and Hazard Mapping under Uncertainty in the Sungai Johor Basin , Malaysia*. PhD thesis, TU Delft, 2018.

[4] Douglas E. Alsdorf, Ernesto Rodriguez, and Dennis P. Lettenmaier. Measuring surface water from space. *Reviews of Geophysics*, 45(2):RG2002, may 2007.

[5] P Ankum. Design of Open-Channels and Hydraulic Structures. *Lecture notes for CT3410*, (October), 2002.

[6] George J. Jr. Arcement and Verne R. Schneider. Guide for Selecting Manning ' s Roughness Coefficients for Natural Channels and Flood Plains. 1989.

[7] H. H. Barnes Jr. Roughness Characteristics of Natural Channels. *Technical Report, Geological Survey Water-Supply, United States Government Printing Office, Washington, U.S.A*, page 219, 1987. ISSN 00221694.

[8] S. J. Birkinshaw, G. M. O'Donnell, P. Moore, C. G. Kilsby, H. J. Fowler, and P. A.M. Berry. Using satellite altimetry data to augment flow estimation techniques on the Mekong River. *Hydrological Processes*, 24(26):3811–3825, 2010. ISSN 08856087.

[9] W.L. Cowan. Estimating hydraulic roughness coefficients. *Agricultural Engineering*, 37(7):473–475, 1956.

[10] DHVC and Delft Hydraulics. How to establish stage discharge rating curve. Technical Report November, DHVC, Delft Hydraulics, New Delhi, 1999.

[11] G. Di Baldassarre and A. Montanari. Uncertainty in river discharge observations: A quantitative analysis. *Hydrology and Earth System Sciences*, 13(6):913–921, 2009. ISSN 16077938.

[12] Giuliano Di Baldassarre and Pierluigi Claps. A hydraulic study on the applicability of flood rating curves. *Hydrology Research*, 42(1):10, 2010. ISSN 0029-1277.

[13] J. E. Freer, H. McMillan, J. J. McDonnell, and K. J. Beven. Constraining dynamic TOPMODEL responses for imprecise water table information using fuzzy rule based performance measures. *Journal of Hydrology*, 291(3-4):254–277, 2004.

[14] GitHub Inc. Scientific PYthon Development EnviRonment (SPYDER). Available at https://github.com/spyder-ide/spyder.

[15] Kateryna. https://blog.propelleraero.com/5-things-to-know-about-drone-data-accuracy, 2016.

[16] J G León, S Calmant, F Seyler, M.-P Bonnet, M Cauhopé, F Frappart, N Filizola, and P Fraizy. Rating curves and estimation of average water depth at the upper Negro River based on satellite altimeter data and modeled discharges. *Journal of Hydrology*, 328(3):481—-496, 2006.

[17] W.M.J. Luxemburg and A.M.J. Coenders. CIE4440 Hydrological Processes and Measurements (Lecture notes), 2015.

[18] R. Manning. On the flow of open channels and pipes. Inst. *Civil Eng. Ireland*, 20:161–207, 1891.

[19] Nasim Mansurov. photographylife.com/iso-shutter-speed-and-aperture-for-beginners, 2018.

[20] Hilary McMillan, Jim Freer, Florian Pappenberger, Tobias Krueger, and Martyn Clark. Impacts of uncertain river flow data on rainfall-runoff model calibration and discharge predictions. *Hydrological Processes*, 24(10):1270–1284, 2010. ISSN 08856087.

[21] NASA/METI/AIST/Japan Spacesytems and U.S./Japan ASTER Science Team. ASTER GDEM is a product of NASA and METI. ASTER Global Digital Elevation Model Version 2 [Data set], 2011.

[22] Asgeir Petersen-Øverleir. A hydraulics perspective on the power-law stage-discharge rating curve. *Report / Norges vassdrags- og energidirektorat*, (5-05):26 s., 2005.

[23] Python Software Foundation. Python Software Foundation. Python Language Reference, version 2.7. Available at http://www.python.org.

[24] Bart Strijker. A Physics-Based approach for Rating Curves to Reduce Uncertainties A New Concept for Hydrological Model Calibration. Additional Thesis, Delft University of Technology, 2017.

[25] Ven Te Chow. *Open Channel Hydraulics*. McGraw-Hill Book Company, Inc; New York, New York, 1959.

[26] Albert I. J. M. Van Dijk, G. Robert Brakenridge, Albert J. Kettner, Hylke E. Beck, Tom De Groeve, and Jaap Schellekens. River gauging at global scale using optical and passive microwave remote sensing. *Water Resources Research*, 52:6404–6418, 2016.

[27] VC Technology Ltd. Litchi for iOS (version 2.2) (Software). Available in App Store and Google Play, 2017.

[28] Wikimedia Foundation. https://en.wikipedia.org/wiki/Root-mean-square_deviation, 2018.

[29] Kun Yan, Giuliano Di Baldassarre, Dimitri P. Solomatine, and Guy J.-P. Schumann. A review of low-cost space-borne data for flood modelling: topography, flood extent and water level. *Hydrological Processes*, 29(15):3368–3387, jul 2015.

A

Fieldwork Data-forms

This Appendix shows a set of forms and tables that have been made to aid flight planning and data collection. All have been made in Microsoft Excel and can be shared if wanted. Figures A.1 and A.2 present the data form used to collect all relevant information about the measuring location. Figure A.3 shows the form that is made to log the levelling measurements for GCP elevation and possibly location. After collection, the information should be digitalised as soon as possible.

Figures C.3 to C.5 present a set of tables that are used for flight planning (See Section 3.2.2).

General Information			
Name Site:		Date:	
Time of arrival:		Time of flight:	
Weather Conditions			
Precipitation:	Dry / Drizzle / Rain	(Est.) Temperature:	°C
Light:	Clear / Vail / Lightly Clouded / Medium Clouded / Very Clouded		
Wind:	Still / Soft / Medium / Hard	Direction:	
Section Details			
Length:	m	Width:	m
Flowing Water: YES / NO		Stagnant Water: YES / NO	
(Est.) Depth:	m	(Est.) Depth:	m
(Est.) Flow:	$L/m^3/s$	(Est.) Flow:	$L/m^3/s$
Comments on vegetation:			
Slope and Roughness			
Length between markers:	m		
Upstr. elevation:	m	Downstr. elevation:	m
Comments on slope measurement:			
Bottom Composition:			
Flight Details			
Length Flypath:	m	Flight Duration:	min
Speed:	km/h	Shutterspeed:	1/ sec
Min. GSD:	cm/pix	Altitude:	m
GSD:	cm/pix	Photo Interval:	sec
Additional Comments:			

Figure A.1: Site-form 1: General information

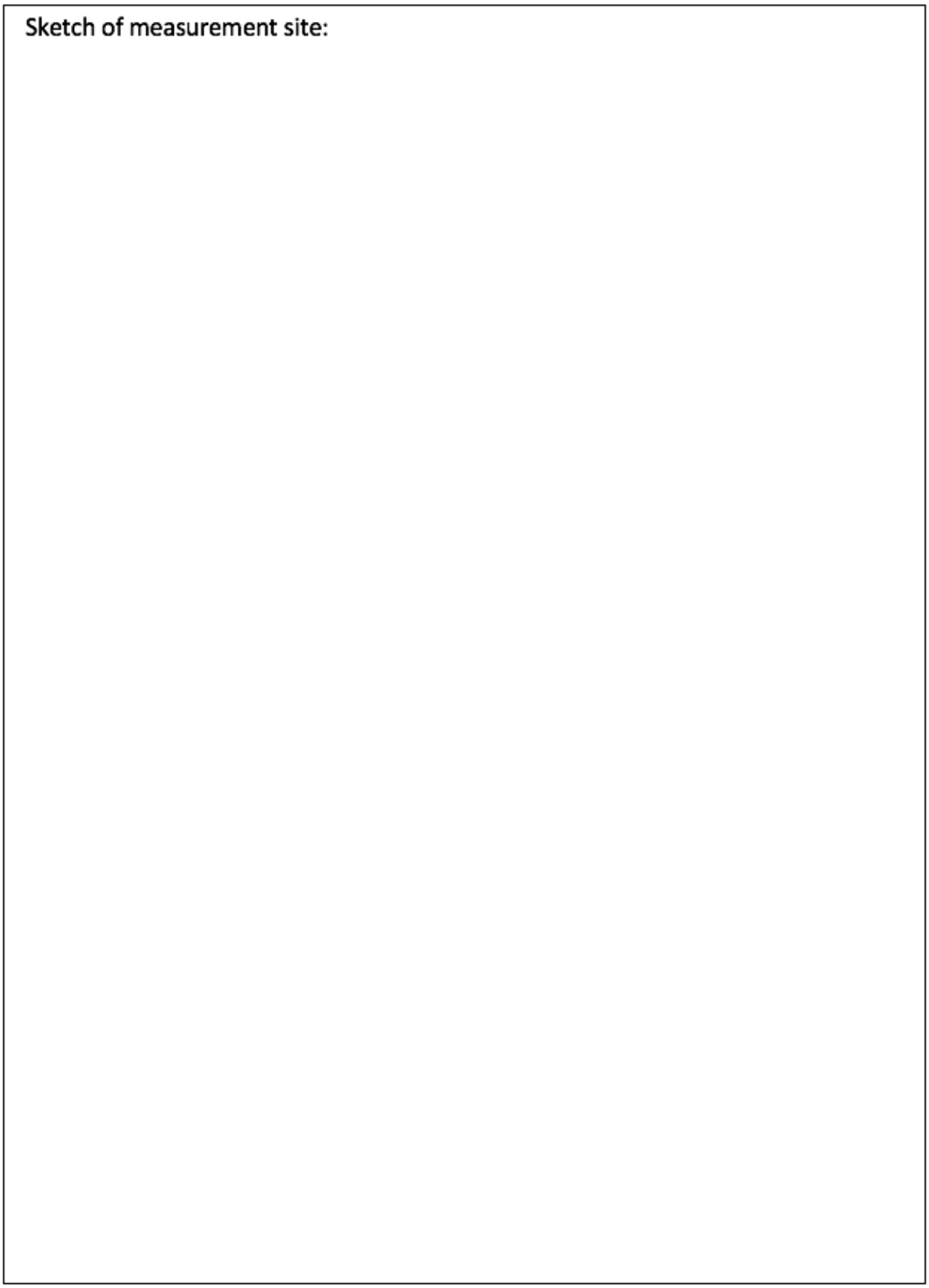

Figure A.2: Site-form 2: Situation sketch

Point ID:		
Level / Theodolite		
	Position1:	Position2:
Elevation / Middle mark:	mm	mm
Upper mark:	mm	mm
Lower mark:	mm	mm
(Upper + Lower) / 2:	mm	mm
Same as Middle? (±5mm):	YES / NO	YES / NO
Distance (Upper - Lower):	mm	mm
Distance Measuring Tape:	mm	mm
Angle:	°	°
(D)GPS		
Coordinate system:	WGS84:	UTM / DD / DMS
Vertical Datum:		
Y / Latitude / Southing:		
X / Longitude / Easting:		
Altitude:		
Comments/notes:		

Point ID:		
Level / Theodolite		
	Position1:	Position2:
Elevation / Middle mark:	mm	mm
Upper mark:	mm	mm
Lower mark:	mm	mm
(Upper + Lower) / 2:	mm	mm
Same as Middle? (±5mm):	YES / NO	YES / NO
Distance (Upper - Lower):	mm	mm
Distance Measuring Tape:	mm	mm
Angle:	°	°
(D)GPS		
Coordinate system:	WGS84:	UTM / DD / DMS
Vertical Datum:		
Y / Latitude / Southing:		
X / Longitude / Easting:		
Altitude:		
Comments/notes:		

Point ID:		
Level / Theodolite		
	Position1:	Position2:
Elevation / Middle mark:	mm	mm
Upper mark:	mm	mm
Lower mark:	mm	mm
(Upper + Lower) / 2:	mm	mm
Same as Middle? (±5mm):	YES / NO	YES / NO
Distance (Upper - Lower):	mm	mm
Distance Measuring Tape:	mm	mm
Angle:	°	°
(D)GPS		
Coordinate system:	WGS84:	UTM / DD / DMS
Vertical Datum:		
Y / Latitude / Southing:		
X / Longitude / Easting:		
Altitude:		
Comments/notes:		

Point ID:		
Level / Theodolite		
	Position1:	Position2:
Elevation / Middle mark:	mm	mm
Upper mark:	mm	mm
Lower mark:	mm	mm
(Upper + Lower) / 2:	mm	mm
Same as Middle? (±5mm):	YES / NO	YES / NO
Distance (Upper - Lower):	mm	mm
Distance Measuring Tape:	mm	mm
Angle:	°	°
(D)GPS		
Coordinate system:	WGS84:	UTM / DD / DMS
Vertical Datum:		
Y / Latitude / Southing:		
X / Longitude / Easting:		
Altitude:		
Comments/notes:		

Point ID:		
Level / Theodolite		
	Position1:	Position2:
Elevation / Middle mark:	mm	mm
Upper mark:	mm	mm
Lower mark:	mm	mm
(Upper + Lower) / 2:	mm	mm
Same as Middle? (±5mm):	YES / NO	YES / NO
Distance (Upper - Lower):	mm	mm
Distance Measuring Tape:	mm	mm
Angle:	°	°
(D)GPS		
Coordinate system:	WGS84:	UTM / DD / DMS
Vertical Datum:		
Y / Latitude / Southing:		
X / Longitude / Easting:		
Altitude:		
Comments/notes:		

Point ID:		
Level / Theodolite		
	Position1:	Position2:
Elevation / Middle mark:	mm	mm
Upper mark:	mm	mm
Lower mark:	mm	mm
(Upper + Lower) / 2:	mm	mm
Same as Middle? (±5mm):	YES / NO	YES / NO
Distance (Upper - Lower):	mm	mm
Distance Measuring Tape:	mm	mm
Angle:	°	°
(D)GPS		
Coordinate system:	WGS84:	UTM / DD / DMS
Vertical Datum:		
Y / Latitude / Southing:		
X / Longitude / Easting:		
Altitude:		
Comments/notes:		

Figure A.3: GCP data-form

B

Fieldwork Procedures

This appendix provides a document containing a general description of fieldwork procedures. It does not alter from the information given in Chapter 3. Two forms that were already shared with HCB-staff in the preparation phase of the fieldwork in Mozambique, are combined and improved based on the findings of this study.

Here follows a description of the tasks that need to be performed when collecting the field data, as well as important things to keep in mind when doing so. Most importantly, make sure you have enough time and measure as accurate and precise as possible. It goes without saying that proper preparation will result in better performance. Think about preparing flight-paths and making sure all UAV equipment is fully charged and updated with latest software.

Needed materials

- UAV (e.g. DJI Phantom 4) with sufficient batteries and spare propellers
- Mobile phone or tablet with aerial surveying software (e.g. Litchi)
- Spatial referencing instrumentation (e.g. theodolite, level, (D)GPS, or a combination of these)
- Measuring-tape
- Markers / Ground Control Points (at least 10)
- Recommended: power-bank, calculator, stopwatch, clipboard, iPad/tablet (to write down data digitally)

Workflow

Reconnaissance:

1. Reconnaissance of measuring location.

   Explore the river for what would be the best section to perform measurements on. Note that river flow will be estimated using Manning's formula, which theoretically only holds for steady uniform flow conditions, meaning no change in flow over time and uniformly distributed water depth over the length of the reach. Therefore, it would benefit the measured section if conditions for uniform-flow are achieved as much as possible. Keep in mind:

   - Sections should be 100 – 300 meters long in order to get proper averages. Obviously a reach of 300 meters is preferred above a reach of 100 meters. The longer the section, the better the estimate of the slope will be.
   - Out of reach of backwater-effects caused by e.g. river confluences, water off-take, big changes in river profile/slope, and obstructions (e.g. bridges).

- A straight section would be most beneficial for easy processing of the results. So, no bends if possible.
- The less trees and bushes, the better. High grass is also better to avoid but is easier to cut away if needed. Avoid high reeds and also be aware of possible obstruction like power-lines.
- At least one discharge measurement needs to be available for the section in order to calibrate the Manning's coefficient.

Topographical survey part 1 - Measuring marker locations and elevations:

Always make sure that the (zero of the) gauge, if present, is included in the topographical survey. If there is no gauge, install a fixed reference point that can be used to connect a gauge (and future measurements) to (transferir a cota).

2. Read the water level on the (staff-)gauge.
3. Positioning of the markers/ground control points (GCPs).
    - Some pre-testing has showed that the best way is to use markers that are square plates of about 40x40 cm with 4 tiles of 20x20 (2 black and 2 white).

B	W
W	B

    - A minimum of 10 markers should be used but more is better.
    - Try to maximize putting markers on different height-levels in the main channel and floodplain.
    - The markers should be spread out over the area as much as possible to minimize extrapolation.
    - Do not place markers in close vicinity of trees as this causes larger errors.
    - Do not put markers on high grass. Very short grass does not seem to be a problem. If there is a lot of high grass in the measurement area, it should be cut away as much as possible.
    - If there is a steep and abrupt slope, place markers on both side of the edges.
    - Placing markers along the edge of the waterline helps identify the waterline as this has proven to be difficult to see in some cases.
    - Use 2 markers to form a line normal to the flow direction and 2 for a line parallel to the flow direction (e.g. by creating a 90° triangle using prepared pieces of rope). This will be helpful when a local grid-system is to be set up.
4. Sketch the site including the markers for notation of location data, and start filling in the site-form (Appendix A). Don't forget to comment on the bottom-composition and vegetation.
5. Collect location and elevation data of the markers.

    This can be done by means of spatial referencing instrumentation (e.g.: (dumpy) level, total station, DGPS). One can also use a measuring-tape to create a system of triangles with known distances. Use the data-form (Appendix A) and sketch to write down all information. The following procedure is recommended when using a levelling-instrument without a degree-circle for elevation-measurements and a measuring-tape for distance measurements..

    - Write down values for upper, lower, and middle indicator line.
    - Let someone else DOUBLE-CHECK these values.
    - The average value of the upper and lower line should equal the value of the middle line. CHECK THIS RIGHT AWAY AND NOT AFTERWARDS. Use a calculator to make it easier and faster.
    - If correct, this checked middle value is the altitude value of the marker-point.

- The difference (in cm) between the upper and the lower value is the distance to the marker-point in meters. However, this distance is less precise than using a measuring-tape and is therefore recommended to only be used to provide a method to check measuring-tape measurements.
- Measure marker-to-marker distances with measuring-tape. Use sketch to write down information.

Note: When the level needs to be re-located, make sure to measure at least 1 of the same markers as from the previous level-location in order to link elevation measurements. When a level with degree-circle is used, and the angles are used to determine GCP locations, at least 2 overlapping measurements are necessary. **Again: Do not forget to include the staff-gauge in the elevation measurements.** When all markers are successfully included in the ground-survey, they should remain on the exact same location until aerial photography is finished.

6. When present, measure the slope of the water surface. Make sure the distance over which slope is measured is as long as possible. If there is still some water flowing, measure the water level by for example putting a rock along the shoreline in such a way that its surface is equal to the water surface. Do this at the beginning and the end of a section to make an estimate of the water surface slope.

Topographical survey part 2 - Aerial image collection:

7. Prepare and/or fine-tune flight-plan. Important aspects of the flight-plan are overlap, altitude, GSD and flight speed. **Preferable this is done in advance as much as possible (Section 3.2.2 and Appendix C)**. When the Litchi application is used, keep in mind that:
    - Use either ”Auto” or ”Custom” for the ’heading’ in mission settings. Auto: the aircraft will point towards the next waypoint. This is probably easiest. Custom: the aircraft will assume the heading that you have to manually define for each waypoint.
    - Make a flightpath by adding waypoints. In waypoint 1, set the adjustment of the gimbal-angle to -80° as an action-point.
    - Set the ’finish action’ in Litchi to ”RTH” (return to home) and the ’path mode’ to ”Straight Lines” to make it fly in straight
    - Switch controller to ”P” mode in order to fly the mission. While flying the mission, the drone can not be adjusted manually. **When in trouble, this can be interrupted at any time by switching to ”S” mode.**
8. Check camera settings. In general automatic camera settings will suffice, but it is important to check this. It is recommended to shortly fly to the chosen altitude to verify lighting of the photos. If the automated camera setting show a over- or under-lighted image, the settings can be adjusted manually. When manual adjustment of the camera settings is required:
    - ISO should be set to the lowest value because high ISO values will induce additional noise to the images. (ISO indicates light-sensitivity of the camera; a lower value means a lower sensitivity to light.)
    - Aperture value should be high enough to result in sufficient focal depth. (Aperture refers to the opening of the lens. It controls the amount of light passed to the camera sensor but also controls the depth of the field. High aperture value means more of the picture will be sharp.)
    - Shutter speed should be as high as possible to minimize blur.
9. Collect aerial images:
    - Using RAW data for the photo-setting is better than JPG, as JPG compression may induce unwanted noise to the images.
    - Take images at the highest possible resolution.
    - Fly in lanes perpendicular to flow-direction. Make sure all markers are properly visible and not obstructed by people for example.

- It is better to have too many photos than too few.
- Pay attention to the photo-interval.
- Additionally one can also fly in lanes parallel to flow direction to improve accuracy of the DEM. This will however increase processing time.

10. Fill in flight-details on site-form 1.

Completion

11. Read the water level on (staff-)gauge at the end of data-collection.

12. Collect markers and any other material. When ground-survey is performed with a levelling device, marker coordinates can be recorded with GPS while collecting them. These additional GPS measurements can be used as a back-up and for geo-referencing. Note that in general with GPS coordinates a lower accuracy is achieved than by using a level and/or a measuring-tape.

C

Flight Planning Example

This Annex should be regarded as an addition to Section 3.2.2. Figures C.3 to C.5 show a set of tables (made in Excel) that can be used for flight planning, and it will provide an example in doing so. The example is made for the measuring site at Rio Luia.

During flight planning all above mentioned aspects have to be considered in an iterative manner and some parameters can only really be fine-tuned on site. Appendix A (Figures C.3, C.4 and C.5) shows a set of tables that have been made to aid in this process. The iterative process includes:

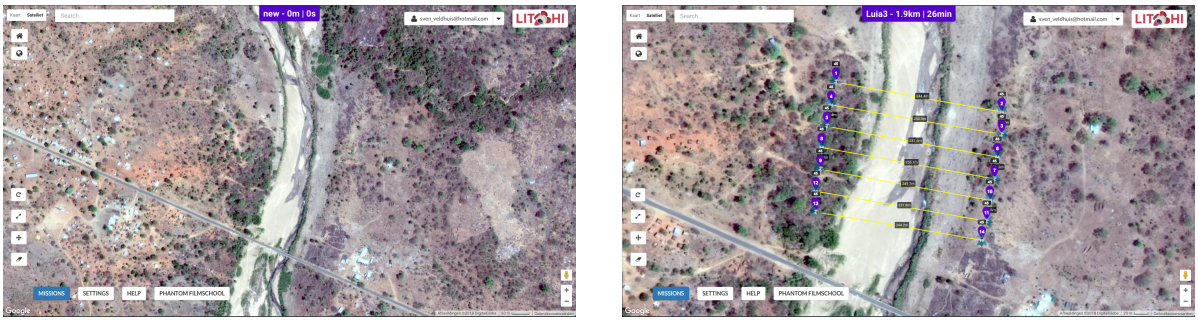

(a) (b)

Figure C.1: Litchi online mission hub: https://flylitchi.com/hub.

1. Look at the size of the measuring site (Figure C.1a) to make an initial guess of the required flight altitude. Personal experience has taught that for a river width of about $200\ m$ an minimum altitude of about $50\ m$ is required.

   We use an altitude of $45\ m$ in this example.

2. Based on this altitude, determine the maximum distance between parallel flight lanes to safeguard sufficient overlap of the images.

   Figure C.2a shows this to be $31\ m$ for an altitude of $45\ m$. Note that the required sideways overlap is 60%.

3. Using this max sideways distance, plan a flight route in Litchi to determine the total distance and flight duration. This also requires assuming an initial flight speed that allows you to cover a section of at least 200 m in length (for very wide rivers it might not be possible to cover 200 m). Keep battery life in mind in doing so. Personal experience has taught that speeds between 1.5 m/s and 2.1 m/s are usually a save guess.

   Figure C.1b. A velocity of $6.1\ km/h$ or $1.69\ m/s$ is used. Total distance is established to be $1.9\ km$ with a flight duration of approximately $26\ min$.

4. Based on the flight speed and the GSD (corresponding to altitude), check which shutter speeds can be used when staying above minimum GSD. If only very high shutter speeds (e.g. $\frac{1}{640}$ to $\frac{1}{1000}$) can be used it might be worth decreasing flight speed to allow lower shutter speeds to still be applicable. Very high shutter speeds can only be used on sunny days.

   Figure C.2a from Table C.3 shows the GSD to be $1.94\ cm/pix$ for the chosen altitude. In Figure C.2b (Table C.4) it can be seen that for chosen flight speed, a shutter speed (SS) of $1/400\ s$ requires a minimum GSD of $1.27\ cm/pix$. Expected sunny weather did not give cause to plan for the possibility of poor light-conditions leading to a SS less than $1/400\ s$. The GSD of $1.94\ cm/pix$ therefore meets the minimum requirements.

5. Settle on an assumable save flight altitude and flight speed and adjust Litchi flight plan accordingly.

   All requirements are met so no need for adjustments: $H = 45\ m$ and $v = 1.69\ m/s$.

6. When on site and ready to fly, use DJI Go to bring drone to planned altitude and test auto camera settings for shutter speed, ISO, and aperture to judge brightness of the image. When slightly dark, the pilot can manually change these setting to try to improve the image. Keep in mind that ISO should be as low as possible to reduce noise in the image. Bring the drone back afterwards.

7. Verify if the now applicable shutter speed and flight speed corresponds to a high enough GSD with the planned flight altitude. If not, altitude or flight speed can still be adjusted in Litchi flight plan to safeguard minimum GSD.

   Local lighting conditions allowed a SS of $1/800\ s$, therefore being well within the planned limits of a SS of $1/400\ s$. If the SS of less than $1/400\ s$ would have been necessary for properly illuminated photographs, the minimum GSD corresponding to that SS should have been checked before flight, possibly leading to an adjustment of either altitude (to increase GSD) or speed (to decrease minimum GSD)

8. When the flight plan is complete and the flight speed and altitude are final, determine the required photo-interval to guaranty sufficient overlap in forward direction (80%).

   Figure C.2c (Table C.5) shows that the required photo-interval for the chosen flight speed and altitude is $6.9\ s$. In practise this is rounded up to $7\ s$.

9. Use Litchi to commence the flight and start taking photographs.

H [m]	GSD [cm/pixels]	Dw [m]	Dh [m]	0.8H [m]	0.6W [m]	Max_Side [m]
10	0.43	17.2	12.9	10.3	10.3	6.9
15	0.65	25.8	19.4	15.5	15.5	10.3
20	0.86	34.4	25.8	20.7	20.7	13.8
25	1.08	43.1	32.3	25.8	25.8	17.2
30	1.29	51.7	38.8	31.0	31.0	20.7
35	1.51	60.3	45.2	36.2	36.2	24.1
40	1.72	68.9	51.7	41.3	41.3	27.6
45	1.94	77.5	58.1	46.5	46.5	31.0
50	2.15	86.1	64.6	51.7	51.7	34.4

(a)

		SS 1/1000:		SS 1/800:		SS 1/640:		SS 1/500:		SS 1/400:	
Vel [km/h]	Vel [m/s]	Movement photo [cm]	Min GSD (cm)	Movement photo [cm]	Min GSD (cm)	Movement photo [cm]	Min GSD (cm)	Movement photo [cm]	Min GSD (cm)	Movement photo [cm]	Min GSD (cm)
4.5	1.25	0.1250	0.3750	0.1563	0.4688	0.2500	0.7500	0.2500	0.7500	0.3125	0.9375
4.6	1.28	0.1278	0.3833	0.1597	0.4792	0.2556	0.7667	0.2556	0.7667	0.3194	0.9583
4.7	1.31	0.1306	0.3917	0.1632	0.4896	0.2611	0.7833	0.2611	0.7833	0.3264	0.9792
4.8	1.33	0.1333	0.4000	0.1667	0.5000	0.2667	0.8000	0.2667	0.8000	0.3333	1.0000
4.9	1.36	0.1361	0.4083	0.1701	0.5104	0.2722	0.8167	0.2722	0.8167	0.3403	1.0208
5	1.39	0.1389	0.4167	0.1736	0.5208	0.2778	0.8333	0.2778	0.8333	0.3472	1.0417
5.1	1.42	0.1417	0.4250	0.1771	0.5313	0.2833	0.8500	0.2833	0.8500	0.3542	1.0625
5.2	1.44	0.1444	0.4333	0.1806	0.5417	0.2889	0.8667	0.2889	0.8667	0.3611	1.0833
5.3	1.47	0.1472	0.4417	0.1840	0.5521	0.2944	0.8833	0.2944	0.8833	0.3681	1.1042
5.4	1.50	0.1500	0.4500	0.1875	0.5625	0.3000	0.9000	0.3000	0.9000	0.3750	1.1250
5.5	1.53	0.1528	0.4583	0.1910	0.5729	0.3056	0.9167	0.3056	0.9167	0.3819	1.1458
5.6	1.56	0.1556	0.4667	0.1944	0.5833	0.3111	0.9333	0.3111	0.9333	0.3889	1.1667
5.7	1.58	0.1583	0.4750	0.1979	0.5938	0.3167	0.9500	0.3167	0.9500	0.3958	1.1875
5.8	1.61	0.1611	0.4833	0.2014	0.6042	0.3222	0.9667	0.3222	0.9667	0.4028	1.2083
5.9	1.64	0.1639	0.4917	0.2049	0.6146	0.3278	0.9833	0.3278	0.9833	0.4097	1.2292
6	1.67	0.1667	0.5000	0.2083	0.6250	0.3333	1.0000	0.3333	1.0000	0.4167	1.2500
6.1	1.69	0.1694	0.5083	0.2118	0.6354	0.3389	1.0167	0.3389	1.0167	0.4236	1.2708
6.2	1.72	0.1722	0.5167	0.2153	0.6458	0.3444	1.0333	0.3444	1.0333	0.4306	1.2917

(b)

Vel [km/h]	Vel [m/s]	Dmax [m]	H = 10 m P10 [s/ph]	H = 15 m P15 [s/ph]	H = 20 m P20 [s/ph]	H = 25 m P25 [s/ph]	H = 30 m P30 [s/ph]	H = 35 m P35 [s/ph]	H = 40 m P40 [s/ph]	H = 45 m P45 [s/ph]
4.5	1.25	2400	2.1	3.1	4.1	5.2	6.2	7.2	8.3	9.3
4.6	1.28	2453	2.0	3.0	4.0	5.1	6.1	7.1	8.1	9.1
4.7	1.31	2507	2.0	3.0	4.0	4.9	5.9	6.9	7.9	8.9
4.8	1.33	2560	1.9	2.9	3.9	4.8	5.8	6.8	7.8	8.7
4.9	1.36	2613	1.9	2.8	3.8	4.7	5.7	6.6	7.6	8.5
5	1.39	2667	1.9	2.8	3.7	4.7	5.6	6.5	7.4	8.4
5.1	1.42	2720	1.8	2.7	3.6	4.6	5.5	6.4	7.3	8.2
5.2	1.44	2773	1.8	2.7	3.6	4.5	5.4	6.3	7.2	8.0
5.3	1.47	2827	1.8	2.6	3.5	4.4	5.3	6.1	7.0	7.9
5.4	1.50	2880	1.7	2.6	3.4	4.3	5.2	6.0	6.9	7.8
5.5	1.53	2933	1.7	2.5	3.4	4.2	5.1	5.9	6.8	7.6
5.6	1.56	2987	1.7	2.5	3.3	4.2	5.0	5.8	6.6	7.5
5.7	1.58	3040	1.6	2.4	3.3	4.1	4.9	5.7	6.5	7.3
5.8	1.61	3093	1.6	2.4	3.2	4.0	4.8	5.6	6.4	7.2
5.9	1.64	3147	1.6	2.4	3.2	3.9	4.7	5.5	6.3	7.1
6	1.67	3200	1.6	2.3	3.1	3.9	4.7	5.4	6.2	7.0
6.1	1.69	3253	1.5	2.3	3.0	3.8	4.6	5.3	6.1	6.9
6.2	1.72	3307	1.5	2.3	3.0	3.8	4.5	5.3	6.0	6.8
6.3	1.75	3360	1.5	2.2	3.0	3.7	4.4	5.2	5.9	6.6

(c)

Figure C.2: Flightplanning

Sw [mm]	Fr [mm]	imW [pixels]	imH [pixels]	Bty_life [min]
6.2	3.6	4000	3000	32

H [m]	GSD [cm/pixels]	Dw [m]	Dh [m]	0.8H [m]	0.6W [m]	Max_Side [m]
10	0.43	17.2	12.9	10.3	10.3	6.9
15	0.65	25.8	19.4	15.5	15.5	10.3
20	0.86	34.4	25.8	20.7	20.7	13.8
25	1.08	43.1	32.3	25.8	25.8	17.2
30	1.29	51.7	38.8	31.0	31.0	20.7
35	1.51	60.3	45.2	36.2	36.2	24.1
40	1.72	68.9	51.7	41.3	41.3	27.6
45	1.94	77.5	58.1	46.5	46.5	31.0
50	2.15	86.1	64.6	51.7	51.7	34.4
55	2.37	94.7	71.0	56.8	56.8	37.9
60	2.58	103.3	77.5	62.0	62.0	41.3
65	2.80	111.9	84.0	67.2	67.2	44.8
70	3.01	120.6	90.4	72.3	72.3	48.2
75	3.23	129.2	96.9	77.5	77.5	51.7
80	3.44	137.8	103.3	82.7	82.7	55.1
85	3.66	146.4	109.8	87.8	87.8	58.6
90	3.88	155.0	116.3	93.0	93.0	62.0
95	4.09	163.6	122.7	98.2	98.2	65.4
100	4.31	172.2	129.2	103.3	103.3	68.9

Figure C.3: Table to establish GSD and overlap-distance for a given altitude and speed.

Vel [km/h]	Vel [m/s]	SS 1/1000: Movement photo [cm]	0.001 Min GSD (cm)	SS 1/800: Movement photo [cm]	0.00125 Min GSD (cm)	SS 1/640: Movement photo [cm]	0.0015625 Min GSD (cm)	SS 1/500: Movement photo [cm]	0.002 Min GSD (cm)	SS 1/400: Movement photo [cm]	0.0025 Min GSD (cm)
4.5	1.25	0.1250	0.3750	0.1563	0.4688	0.2500	0.7500	0.2500	0.7500	0.3125	0.9375
4.6	1.28	0.1278	0.3833	0.1597	0.4792	0.2556	0.7667	0.2556	0.7667	0.3194	0.9583
4.7	1.31	0.1306	0.3917	0.1632	0.4896	0.2611	0.7833	0.2611	0.7833	0.3264	0.9792
4.8	1.33	0.1333	0.4000	0.1667	0.5000	0.2667	0.8000	0.2667	0.8000	0.3333	1.0000
4.9	1.36	0.1361	0.4083	0.1701	0.5104	0.2722	0.8167	0.2722	0.8167	0.3403	1.0208
5	1.39	0.1389	0.4167	0.1736	0.5208	0.2778	0.8333	0.2778	0.8333	0.3472	1.0417
5.1	1.42	0.1417	0.4250	0.1771	0.5313	0.2833	0.8500	0.2833	0.8500	0.3542	1.0625
5.2	1.44	0.1444	0.4333	0.1806	0.5417	0.2889	0.8667	0.2889	0.8667	0.3611	1.0833
5.3	1.47	0.1472	0.4417	0.1840	0.5521	0.2944	0.8833	0.2944	0.8833	0.3681	1.1042
5.4	1.50	0.1500	0.4500	0.1875	0.5625	0.3000	0.9000	0.3000	0.9000	0.3750	1.1250
5.5	1.53	0.1528	0.4583	0.1910	0.5729	0.3056	0.9167	0.3056	0.9167	0.3819	1.1458
5.6	1.56	0.1556	0.4667	0.1944	0.5833	0.3111	0.9333	0.3111	0.9333	0.3889	1.1667
5.7	1.58	0.1583	0.4750	0.1979	0.5938	0.3167	0.9500	0.3167	0.9500	0.3958	1.1875
5.8	1.61	0.1611	0.4833	0.2014	0.6042	0.3222	0.9667	0.3222	0.9667	0.4028	1.2083
5.9	1.64	0.1639	0.4917	0.2049	0.6146	0.3278	0.9833	0.3278	0.9833	0.4097	1.2292
6	1.67	0.1667	0.5000	0.2083	0.6250	0.3333	1.0000	0.3333	1.0000	0.4167	1.2500
6.1	1.69	0.1694	0.5083	0.2118	0.6354	0.3389	1.0167	0.3389	1.0167	0.4236	1.2708
6.2	1.72	0.1722	0.5167	0.2153	0.6458	0.3444	1.0333	0.3444	1.0333	0.4306	1.2917
6.3	1.75	0.1750	0.5250	0.2188	0.6562	0.3500	1.0500	0.3500	1.0500	0.4375	1.3125
6.4	1.78	0.1778	0.5333	0.2222	0.6667	0.3556	1.0667	0.3556	1.0667	0.4444	1.3333
6.5	1.81	0.1806	0.5417	0.2257	0.6771	0.3611	1.0833	0.3611	1.0833	0.4514	1.3542
6.6	1.83	0.1833	0.5500	0.2292	0.6875	0.3667	1.1000	0.3667	1.1000	0.4583	1.3750
6.7	1.86	0.1861	0.5583	0.2326	0.6979	0.3722	1.1167	0.3722	1.1167	0.4653	1.3958
6.8	1.89	0.1889	0.5667	0.2361	0.7083	0.3778	1.1333	0.3778	1.1333	0.4722	1.4167
6.9	1.92	0.1917	0.5750	0.2396	0.7187	0.3833	1.1500	0.3833	1.1500	0.4792	1.4375
7	1.94	0.1944	0.5833	0.2431	0.7292	0.3889	1.1667	0.3889	1.1667	0.4861	1.4583
7.1	1.97	0.1972	0.5917	0.2465	0.7396	0.3944	1.1833	0.3944	1.1833	0.4931	1.4792
7.2	2.00	0.2000	0.6000	0.2500	0.7500	0.4000	1.2000	0.4000	1.2000	0.5000	1.5000
7.3	2.03	0.2028	0.6083	0.2535	0.7604	0.4056	1.2167	0.4056	1.2167	0.5069	1.5208
7.4	2.06	0.2056	0.6167	0.2569	0.7708	0.4111	1.2333	0.4111	1.2333	0.5139	1.5417
7.5	2.08	0.2083	0.6250	0.2604	0.7812	0.4167	1.2500	0.4167	1.2500	0.5208	1.5625
7.6	2.11	0.2111	0.6333	0.2639	0.7917	0.4222	1.2667	0.4222	1.2667	0.5278	1.5833
7.7	2.14	0.2139	0.6417	0.2674	0.8021	0.4278	1.2833	0.4278	1.2833	0.5347	1.6042
7.8	2.17	0.2167	0.6500	0.2708	0.8125	0.4333	1.3000	0.4333	1.3000	0.5417	1.6250
7.9	2.19	0.2194	0.6583	0.2743	0.8229	0.4389	1.3167	0.4389	1.3167	0.5486	1.6458
8	2.22	0.2222	0.6667	0.2778	0.8333	0.4444	1.3333	0.4444	1.3333	0.5556	1.6667
8.1	2.25	0.2250	0.6750	0.2812	0.8437	0.4500	1.3500	0.4500	1.3500	0.5625	1.6875
8.2	2.28	0.2278	0.6833	0.2847	0.8542	0.4556	1.3667	0.4556	1.3667	0.5694	1.7083
8.3	2.31	0.2306	0.6917	0.2882	0.8646	0.4611	1.3833	0.4611	1.3833	0.5764	1.7292
8.4	2.33	0.2333	0.7000	0.2917	0.8750	0.4667	1.4000	0.4667	1.4000	0.5833	1.7500
8.5	2.36	0.2361	0.7083	0.2951	0.8854	0.4722	1.4167	0.4722	1.4167	0.5903	1.7708
8.6	2.39	0.2389	0.7167	0.2986	0.8958	0.4778	1.4333	0.4778	1.4333	0.5972	1.7917
8.7	2.42	0.2417	0.7250	0.3021	0.9062	0.4833	1.4500	0.4833	1.4500	0.6042	1.8125
8.8	2.44	0.2444	0.7333	0.3056	0.9167	0.4889	1.4667	0.4889	1.4667	0.6111	1.8333
8.9	2.47	0.2472	0.7417	0.3090	0.9271	0.4944	1.4833	0.4944	1.4833	0.6181	1.8542
9	2.50	0.2500	0.7500	0.3125	0.9375	0.5000	1.5000	0.5000	1.5000	0.6250	1.8750
9.1	2.53	0.2528	0.7583	0.3160	0.9479	0.5056	1.5167	0.5056	1.5167	0.6319	1.8958
9.2	2.56	0.2556	0.7667	0.3194	0.9583	0.5111	1.5333	0.5111	1.5333	0.6389	1.9167
9.3	2.58	0.2583	0.7750	0.3229	0.9687	0.5167	1.5500	0.5167	1.5500	0.6458	1.9375
9.4	2.61	0.2611	0.7833	0.3264	0.9792	0.5222	1.5667	0.5222	1.5667	0.6528	1.9583
9.5	2.64	0.2639	0.7917	0.3299	0.9896	0.5278	1.5833	0.5278	1.5833	0.6597	1.9792
9.6	2.67	0.2667	0.8000	0.3333	1.0000	0.5333	1.6000	0.5333	1.6000	0.6667	2.0000
9.7	2.69	0.2694	0.8083	0.3368	1.0104	0.5389	1.6167	0.5389	1.6167	0.6736	2.0208
9.8	2.72	0.2722	0.8167	0.3403	1.0208	0.5444	1.6333	0.5444	1.6333	0.6806	2.0417
9.9	2.75	0.2750	0.8250	0.3437	1.0313	0.5500	1.6500	0.5500	1.6500	0.6875	2.0625
10	2.78	0.2778	0.8333	0.3472	1.0417	0.5556	1.6667	0.5556	1.6667	0.6944	2.0833

Figure C.4: Table to establish minimum needed GSD for a given flight- and shutter speed.

Vel [km/h]	Vel [m/s]	Dmax [m]	H = 10 m P10 [s/ph]	H = 15 m P15 [s/ph]	H = 20 m P20 [s/ph]	H = 25 m P25 [s/ph]	H = 30 m P30 [s/ph]	H = 35 m P35 [s/ph]	H = 40 m P40 [s/ph]	H = 45 m P45 [s/ph]	H = 50 m P50 [s/ph]	H = 55 m P55 [s/ph]	H = 60 m P60 [s/ph]	H = 65 m P65 [s/ph]	H = 70 m P70 [s/ph]	H = 75 m P75 [s/ph]	H = 80 m P80 [s/ph]	H = 85 m P85 [s/ph]	H = 90 m P90 [s/ph]	H = 95 m P95 [s/ph]	H = 100 m P100 [s/ph]
4.5	1.25	2400	2.1	3.1	4.1	5.2	6.2	7.2	8.3	9.3	10.3	11.4	12.4	13.4	14.5	15.5	16.5	17.6	18.6	19.6	20.7
4.6	1.28	2453	2.0	3.0	4.0	5.1	6.1	7.1	8.1	9.1	10.1	11.1	12.1	13.1	14.2	15.2	16.2	17.2	18.2	19.2	20.2
4.7	1.31	2507	2.0	3.0	4.0	4.9	5.9	6.9	7.9	8.9	9.9	10.9	11.9	12.9	13.9	14.8	15.8	16.8	17.8	18.8	19.8
4.8	1.33	2560	1.9	2.9	3.9	4.8	5.8	6.8	7.8	8.7	9.7	10.7	11.6	12.6	13.6	14.5	15.5	16.5	17.4	18.4	19.4
4.9	1.36	2613	1.9	2.8	3.8	4.7	5.7	6.6	7.6	8.5	9.5	10.4	11.4	12.3	13.3	14.2	15.2	16.1	17.1	18.0	19.0
5	1.39	2667	1.9	2.8	3.7	4.7	5.6	6.5	7.4	8.4	9.3	10.2	11.2	12.1	13.0	14.0	14.9	15.8	16.7	17.7	18.6
5.1	1.42	2720	1.8	2.7	3.6	4.6	5.5	6.4	7.3	8.2	9.1	10.0	10.9	11.9	12.8	13.7	14.6	15.5	16.4	17.3	18.2
5.2	1.44	2773	1.8	2.7	3.6	4.5	5.4	6.3	7.2	8.0	8.9	9.8	10.7	11.6	12.5	13.4	14.3	15.2	16.1	17.0	17.9
5.3	1.47	2827	1.8	2.6	3.5	4.4	5.3	6.1	7.0	7.9	8.8	9.7	10.5	11.4	12.3	13.2	14.0	14.9	15.8	16.7	17.5
5.4	1.50	2880	1.7	2.6	3.4	4.3	5.2	6.0	6.9	7.8	8.6	9.5	10.3	11.2	12.1	12.9	13.8	14.6	15.5	16.4	17.2
5.5	1.53	2933	1.7	2.5	3.4	4.2	5.1	5.9	6.8	7.6	8.5	9.3	10.1	11.0	11.8	12.7	13.5	14.4	15.2	16.1	16.9
5.6	1.56	2987	1.7	2.5	3.3	4.2	5.0	5.8	6.6	7.5	8.3	9.1	10.0	10.8	11.6	12.5	13.3	14.1	14.9	15.8	16.6
5.7	1.58	3040	1.6	2.4	3.3	4.1	4.9	5.7	6.5	7.3	8.2	9.0	9.8	10.6	11.4	12.2	13.1	13.9	14.7	15.5	16.3
5.8	1.61	3093	1.6	2.4	3.2	4.0	4.8	5.6	6.4	7.2	8.0	8.8	9.6	10.4	11.2	12.0	12.8	13.6	14.4	15.2	16.0
5.9	1.64	3147	1.6	2.4	3.2	3.9	4.7	5.5	6.3	7.1	7.9	8.7	9.5	10.2	11.0	11.8	12.6	13.4	14.2	15.0	15.8
6	1.67	3200	1.6	2.3	3.1	3.9	4.7	5.4	6.2	7.0	7.8	8.5	9.3	10.1	10.9	11.6	12.4	13.2	14.0	14.7	15.5
6.1	1.69	3253	1.5	2.3	3.0	3.8	4.6	5.3	6.1	6.9	7.6	8.4	9.1	9.9	10.7	11.4	12.2	13.0	13.7	14.5	15.2
6.2	1.72	3307	1.5	2.3	3.0	3.8	4.5	5.3	6.0	6.9	7.5	8.3	9.0	9.8	10.5	11.3	12.0	12.8	13.5	14.3	15.0
6.3	1.75	3360	1.5	2.2	3.0	3.7	4.4	5.2	5.9	6.6	7.4	8.1	8.9	9.6	10.3	11.1	11.8	12.5	13.3	14.0	14.8
6.4	1.78	3413	1.5	2.2	2.9	3.6	4.4	5.1	5.8	6.5	7.3	8.0	8.7	9.4	10.2	10.9	11.6	12.4	13.1	13.8	14.5
6.5	1.81	3467	1.4	2.1	2.9	3.6	4.3	5.0	5.7	6.4	7.2	7.9	8.6	9.3	10.0	10.7	11.4	12.2	12.9	13.6	14.3
6.6	1.83	3520	1.4	2.1	2.8	3.5	4.2	4.9	5.6	6.3	7.1	7.9	8.5	9.2	9.9	10.6	11.3	12.0	12.7	13.4	14.1
6.7	1.86	3573.33333	1.4	2.1	2.8	3.5	4.2	4.9	5.6	6.3	7.0	7.8	8.3	9.0	9.7	10.4	11.1	11.8	12.5	13.2	13.9
6.8	1.89	3627	1.4	2.1	2.7	3.4	4.1	4.8	5.5	6.2	6.8	7.5	8.2	8.9	9.6	10.3	10.9	11.6	12.3	13.0	13.7
6.9	1.92	3680	1.3	2.0	2.7	3.4	4.0	4.7	5.4	6.1	6.7	7.4	8.1	8.8	9.4	10.1	10.8	11.5	12.1	12.8	13.5
7	1.94	3733	1.3	2.0	2.7	3.3	4.0	4.7	5.3	6.0	6.6	7.3	8.0	8.6	9.3	10.0	10.6	11.3	12.0	12.6	13.3
7.1	1.97	3786.66667	1.3	2.0	2.6	3.3	3.9	4.6	5.2	5.9	6.5	7.2	7.9	8.5	9.2	9.8	10.5	11.1	11.8	12.4	13.1
7.2	2.00	3840	1.3	1.9	2.6	3.2	3.9	4.5	5.2	5.8	6.5	7.1	7.8	8.4	9.0	9.7	10.3	11.0	11.6	12.3	12.9
7.3	2.03	3893	1.3	1.9	2.5	3.2	3.8	4.5	5.1	5.8	6.4	7.0	7.6	8.3	8.9	9.6	10.2	10.8	11.5	12.1	12.7
7.4	2.06	3947	1.3	1.9	2.5	3.1	3.8	4.4	5.0	5.7	6.3	6.9	7.5	8.2	8.8	9.4	10.1	10.7	11.3	11.9	12.6
7.5	2.08	4000	1.2	1.9	2.5	3.1	3.7	4.3	5.0	5.6	6.2	6.8	7.4	8.1	8.7	9.3	9.9	10.5	11.2	11.8	12.4
7.6	2.11	4053	1.2	1.8	2.4	3.1	3.7	4.3	4.9	5.5	6.1	6.7	7.3	8.0	8.6	9.2	9.8	10.4	11.0	11.6	12.2
7.7	2.14	4107	1.2	1.8	2.4	3.0	3.6	4.2	4.8	5.4	6.0	6.6	7.2	7.9	8.5	9.1	9.7	10.3	10.9	11.5	12.1
7.8	2.17	4160	1.2	1.8	2.4	3.0	3.6	4.2	4.8	5.4	6.0	6.6	7.2	7.8	8.3	8.9	9.5	10.1	10.7	11.3	11.9
7.9	2.19	4213	1.2	1.8	2.4	2.9	3.5	4.1	4.7	5.3	5.9	6.5	7.1	7.7	8.2	8.8	9.4	10.0	10.6	11.2	11.8
8	2.22	4267	1.2	1.7	2.3	2.9	3.5	4.1	4.7	5.2	5.8	6.4	7.0	7.6	8.1	8.7	9.3	9.9	10.5	11.0	11.6
8.1	2.25	4320	1.1	1.7	2.3	2.9	3.4	4.0	4.6	5.2	5.7	6.3	6.9	7.5	8.0	8.6	9.2	9.8	10.3	10.8	11.5
8.2	2.28	4373.33333	1.1	1.7	2.3	2.8	3.4	4.0	4.5	5.1	5.7	6.2	6.8	7.4	7.9	8.5	9.1	9.7	10.2	10.8	11.3
8.3	2.31	4427	1.1	1.7	2.2	2.8	3.4	3.9	4.5	5.0	5.6	6.2	6.7	7.3	7.8	8.4	9.0	9.6	10.1	10.6	11.2
8.4	2.33	4480	1.1	1.7	2.2	2.8	3.3	3.9	4.4	5.0	5.5	6.1	6.6	7.2	7.8	8.3	8.9	9.4	10.0	10.5	11.1
8.5	2.36	4533	1.1	1.6	2.2	2.7	3.3	3.8	4.4	4.9	5.5	6.0	6.6	7.1	7.7	8.2	8.8	9.3	9.8	10.4	10.9
8.6	2.39	4586.66667	1.1	1.6	2.2	2.7	3.2	3.8	4.3	4.9	5.4	5.9	6.5	7.0	7.6	8.1	8.7	9.2	9.7	10.3	10.8
8.7	2.42	4640	1.1	1.6	2.1	2.7	3.2	3.7	4.3	4.8	5.3	5.9	6.4	6.9	7.5	8.0	8.6	9.1	9.6	10.2	10.7
8.8	2.44	4693	1.1	1.6	2.1	2.6	3.2	3.7	4.2	4.8	5.3	5.8	6.3	6.9	7.4	7.9	8.5	9.0	9.5	9.9	10.6
8.9	2.47	4747	1.0	1.6	2.1	2.6	3.1	3.7	4.2	4.7	5.2	5.7	6.3	6.8	7.3	7.8	8.4	8.9	9.4	9.9	10.4
9	2.50	4800	1.0	1.6	2.1	2.6	3.1	3.6	4.1	4.7	5.2	5.7	6.2	6.7	7.2	7.8	8.3	8.8	9.3	9.8	10.3
9.1	2.53	4853.33333	1.0	1.5	2.0	2.6	3.1	3.6	4.1	4.6	5.1	5.6	6.1	6.6	7.1	7.6	8.1	8.7	9.2	9.7	10.2
9.2	2.56	4907	1.0	1.5	2.0	2.5	3.0	3.5	4.0	4.5	5.0	5.6	6.0	6.6	7.0	7.6	8.1	8.6	9.0	9.6	10.1
9.3	2.58	4960	1.0	1.5	2.0	2.5	3.0	3.5	4.0	4.5	4.9	5.5	5.9	6.5	6.9	7.5	8.0	8.5	9.0	9.5	10.0
9.4	2.61	5013	1.0	1.5	2.0	2.5	3.0	3.5	4.0	4.5	4.9	5.4	5.9	6.4	6.9	7.3	7.9	8.4	8.9	9.4	9.9
9.5	2.64	5066.66667	1.0	1.5	2.0	2.4	2.9	3.4	3.9	4.4	4.9	5.4	5.9	6.4	6.9	7.3	7.8	8.3	8.8	9.3	9.8
9.6	2.67	5120	1.0	1.5	1.9	2.4	2.9	3.4	3.9	4.4	4.8	5.3	5.8	6.3	6.8	7.3	7.8	8.2	8.7	9.2	9.7
9.7	2.69	5173	1.0	1.4	1.9	2.4	2.9	3.4	3.9	4.4	4.8	5.3	5.8	6.2	6.7	7.2	7.7	8.1	8.6	9.1	9.6
9.8	2.72	5227	0.9	1.4	1.9	2.4	2.8	3.3	3.8	4.3	4.7	5.2	5.7	6.2	6.6	7.1	7.6	8.1	8.5	9.0	9.5
9.9	2.75	5280	0.9	1.4	1.9	2.3	2.8	3.3	3.8	4.2	4.7	5.2	5.6	6.1	6.6	7.0	7.5	8.0	8.5	8.9	9.4
10	2.78	5333	0.9	1.4	1.9	2.3	2.8	3.3	3.7	4.2	4.7	5.1	5.6	6.0	6.5	7.0	7.4	7.9	8.4	8.8	9.3

Figure C.5: Table to establish required photo interval for a given altitude and speed.

D

DEMs and Orthophotos

In addition to Section 5.1, this appendix displays the orthomosiacs and DEMs of the remaining rivers.

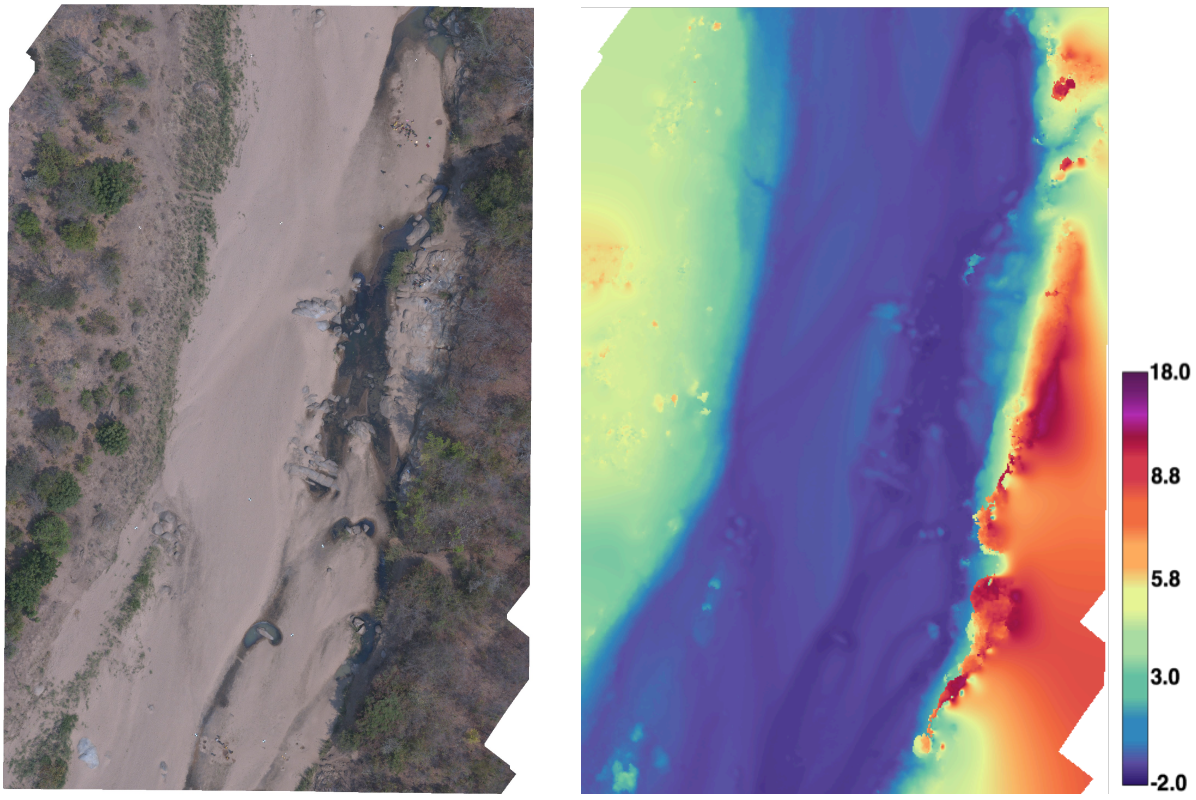

(a) Orthomosaic Rio Duângua (b) DEM Rio Duângua

Figure D.1: Images of the six processed river-reaches with downstream direction facing downwards (colour-scale in meters). Chronologically ordered by time of measurements.
a, b: Rio Duângua
(cont. on next page)

(c) Orthomosaic Rio Mucanha

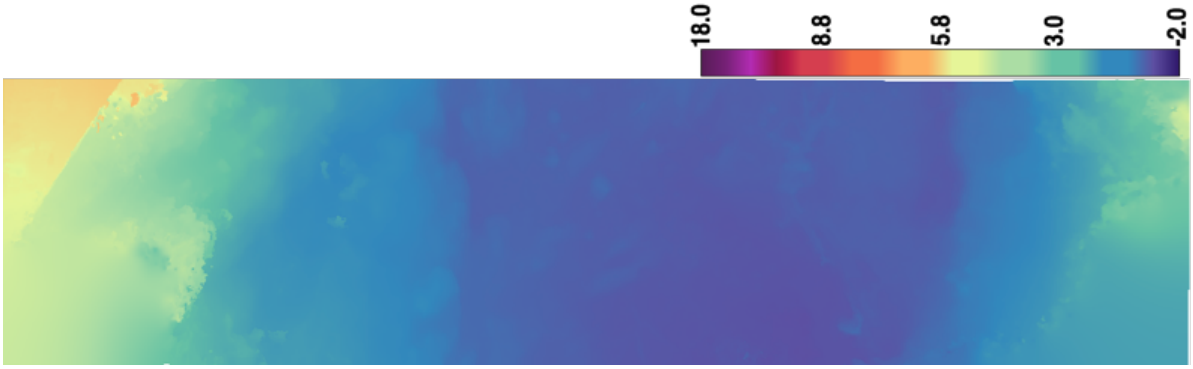

(d) DEM Rio Mucanha

(e) Orthomosaic Rio Muze

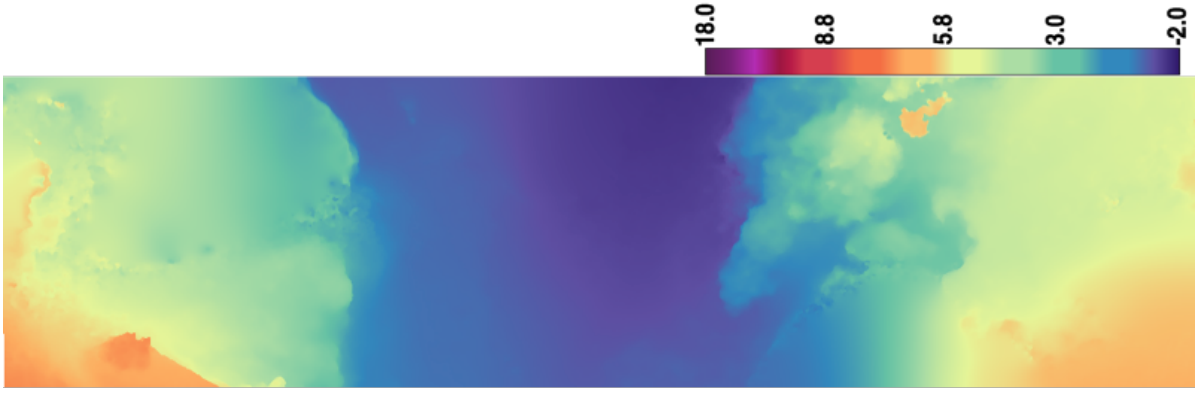

(f) DEM Rio Muze

Figure D.1: Images of the six processed river-reaches with downstream direction facing downwards. Chronologically ordered by time of measurements (colour-scale in meters).
c, d: Rio Mucanha - e, f: Rio Muze
(cont. on next page)

(g) Orthomosaic Rio Cherisse

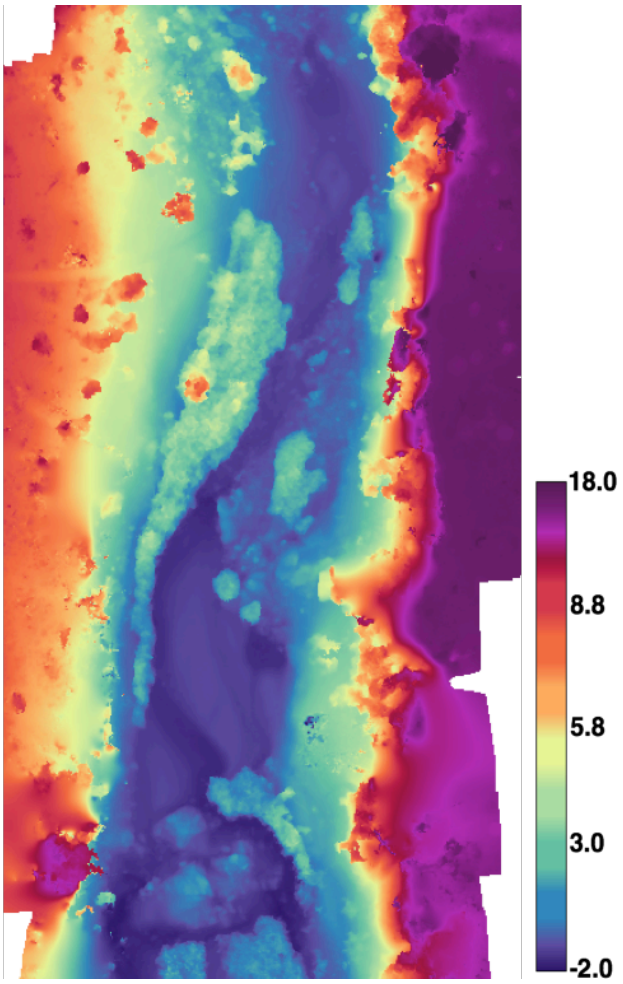

(h) DEM Rio Cherisse

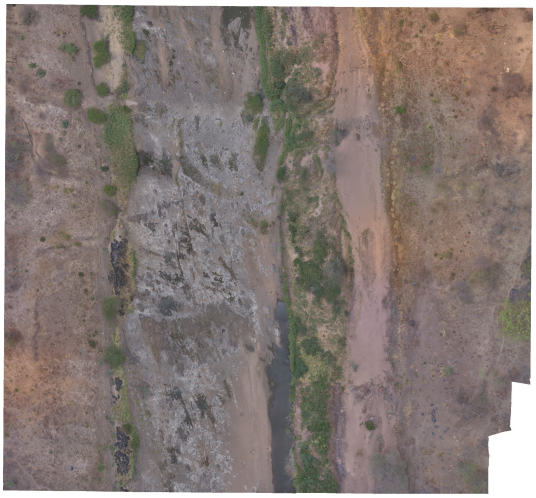

(i) Orthomosaic Rio Capoche

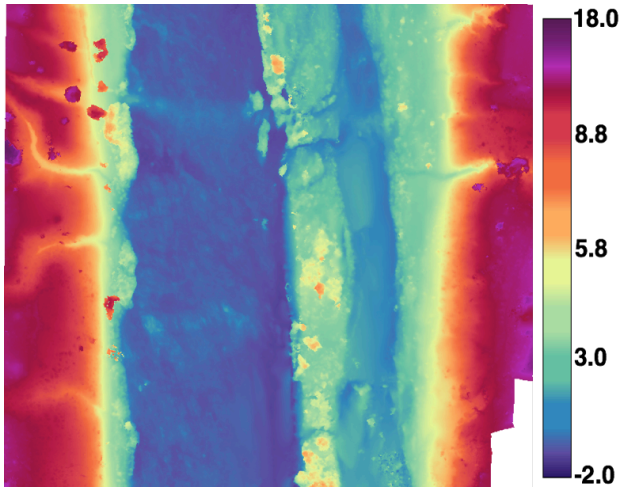

(j) DEM Rio Capoche

Figure D.1: Images of the six processed river-reaches with downstream direction facing downwards. Chronologically ordered by time of measurements (colour-scale in meters). g, h: Rio Cherisse - i, j: Rio Capoche

E

GDEM-based Regional Slopes

This appendix shows the elevation-profiles derived from ASTGDEM Version 2 [21], together with the regional slope based on a reach of $20\ km$ around the measuring sites of the additional tributaries. Graphs for Rio Luia can be seen in Figure 5.5.

Table E.1 shows an overview of the derived and computed slopes for all six processed tributaries. Here, the overall slope reflects the slope over the full length of the tributary, the regional slope corresponds with the slope derived from a reach stretching from $10\ km$ up- to $10\ km$ downstream of the measuring site, and the local slope being calculated with proposed method using $^{\mathrm{d}C}/_{\mathrm{d}y}$ and the computed DEMs (Section 3.2.6). In general it can be seen that even though there is a difference of about a factor 2 between the regional and the local slopes, the orders of magnitude do correspond. From this set there is no obvious pattern of over- of underestimation of the local slope. This leads to suggest that the slope based on the computed DEMs might be too local and longer stretches of the river are needed for better slope estimation. This can also be seen by looking at the graphs, as the slope in direct vicinity of the measuring point usually differs from the regional slope. However, these graphs do have to be interpreted with caution as (1) the GDEM they are based on only has a resolution of about $30\ m$ and (2) the (RMSE) of the GDEM-data is known to be in the range from 7 up to $25\ m$ [21] [3]. The local slope might be representable for very low flow conditions in the processed reach, but for higher flows the water surface will probably tend towards the derived regional slope.

River	Overall Slope ($\cdot 10^{-3}$)	Regional Slope around MS ($\cdot 10^{-3}$)	Computed Local Slope at MS ($\cdot 10^{-3}$)
Duângua	5.70	5.16	2.21
Mucanha	3.83	2.40	5.96*
Muze	2.96	2.97	5.96*
Cherisse	4.91	2.62	6.07
Capoche	3.52	2.02	1.09
Luia	3.47	1.32	2.23

Table E.1: Overview of difference in slope calculation, MS = Measuring Site. *These computed values were known to be very inaccurate.

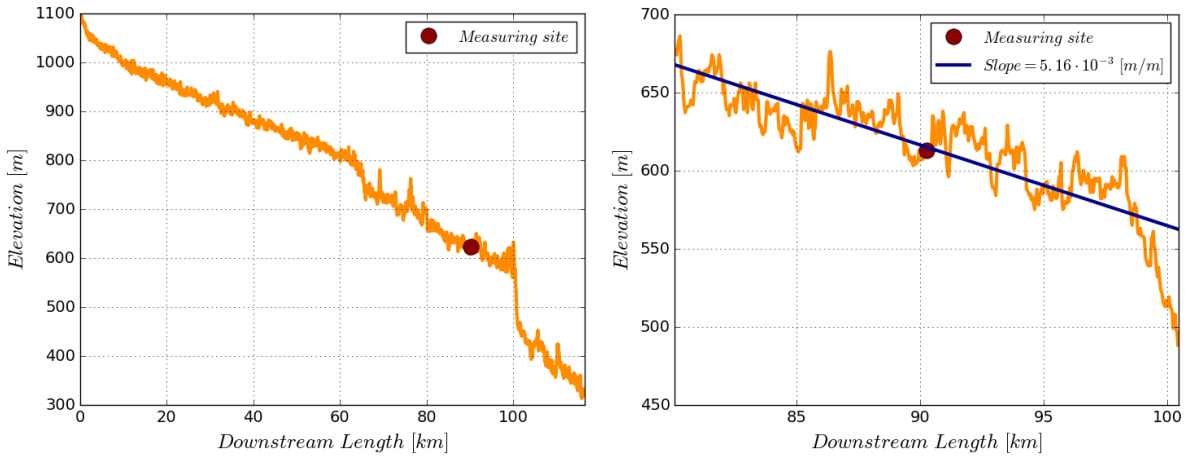

(a) Full length of the river.

(b) $\pm 20\ km$ around the measuring site

Figure E.1: Elevation profile of Rio Duângua based on ASTGDEM and local slope around measuring site.

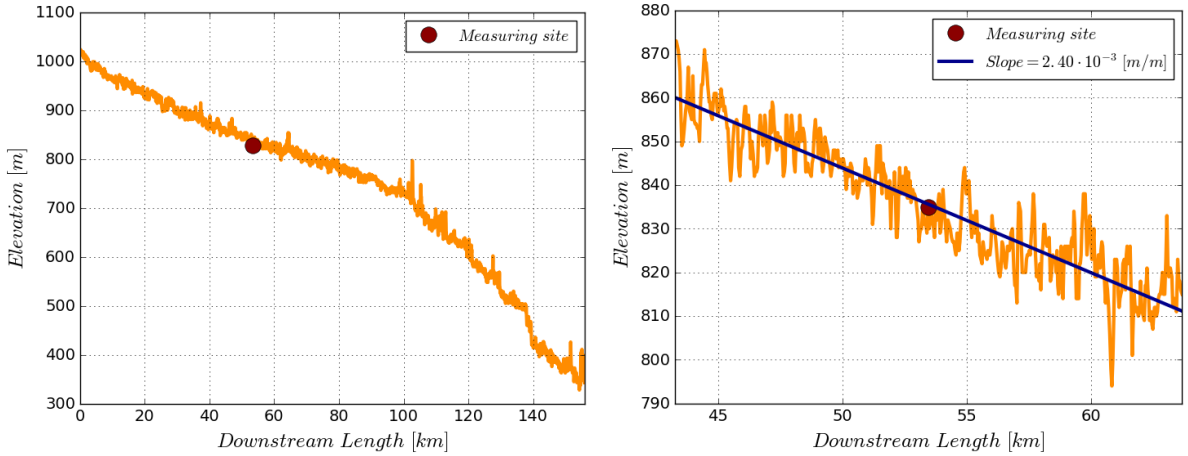

(a) Full length of the river.

(b) $\pm 20\ km$ around the measuring site

Figure E.2: Elevation profile of Rio Mucanha based on ASTGDEM and local slope around measuring site.

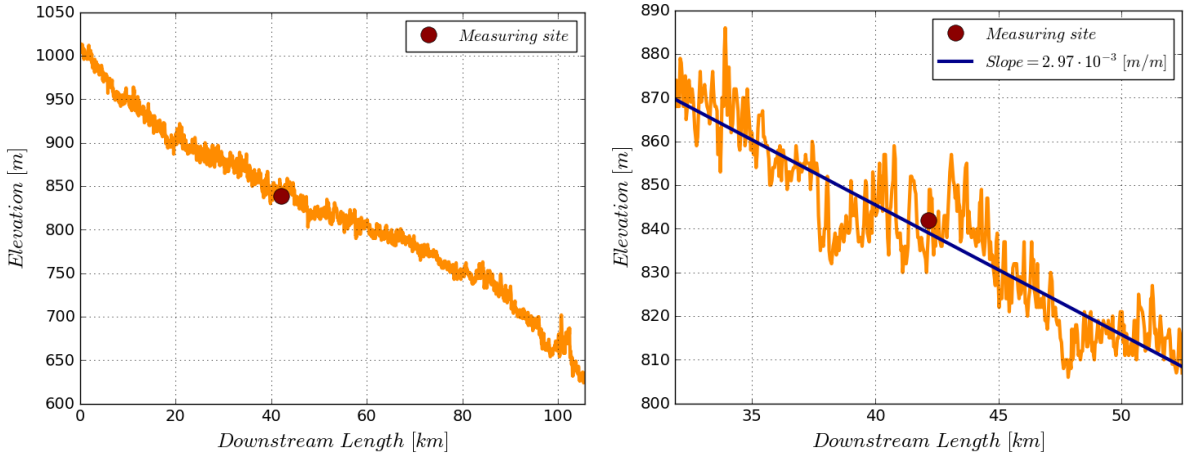

(a) Full length of the river.

(b) $\pm 20\ km$ around the measuring site

Figure E.3: Elevation profile of Rio Muze based on ASTGDEM and local slope around measuring site.

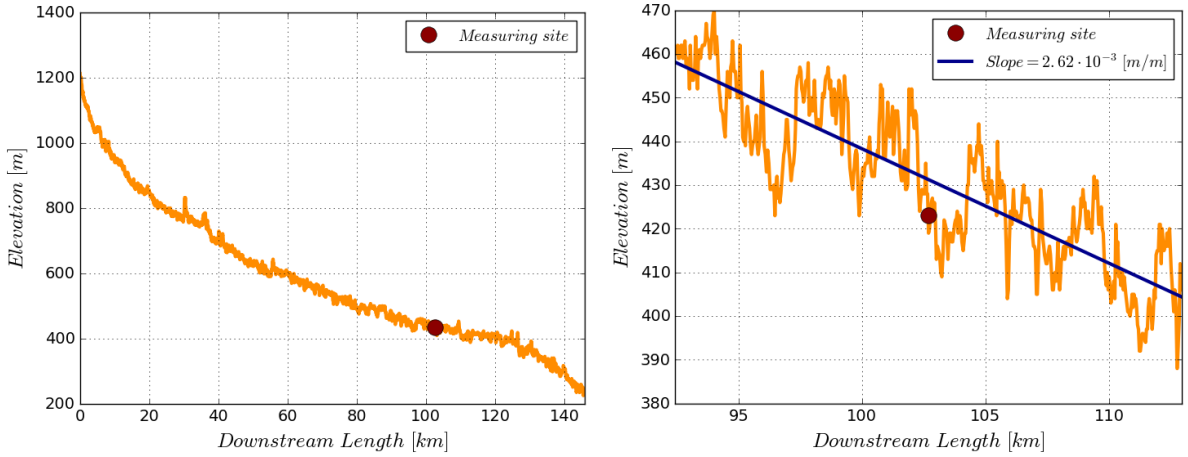

(a) Full length of the river.

(b) $\pm 20\ km$ around the measuring site

Figure E.4: Elevation profile of Rio Cherisse based on ASTGDEM and local slope around measuring site.

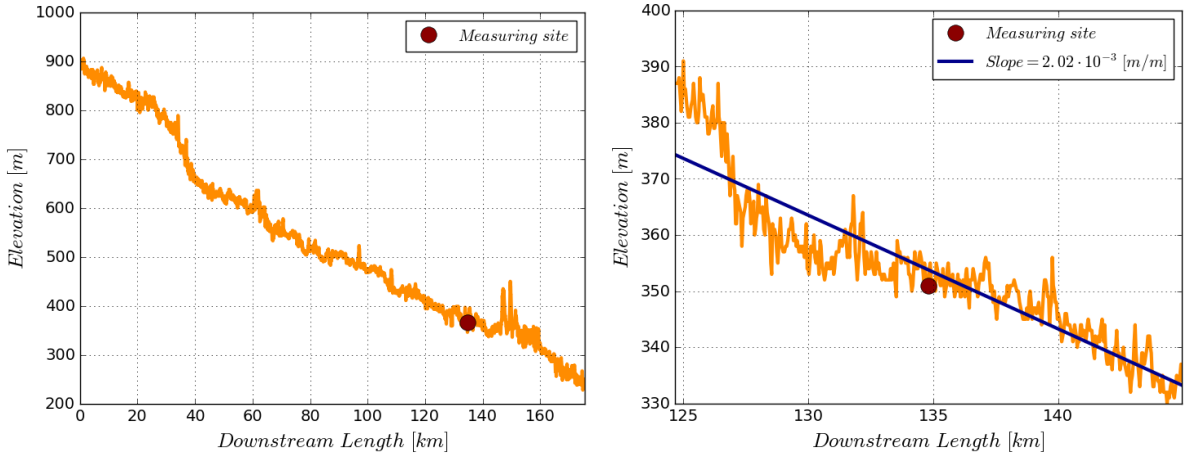

(a) Full length of the river.

(b) $\pm 20\ km$ around the measuring site

Figure E.5: Elevation profile of Rio Capoche based on ASTGDEM and local slope around measuring site.

F

Errors of Ground Control Points

Here, Photoscan's error calculation of the GCPs is presented per measured tributary. The photogrammetry software calculates the RMSE of the GCPs in both X, Y and Z directions of the 3D model. The error is based on the difference between the location/elevation assigned to the GCP by the modeller and the location/elevation calculated by the program. Z error is represented by ellipse color. X,Y errors are represented by ellipse shape. Estimated GCP locations are marked with a dot or crossing.

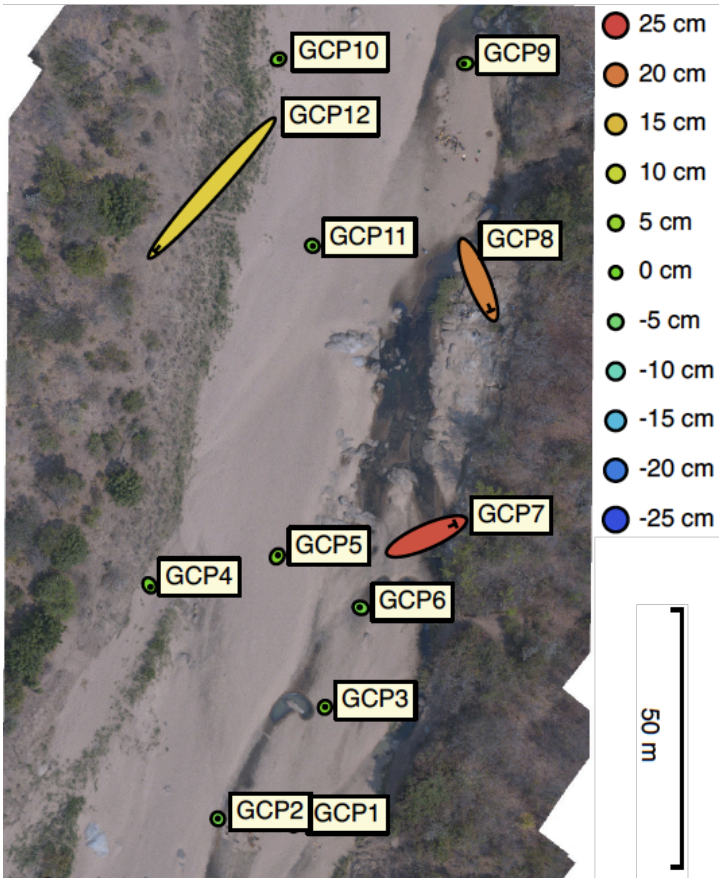

(a) Graphical presentation

Label	X error (m)	Y error (m)	Z error (m)	Total (m)	Image (pix)
GCP1	-0.29485	-0.34244	0.0112208	0.452026	0.130 (10)
GCP2	-0.0559811	0.11709	-0.0222443	0.131677	0.165 (12)
GCP3	0.0818923	0.174512	0.0174235	0.193557	0.113 (16)
GCP4	0.375978	-0.638067	0.00331981	0.740608	0.209 (14)
GCP5	0.2701	0.448304	0.0194513	0.523745	0.164 (18)
GCP6	-0.419654	0.163918	-0.0217325	0.451055	0.167 (14)
GCP9	-0.608042	-0.0420357	0.00176118	0.609495	0.124 (14)
GCP10	0.455225	0.218594	0.00418133	0.505005	0.121 (9)
GCP11	0.19532	-0.0999034	-0.0134008	0.219796	0.138 (13)
Total	**0.349967**	**0.308389**	**0.0148554**	**0.466692**	**0.152**

(b) Quantitative presentation

Figure F.1: GCP errors for Rio Duangua

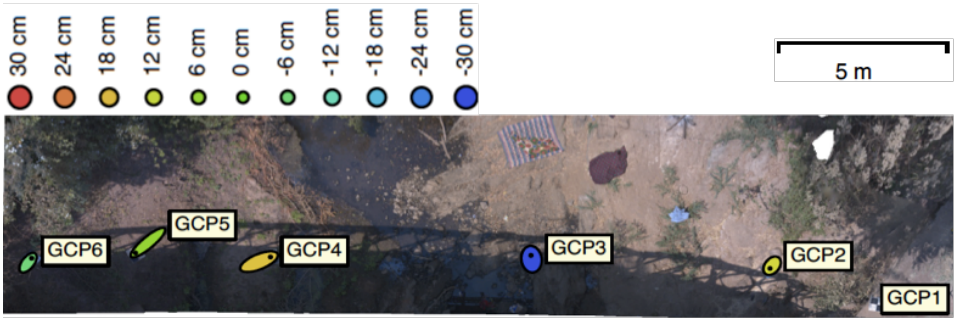

(a) Graphical presentation

Label	X error (cm)	Y error (cm)	Z error (cm)	Total (cm)	Image (pix)
GCP2	-3.36972	-4.64472	13.5369	14.7029	0.281 (14)
GCP3	-0.804916	6.62678	-29.9822	30.7163	0.282 (15)
GCP4	18.4128	8.12741	17.1743	26.4583	0.270 (14)
GCP5	-20.1034	-18.0199	5.71793	27.5963	0.162 (10)
GCP6	5.86539	7.90966	-6.4527	11.773	0.105 (5)
Total	**12.5665**	**10.1865**	**17.038**	**23.4941**	**0.250**

(b) Quantitative presentation

Figure F.2: GCP errors for Rio Mucanha

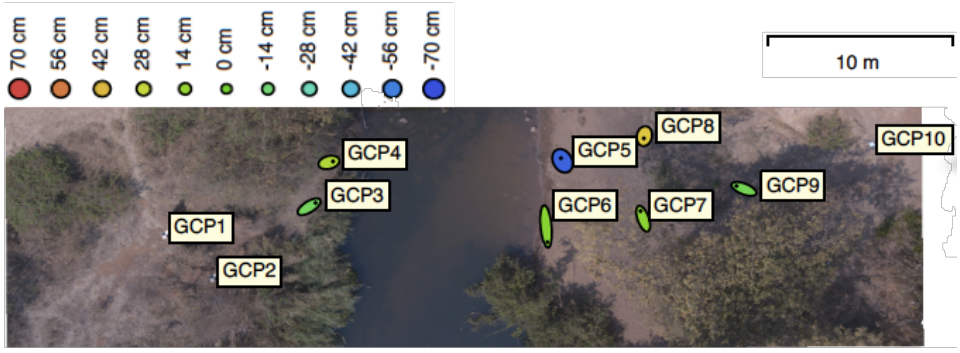

(a) Graphical presentation

Label	X error (cm)	Y error (cm)	Z error (cm)	Total (cm)	Image (pix)
GCP3	69.8103	42.6276	-9.10441	82.3011	0.475 (24)
GCP4	45.1876	11.2432	21.6438	51.3496	0.431 (25)
GCP6	15.9567	-168.955	8.71664	169.931	0.636 (27)
GCP5	-16.9225	28.8844	-63.6001	71.8725	0.538 (26)
GCP8	-5.78284	-25.5181	38.7222	46.7335	0.479 (22)
GCP9	-79.5798	30.6313	-6.98722	85.5573	0.593 (16)
GCP7	-28.7835	80.7525	10.2876	86.344	0.785 (22)
Total	**45.7497**	**75.0562**	**30.0627**	**92.8991**	**0.570**

(b) Quantitative presentation

Figure F.3: GCP errors for Rio Muze

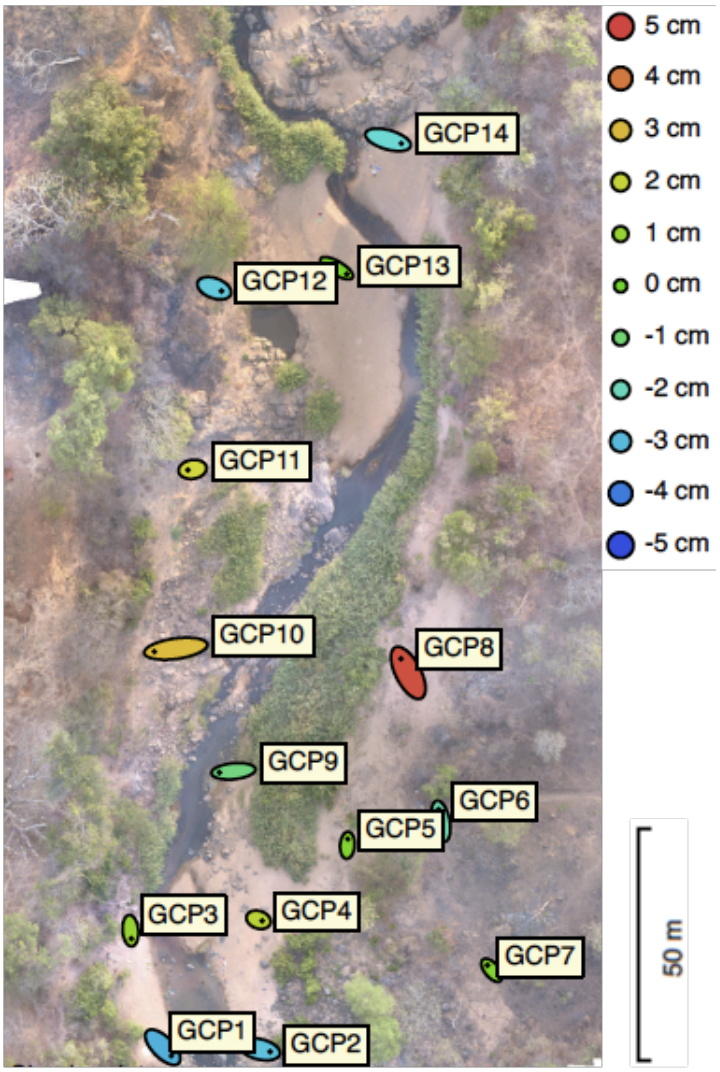

(a) Graphical presentation

Label	X error (m)	Y error (m)	Z error (m)	Total (m)	Image (pix)
GCP1	1.22617	-1.24061	-0.0311609	1.74459	0.167 (13)
GCP2	1.48698	-0.355715	-0.0288463	1.52921	0.169 (12)
GCP3	0.0927005	-1.14043	0.0109165	1.14424	0.085 (17)
GCP4	0.505321	-0.169508	0.0179984	0.533297	0.149 (18)
GCP5	0.0627184	0.913099	0.00581032	0.915269	0.158 (17)
GCP6	-0.340377	1.70426	-0.018523	1.73801	0.200 (13)
GCP7	-0.621208	0.738295	0.00512003	0.964887	0.155 (9)
GCP8	-1.05879	2.05141	0.0472145	2.30901	0.138 (17)
GCP9	-2.01899	-0.188078	-0.0118029	2.02776	0.154 (19)
GCP10	-3.09222	-0.426808	0.029059	3.12167	0.097 (18)
GCP11	-0.66542	-0.1027	0.0228839	0.673687	0.141 (11)
GCP12	1.0385	-0.384891	-0.0272582	1.10787	0.139 (12)
GCP13	1.46006	-0.851257	0.00286111	1.6901	0.238 (19)
GCP14	1.92455	-0.547065	-0.0242833	2.00094	0.175 (17)
Total	**1.37841**	**0.959416**	**0.0234928**	**1.6796**	**0.159**

(b) Quantitative presentation

Figure F.4: GCP errors for Rio Cherisse

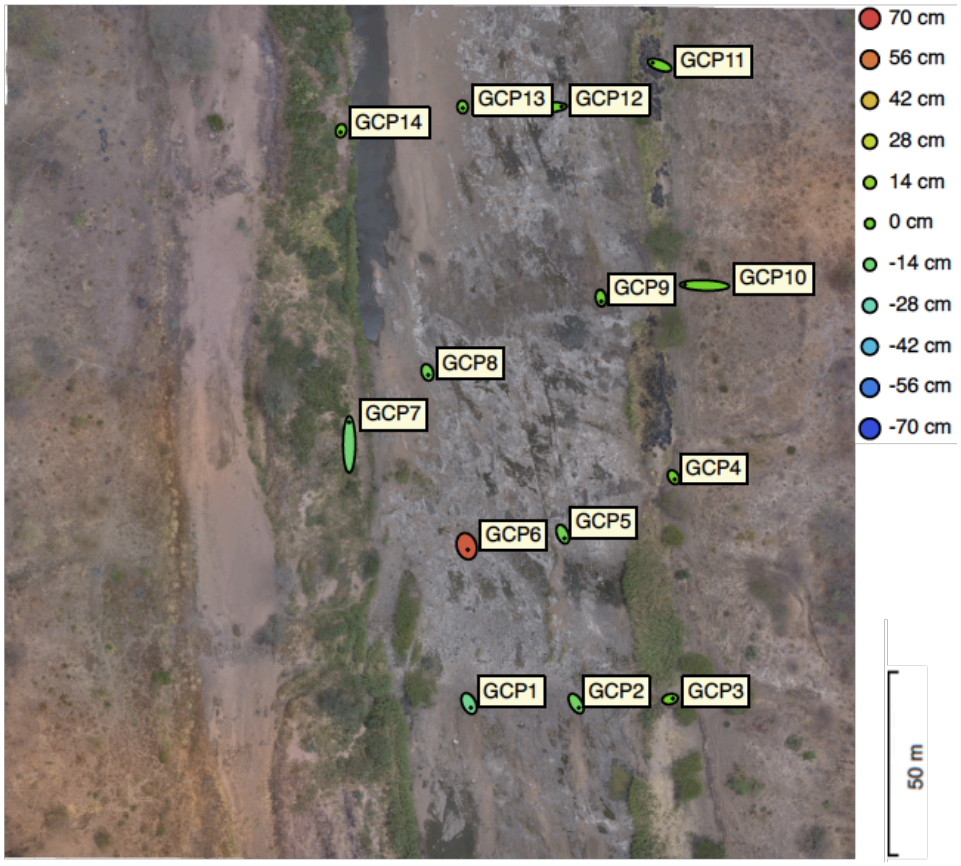

(a) Graphical presentation

Label	X error (m)	Y error (m)	Z error (m)	Total (m)	Image (pix)
GCP3	0.769531	0.163029	0.000596141	0.786611	0.165 (8)
GCP2	0.71953	-1.18524	-0.10699	1.39067	0.233 (10)
GCP1	0.531403	-1.11416	-0.204466	1.25122	0.153 (12)
GCP4	0.328716	-0.575253	0.0117873	0.662653	0.121 (10)
GCP5	0.476717	-1.10753	-0.0719389	1.20791	0.130 (16)
GCP6	0.292484	-0.954607	0.643592	1.18787	0.197 (16)
GCP7	0.015764	6.02758	-0.146073	6.02937	0.087 (14)
GCP8	0.230733	-0.711119	-0.0891508	0.752912	0.181 (12)
GCP10	-5.32704	0.181775	0.00792852	5.33015	0.088 (9)
GCP9	0.132253	-0.897526	-0.0198094	0.907434	0.089 (10)
GCP14	-0.11557	-0.439764	0.0174206	0.45503	0.100 (10)
GCP13	0.0381857	-0.30435	-0.0265517	0.307883	0.156 (10)
GCP12	3.81377	0.238021	-0.0163348	3.82122	0.152 (10)
GCP11	-1.90648	0.679162	-0.000125475	2.02384	0.258 (5)
Total	**1.86041**	**1.76517**	**0.189698**	**2.57156**	**0.155**

(b) Quantitative presentation

Figure F.5: GCP errors for Rio Capoche

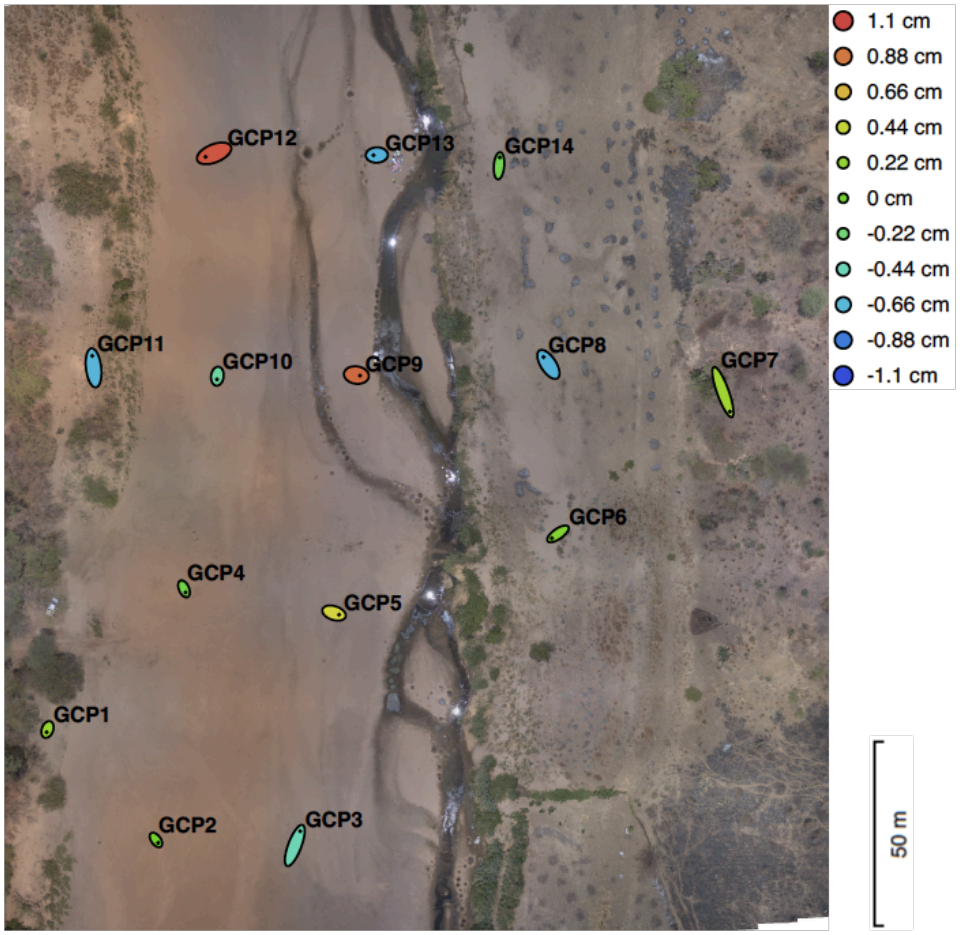

(a) Graphical presentation

Label	X error (m)	Y error (m)	Z error (m)	Total (m)	Image (pix)
GCP1	-0.140302	-0.372769	0.00235166	0.398305	0.069 (10)
GCP2	0.288382	-0.394789	3.79628e-06	0.488899	0.053 (9)
GCP3	0.741185	1.95053	-0.00432544	2.08661	0.085 (11)
GCP4	0.220909	-0.500107	-0.000721864	0.546725	0.056 (15)
GCP5	0.683551	-0.219697	0.00505611	0.718007	0.122 (14)
GCP6	-0.833057	-0.580437	0.000987693	1.01533	0.145 (12)
GCP7	0.955228	-2.66542	0.00273674	2.83142	0.085 (8)
GCP8	-0.661493	1.01366	-0.00691417	1.21043	0.129 (14)
GCP9	0.519377	-0.0726518	0.00928001	0.524516	0.122 (14)
GCP10	-0.0562841	-0.434396	-0.00368069	0.438042	0.047 (12)
GCP11	-0.189988	1.62921	-0.00674099	1.64026	0.060 (13)
GCP12	-1.15846	-0.468845	0.0100667	1.24978	0.071 (11)
GCP13	-0.459507	-0.0188262	-0.00688388	0.459944	0.212 (12)
GCP14	0.0904656	1.1345	-0.00118516	1.1381	0.133 (11)
Total	**0.602533**	**1.10912**	**0.00535747**	**1.26223**	**0.110**

(b) Quantitative presentation

Figure F.6: GCP errors for Rio Luia